

Waves and Instabilities at Contact Discontinuities

ELEANOR VICKERS

Doctor ISTVAN BALLAI,
Professor RÓBERT ERDÉLYI



The
University
Of
Sheffield.

University of Sheffield
School of Mathematics and Statistics

A thesis submitted in partial fulfilment of the requirements for the degree of

Doctor of Philosophy

September 2019

Acknowledgements

I would like to offer my thanks to the people and institutions that made this thesis possible.

First, my deepest thanks to my two PhD supervisors, Istvan and Robertus, who were always there to offer support and guidance. Thanks also Michael Ruderman for his insight to some mathematical quandaries.

I would also like to thank my friends and colleagues in SP2RC and PDG for their help and support. Particular thanks to Mihai Barbulescu, who developed the numerical solver, used to find solutions in Chapter 3 and was always ready to help with coding questions. To all of H23 and H25, thank you for being my “rubber ducks” and for helping to answer questions on maths and the Sun .

To Cathy, Felix, Jonny, Harriet and Mo, thank you for many evenings of great food and even better company that helped to keep me sane. To Harriet and Lottie thank you for reminding me I can achieve something, even if it is only small. To Ace, Bane, Garret, Helmholtz, Goldie, Ivellios, Ku and others, thank you for giving me a chance to not be myself. Thanks to Interval, Shakespeare’s and University Arms for being my oases and to those who shared in their sanctuary, in particular, Ben, Callum, Freddie, Hope, Jonny, Mihai and Poppy.

I am also thankful to my family for their constant support, especially to my father, who has helped me with my maths homework for many years longer than most parents.

Most of all, I would like to thank my partner, Iby, for being there through thick and thin, sharing in my highs and supporting me in my lows. The last few years would have felt impossible without you to lean on.

Finally, I acknowledge the funding received from the UK’s Science and Technologies Facilities Council (STFC).

Declaration of Authorship

I hereby declare that except where specific reference is made to the work of others, the contents of this dissertation are original and have not been submitted in whole or in part for consideration for any other degree or qualification in this, or any other university. This dissertation is my own work and contains nothing which is the outcome of work done in collaboration with others, except as specified in the text and Acknowledgements. This dissertation contains fewer than 80,000 words including appendices, bibliography, footnotes, tables and equations.

Eleanor Vickers
September 2019

Abstract

The aim of the present work is to study MHD waves and instabilities at contact discontinuities, in a plasma, with applications to the solar atmosphere. In particular we investigate what effect field inclination has on the characteristics of waves and instabilities.

We initially consider the gravity-free environment and investigate the characteristics of magneto-acoustic surface waves propagating at a single density interface, in the presence of an inclined magnetic field. For linear wave propagation, dispersion relations are obtained for both the time independent and the incompressible, time-dependent cases. Analytical solutions are derived for small inclination angle. For the time-independent case, the inclination of the field renders the frequency of waves to be complex, where the imaginary part describes wave attenuation, due to lateral energy leakage. The time-dependent case confirms the attenuation of leaky waves at a contact discontinuity. We also discuss the transition to the tangential discontinuity as the inclination angle tends to zero. We show that there is no continuous transition from the leaky modes on a contact discontinuity to the surface modes on a tangential discontinuity. However, such a transition exists if we take the average quantities describing the leaky modes.

We extend our study of the effects of magnetic field inclination at a contact discontinuity, by including the gravitational effects. We investigate the nature of the magnetic Rayleigh-Taylor instability at a density interface permeated by an inclined magnetic field in the incompressible MHD limit. Through an ideal MHD analysis, we find that, unlike the tangential case of MRT instability, perturbations of the interface are shown to be unstable for all wavenumbers, thus, due to the inclination of the magnetic field, the critical wavenumber at which waves become unstable disappears. As a result, field inclination produces qualitatively different dynamics than the tangential case, for the gravitationally modified case, as well as for the gravity free analysis. Theoretical results are applied to diagnose the structure of the magnetic field in prominence threads. Our analysis shows that the observed growth time of instability requires only small values of the inclination angle.

List of Publications

This Thesis is based on the following publications:

- Vickers, E., Ballai, I., Erdélyi, R. (2018); Propagation of Leaky MHD Waves at Discontinuities with Tilted Magnetic Field, *Solar Phys.* Volume 293, Issue 10
- Ruderman, M.S., Vickers, E., Ballai, I., Erdélyi, R. (2018); Propagation of Leaky Surface Waves on Contact Magnetohydrodynamic Discontinuities in Incompressible Plasmas, *Physics of Plasmas*, Volume 25, Issue 12
- Vickers, E., Ballai, I., Erdélyi, R.; Magnetic Rayleigh-Taylor Instability at Contact Discontinuity, *Astron. Astrophys.*, Volume 634, A96

Contents

1	Introduction	1
1.1	Solar Structure and Properties	1
1.1.1	Solar Interior	2
1.1.2	Solar Atmosphere	3
1.1.3	Structure and Variations in the Solar Atmosphere	4
1.1.4	Eruptive Events	7
1.1.5	Waves in the solar atmosphere	7
1.2	Outline of Thesis	10
2	Physical and Mathematical Background	11
2.1	Introduction to MHD	11
2.1.1	Assumptions of MHD	12
2.1.2	MHD equations	12
2.1.3	Ideal MHD Limit	14
2.1.4	Linearisation	15
2.2	MHD Waves	16
2.2.1	Sound waves	17
2.2.2	Alfvén Waves	18
2.2.3	Magnetoacoustic waves	18
2.3	Discontinuities and Jump Conditions	20
2.3.1	Jump conditions in the presence of gravity	23
2.4	MHD Waves Propagating Along an Interface	24
2.4.1	Numerical Solutions of The Dispersion Relation	26
2.4.2	Symmetry	30
2.5	Summary and Conclusions	30
3	Leaky MHD Waves	32
3.1	Governing Equation	33
3.2	Solving The Governing Equation	36
3.3	Dispersion Relation	39
3.3.1	Dispersion Relation in Dimensionless Form	40
3.4	Numerical Solutions and Discussion of Results	41
3.5	Symmetry	47
3.6	Conclusions	49

4	Time-Dependent Analysis	51
4.1	Governing equations	52
4.2	Joining solutions at the interface	56
4.3	Finding time-dependent solutions	58
4.4	Small Inclination Angle Approximation	61
4.5	Comparison to Tangential Solutions	63
4.6	x -dependent solutions	67
4.6.1	Delta-function driver	67
4.6.2	Lorentz function driver	68
4.6.3	Sinusoidal Driver	69
4.7	Conclusions	72
5	An Introduction to Instabilities	74
5.1	Gravitational Instabilities	75
5.1.1	Convective instabilities	76
5.2	Hydrodynamic Rayleigh-Taylor Instabilities	78
5.3	RTI for a horizontal magnetic field	81
5.4	RTI for a vertical magnetic field	84
6	MRT Instability	88
6.1	x -propagating waves	88
6.1.1	Continuity conditions	91
6.1.2	Solutions	92
6.2	y -propagating waves	94
6.3	Three-Dimensional Analysis	98
6.3.1	Dispersion relation of waves propagating along the in- terface	98
6.3.1.1	Boundary Conditions	101
6.3.1.2	Derivation of Dispersion Relation	101
6.3.2	Solutions and results	103
6.3.3	Symmetry	107
6.3.4	Applications to Solar Prominences	108
6.4	Conclusions	112
7	Conclusions	113
7.1	Overview of Thesis	113
7.2	Summary of Results	114
7.2.1	Chapter 3	114
7.2.2	Chapter 4	114
7.2.3	Chapter 6	115
7.3	Future Work	116
A	Calculation of residues and time-dependent velocities	118
B	Expressions for time-dependent averages	120
	Bibliography	121

List of Figures

1.1	Schematic representation of the solar layers, from the Sun's core to the outer solar wind. Credit: Kelvinsong (2012)	2
1.2	The VAL model of the solar atmosphere, describing how mean density and temperature vary with height from the solar surface. Credit: Avrett and Loeser (2008)	4
1.3	The structure of a sunspot, including magnetic field lines. Credit: Thomas and Weiss (2004).	5
1.4	Magnetic structuring of prominences. Adapted from: Malherbe and Priest (1983)	6
2.1	Velocities of Alfvén, fast (v_{fast}) and slow (v_{slow}) waves in a homogeneous plasma, for a magnetic field, directed in the horizontal direction. Here, the sound speed is denoted v_s . The relevant velocities are shown for the three cases: sound speed slower than Alfvén speed (left), Alfvén and sound speeds equal (middle), and sound speed greater than Alfvén speed (right). Credit: Jess et al. (2015)	20
2.2	Solutions of the dispersion relation of waves propagating along an interface in the tangential discontinuity case, for $\beta = 0.1$ (above) and $\beta = 10$ (below), for varying density ratio. Solutions are shown with solid blue lines. Critical speeds above the interface are shown in green and below the interface are shown in black. The Alfvén speeds are shown with solid lines, the sound speeds are shown with dotted lines and the cusp speeds are shown with a dashed line.	28
2.3	Solutions of the dispersion relation of waves propagating along an interface in the tangential discontinuity case, for $d = 0.1$ (above) and $d = 0.5$ (below), for varying plasma- β . Solutions are shown with solid blue lines. Critical speeds above the interface are shown in green and below the interface are shown in black. The Alfvén speeds are shown with solid lines, the sound speeds are shown with dotted lines and the cusp speeds are shown with a dashed line.	29

3.1	The plasma is structured into two semi-infinite regions of constant density and gas pressure, with a sharp interface at $z = 0$. A constant magnetic field crosses the interface and it is inclined at an angle θ to the interface.	33
3.2	The variation of the dimensionless phase-speed of the waves, \tilde{c}_{ph} , propagating along the interface in terms of the plasma- β , for two values of density ratio. The real part is plotted in the <i>upper panel</i> and the imaginary part in the <i>lower panel</i> . The characteristic speeds are also shown for reference, using <i>thin lines</i> : the Alfvén (<i>solid line</i>), sound (<i>dotted line</i>) and cusp speeds (<i>dashed line</i>) for the regions above (<i>green lines</i>) and below the interface (<i>black lines</i>).	42
3.3	The variation of the dimensionless phase-speed of the waves, \tilde{c}_{ph} propagating along the interface in terms of the density ratio, for two values of plasma- β . The real part is plotted in the <i>upper panel</i> and the imaginary part in the <i>lower panel</i> . The characteristic speeds are also shown for reference, using <i>thin lines</i> : the Alfvén (<i>solid line</i>), sound (<i>dotted line</i>) and cusp speeds (<i>dashed line</i>) for the regions above (<i>green lines</i>) and below the interface (<i>black lines</i>).	44
3.4	Height dependence of eigenfunctions, corresponding to the eigenvalues found in Figures (3.2) and (3.3), proportional to the value G_+	46
3.5	The invariant orientations of the equilibrium system.	48
4.1	A sketch of the contour in the complex ω -plane used to perform inverse Laplace transforms of perturbations. (Taken from Ruderman, Vickers, Ballai and Erdélyi (2018))	59
4.2	The variation of the real part of horizontal velocity, v_x , with respect to time, 100 km above the interface, for two values of density ratio, $d = 0.09, 9$. The inclination angle is take to be $\theta = 5^\circ$	62
4.3	The real and imaginary parts of the velocity, v_x , the tangential solution for the velocity, u_t and the averaged velocity, $\langle v_x \rangle$, with respect to dimensionless height, kz , across the interface, for $\theta = 0.001$, $d = 0.5$ and kv_1t being the value for the 25th peak.	65
4.4	An intensity plot showing the vertical component of velocity in the (x, z) -plane over a minute, when subject to a Lorentzian driver, for $\theta = 5^\circ$, $d = 0.5$, $v_{A-} = 10 \text{ kms}^{-1}$, $a = 1$ and $l = 50$ km. Solutions are only plotted in the region where $ z < z_m(t)$	70
4.5	An intensity plot showing the vertical component of velocity in the (x, z) -plane over a minute, when subject to a sinusoidal initial driver, for $\theta = 5^\circ$, $d = 0.5$, $v_{A-} = 10 \text{ kms}^{-1}$, $a = 1$ and $l = 50$ km. Solutions are only plotted in the region where $ z < z_m(t)$	71

5.1	Solutions for the hydrodynamic RTI and propagating modes, in terms of wavenumber and density ratio.	80
5.2	A sketch of the equilibrium configuration for the case of a horizontal magnetic field. The equilibrium state consists of a surface separating two regions, each with different density. The magnetic field is horizontal and uniform in each region. The configuration is invariant in the x - and y -directions and perturbations are in the direction of the wavevector \mathbf{k} in the (x, y) -plane.	82
5.3	Frequency of waves in the presence of a horizontal magnetic field, in terms of wavenumber. The real part of solutions is shown in blue and the imaginary part in red, while solutions for different propagation directions are shown with different line-styles.	84
5.4	Imaginary part of the frequency against wavenumber for the case of vertical magnetic field, i.e. normal to the density interface.	87
6.1	2D sketch of the equilibrium configuration for the case of waves propagating in the x -direction. The equilibrium state consists of a surface separating two regions, each with different density. The magnetic field is uniform throughout both regions and is inclined within the (x, z) -plane at an angle, θ , with respect to the x -direction. The configuration is invariant in the x -direction.	89
6.2	Solutions for longitudinally propagating waves, where $d = 0.5$, $v_A = 100 \text{ km s}^{-1}$, $\theta = 5^\circ$. Imaginary part of frequency is plotted in red in lower panel, whereas the real part is shown in blue in the upper panel. The solution to the tangential case is shown in green	93
6.3	Imaginary part of the solution for x -propagating waves, where $d = 0.5$, $v_A = 100 \text{ km s}^{-1}$, $k_x = 0.0025$	94
6.4	2D sketch of the equilibrium configuration for the case of waves propagating in the y -direction. The equilibrium state consists of a surface separating two regions, each with different density. The magnetic field is uniform throughout both regions and is inclined within the (x, z) -plane at an angle, θ , with respect to the x -direction, so has a component $B_z = B_0 \sin \theta$ within the (y, z) -plane. The configuration is invariant in the y -direction.	95
6.5	A solution for transversally propagating waves in terms the wavenumber, k_y , whith $d = 0.5$, $v_A = 100 \text{ km s}^{-1}$, $\theta = 22.5^\circ$	97

6.6	Schematic representation of the equilibrium configuration used in the present section. The equilibrium state consists of a surface separating two regions, each with different density. The magnetic field is uniform throughout both regions and is inclined within the (x, z) -plane at an angle, θ , with respect to the x -direction. The configuration is invariant in the x - and y -directions. Perturbations are described by the wavevector, \mathbf{k} , in the (x, y) -plane.	99
6.7	Solutions for the dispersion relation for waves propagating in the (x, y) -plane, for two propagation directions ($\alpha = 0$ solid line, and $\alpha = \pi/4$ dashed line), with respect to wavenumber, k . The density ratio is $d = 0.5$, the Alfvén speed of the lower plasma is $v_A = 10 \text{ km s}^{-1}$, and the magnetic field inclination angle $\theta = 5^\circ$. The upper panel shows the real part of the frequency, while the imaginary part is plotted in the lower panel. The limiting value of $\Im(\omega)$ when $k \rightarrow \infty$ is shown by the grey horizontal lines, in the lower panel. For illustration we also show the real and imaginary part of the frequency in the case of a tangential discontinuity ($\theta = 0$), plotted here in green.	104
6.8	Imaginary part of the frequency for waves propagating in the (x, y) -plane, for several propagation directions, with respect to the magnetic field inclination, θ . The density ratio is assumed to be $d = 0.5$, the reference Alfvén speed is $v_{A-} = 10 \text{ km s}^{-1}$, and the value of the wavenumber fixed at $k = 10^{-5} \text{ m}^{-1}$	105
6.9	Growth time for $k = 2.5 \times 10^{-3} \text{ m}^{-1}$, $d = 0.5$ $v_A = 10 \text{ kms}^{-1}$, in terms of propagation angle, α and field inclination θ	106
6.10	Growth time for $k = 2.5 \times 10^{-3} \text{ m}^{-1}$, $d = 0.5$ $\theta = \pi/8$, in terms of propagation angle, α and Alfvén speed of the lower plasma, v_A	107
6.11	A diagram showing the dense prominence plasma (orange) supported by magnetic field lines (blue) and how this relates to the contact discontinuity at an interface investigated in the present work.	109
6.12	Solutions of the dispersion relation for a given growth time in terms of magnetic field inclination (θ) and propagation direction (α), for six observed prominence threads, for three possible density ratios. Observational data has been adapted from Okamoto et al. (2007).	111

CHAPTER 1

Introduction

*“The sun is a miasma
Of incandescent plasma”*

1.1 Solar Structure and Properties

The Sun dominates virtually all aspects of life on Earth and, as such, has been an object of fascination throughout human history. Our understanding of the Sun has changed greatly over the millennia; from the belief that it was a great flaming chariot being driven across the sky, to our current understanding of it as a massive nuclear furnace at the centre of our solar system.

Not only does the Sun provide heat and light to the solar system, it also constitutes over 99% of the mass of the system, with a mass of approximately 2×10^{30} kg, making it 330,000 times more massive than the Earth. Given its enormous mass, the gravitational acceleration at its surface is 27 times greater than the Earth’s gravitational acceleration. The mean distance from the Earth to the Sun is 149.6 million km, a distance that light takes approximately 8 minutes to cover.

The incredibly high temperature at the core of the Sun, along with the intense pressure, facilitates the occurrence of fusion; where hydrogen nuclei fuse together to form helium and release energy. This high temperature also causes the electrons to dissociate from the nuclei of the super-heated hydrogen and helium. This “soup” of ions and electrons, controlled by the magnetic field, is known as *plasma* and is often referred to as the fourth state of matter. The collectively free moving positively charged ions and negatively charged electrons enable the plasma to support electric currents, as well as electric and magnetic fields, which in turn affect the dynamics of the plasma. The high-resolution observations in different wavelengths, over the last few decades, revealed, with no doubts, that the magnetic field is at the heart of the solar structure and its dynamical evolution. Thus, if we want to understand how our Sun evolves and how and why the varied solar phenomena take place, we need to understand the effects that the magnetic field has on the solar plasma.

The Sun is a huge plasma sphere, approximately 700 Mm in radius, which is over 100 times larger than the Earth’s radius. However, it is far from homogeneous; instead, it is made up of several different layers and regions with

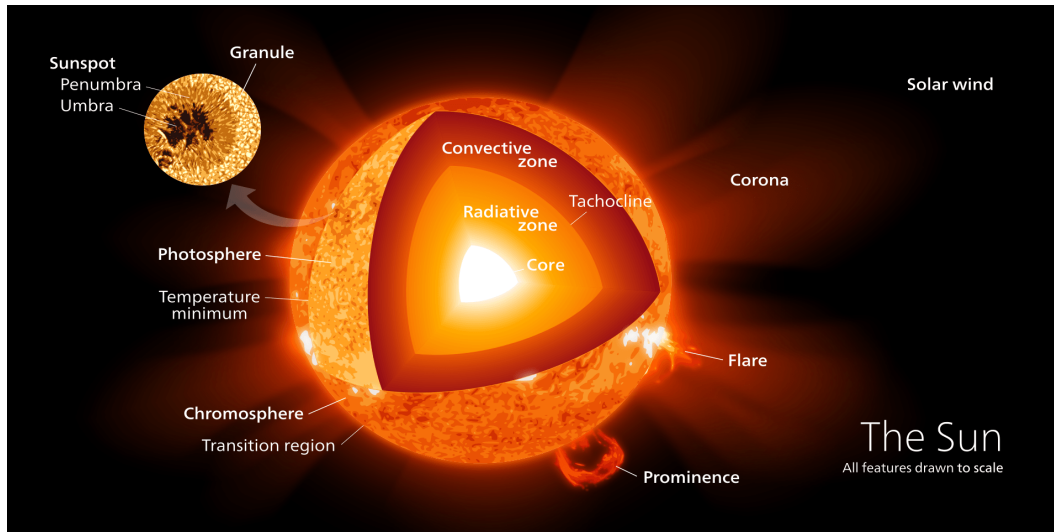


Figure 1.1: Schematic representation of the solar layers, from the Sun's core to the outer solar wind. Credit: Kelvinsong (2012)

different properties, which are shown in figure (1.1) and described below. Most notably for our discussion, the Sun may be split into the *solar interior* and the *solar atmosphere*.

1.1.1 Solar Interior

The interior of the Sun is shielded from our view, only its surface and its atmosphere is visible directly. *Helioseismology* is the science that uses the sound waves, that penetrate the solar interior and get reflected back towards the solar surface, to diagnose the evolution and structure of the solar interior.

In the centre of the Sun, the core has a radius in the region of 150 Mm (0.2 solar radii), so it comprises only approximately 1% of the volume of the Sun. Despite its small size, it contains over one third of the Sun's mass and also has a temperature of 15 million K. At such a high density and pressure, this is the region where 99% of the fusion energy originates. During fusion processes helium nuclei are formed from hydrogen nuclei, mainly by the proton-proton reaction. The end-result of these reactions (in addition to the helium) are two high-frequency gamma-rays, having an energy of 26.2 MeV, and two electron neutrinos, each with an energy of 0.5 MeV. These neutrinos can travel at nearly the speed of light, practically unaffected by matter, but (with great difficulty) can be detected by scientists on Earth, to learn more about the physical mechanisms at the heart of our Sun.

Further out, between 0.2 and 0.7 solar radii, is the radiative zone, where the energy produced in the core radiates outwards, by the absorption and re-emission of photons. The plasma is still incredibly dense and opaque, meaning that absorption and re-emission occurs so many times that the time taken for a photon to travel across the radiative zone is increased to over 100 000 years; a journey that would take about 2 seconds in a vacuum. The density and temperature both decrease over the radiative zone; the density dropping two

orders of magnitude, while the temperature drops an order of magnitude to 1.5 million K.

The outermost layer of the Sun's interior is the convection zone, where energy is transported via the convective instability. The convective instability (covered in more detail in Chapter 5) occurs when the temperature gradient is sufficiently high, such that when plasma is displaced vertically upwards, it may expand, becoming buoyant. The buoyant plasma then rises to the surface, where it radiates energy into the atmosphere, cools and sinks again. At the surface of the Sun, the temperature has fallen to about 6000 K. Unlike the solid body rotation of the radiative zone, the convection zone exhibits differential rotation, where the angular velocity is dependent on latitude. This produces a thin shear layer between the radiative and convective zones, known as the *tachocline* (Spiegel and Zahn, 1992), which is thought to be vital for the generation of the global solar magnetic field, in many solar dynamo models.

1.1.2 Solar Atmosphere

The values for density and temperature given here for layers of the solar atmosphere have been derived from the VAL (Vernazza-Avrett-Loeset) model of the solar atmosphere (Vernazza et al., 1981) and are illustrated in Figure (1.2). This model gives mean values for temperature and density by assuming thermodynamic properties vary only with height. It was constructed by using the equations for radiative transfer, for an optically thick medium. For several constituents of the solar atmosphere (e.g. hydrogen atoms, hydrogen ions, carbon and silicon), these equations were solved for a trial atmosphere, to derive possible radiation spectra. These spectra were then compared against observed data and the trial atmosphere was adjusted until a good agreement with the observed spectrum was achieved.

The lowest level of the solar atmosphere is the photosphere, which, although only 500 km thick, emits the majority of the Sun's visible light. The convective motion from the Sun's interior may be seen as *granulation*. Here, hot bright granules, with cool dark boundaries, are caused by the hot rising plasma and cover most of the solar surface and may be observed directly. They range in size from 0.3 to 2 Mm, with an average diameter of 1.5Mm, and lifetimes of 1 to 20 minutes (Priest, 2014). There are also regions of intense magnetic field, with strengths of the order of a few kG, where convection is inhibited, known as sunspots. Across the photosphere, the temperature decreases from 6 000 K to approximately 4 400 K, and the density gradient is approximately exponential, decreasing two orders of magnitude, to 10^{-6} kg m⁻³. The temperature in the photosphere decreases to its lowest value (approximately 4,300 K), while density and pressure decrease by approximately two and a half orders of magnitude.

Further out is the chromosphere, a region situated between 0.5 - 2.5 Mm; so-called because of its rosy colour, revealed during a solar eclipse. Throughout its height, the temperature rises from 4 400 K to around 100 000 K, while density and pressure decrease by further four orders of magnitude. The chro-

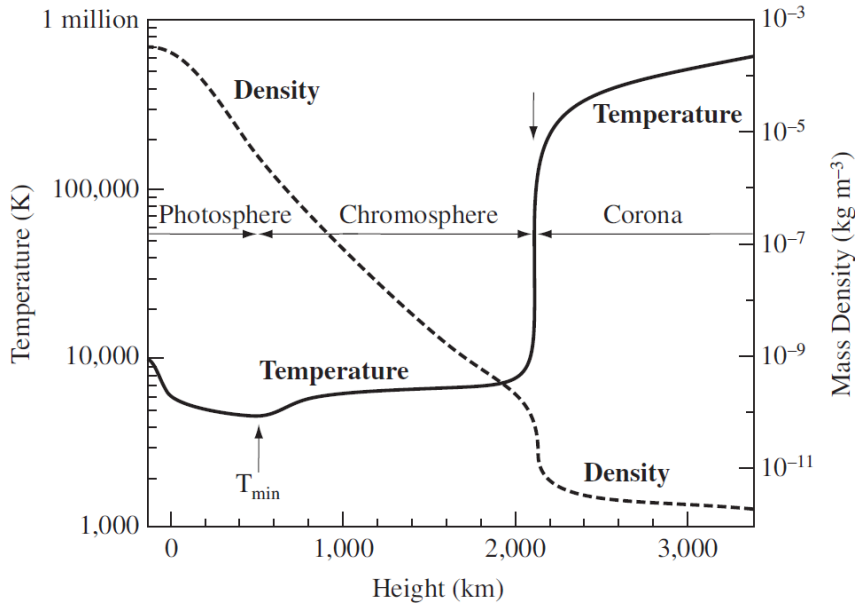


Figure 1.2: The VAL model of the solar atmosphere, describing how mean density and temperature vary with height from the solar surface. Credit: Avrett and Loeser (2008)

mosphere contains many magnetic and plasma structures, most notably its many spicules, which early observers described as a “burning prairie”, and solar prominences (also known as filaments). The solar chromosphere is probably the most dynamic and structured solar atmospheric layer, however its detailed description is beyond the current study. Instead we refer to the remarkable review by Priest (2014).

The outer atmosphere is known as the corona, so named because, when a solar eclipse allowed the corona to be seen clearly, ancient Greeks thought it looked like a crown. Separating the chromosphere from the corona, is a very thin layer (only a few hundred km), termed the *transition region*. Within this thin layer the temperature changes from 100 000 K to over 1 million K, accompanied by a drastic drop in density. There are many theories proposed to explain this huge rise in temperature, but this problem is still not fully understood and is thus known as the *coronal heating problem*, (see e.g. Klimchuk 2006; Parnell and De Moortel 2012). In the corona, magnetic forces dominate, creating significant structuring, including coronal loops. There is no clear distinction between the corona and the solar wind, which extends as far as the heliopause, past the orbit of Pluto, and constitutes a stream of charged particles streaming outwards, emitted by the Sun.

1.1.3 Structure and Variations in the Solar Atmosphere

The magnetic field in the solar atmosphere is profoundly inhomogeneous. Not only does the magnetic field strength vary with height, with the average intensity decreasing with height from the solar surface, the magnetic field lines also accumulate into tubes of intense magnetic field strength, known as flux tubes.

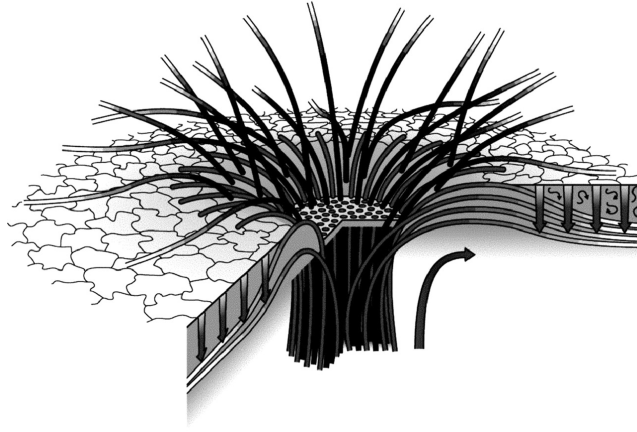


Figure 1.3: The structure of a sunspot, including magnetic field lines. Credit: Thomas and Weiss (2004).

This magnetic field structuring, in turn, applies structure to the plasma, due to the fact that plasma will more readily travel in the direction of magnetic field lines, especially in regions of intense magnetic field. This section will introduce some of the more notable structures of the solar atmosphere. The main premise of this thesis is to explore dynamics at contact discontinuities, where a component of the magnetic field intersects a sharp change in plasma densities ¹. For this reason, this section will particularly focus on examples where magnetic fields are inclined to changes in density.

Sunspots have already been introduced in section (1.1.2), as regions of intense magnetic field. These tend to be approximately 10 Mm across and the field tends to be in the region of a few kG. This intense magnetic field exerts a strong magnetic pressure, which inhibits convection, causing the sunspots to be approximately 2000 K cooler than their surroundings. At the centre of the sunspot, in the *umbra*, magnetic field lines are vertical, opening out more at the edges, becoming inclined, as well as less intense. This means that at the outer edges, the convection is not as diminished as in the centre, manifesting as a brighter ring around the umbra, known as the *penumbra*. Within the umbra, the field is still not homogeneous and there are often bright points, around 100km across, of less intense magnetic field, known as umbral dots. Within the penumbra the magnetic field is inclined with respect to the vertical direction (see Fig. 1.3). As the density gradient between the solar interior and the photosphere is predominantly vertical, where these inclined magnetic field lines open up, they can, in places, cross this density change, and may be viewed as a *contact discontinuity* (a discontinuity with an intersecting magnetic field component, see Section 2.3). The treatment of the penumbra as a discontinuity is valid, provided the lengths scales, in the direction of the density change, of perturbations considered are large in comparison to the scale-height of the density change. For more details on sunspots' structure and properties, see Solanki (2003).

¹A more detailed explanation of discontinuities is given in Section (2.3)

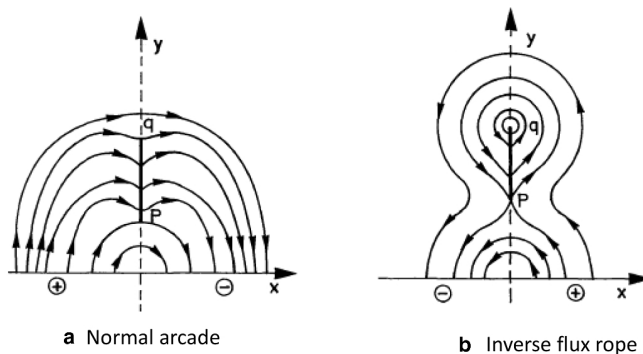


Figure 1.4: Magnetic structuring of prominences. Adapted from: Malherbe and Priest (1983)

Throughout much of the corona are bright *coronal loops*, visible thanks to high resolution observations in X-ray and EUV, made with instruments such as Yohkoh, SDO AIA or TRACE. The emissive plasma in these loops acts as tracer of the magnetic field lines, with plasma in the loops denser than their surroundings (around 10 times denser). The loops' characteristics therefore vary as much as the magnetic fields themselves. Magnetic field intensities in coronal loops vary over two orders of magnitude. Loops may be anchored at both ends by magnetically opposite footpoints, with these “closed” loops extending up to 300Mm up into the solar atmosphere. Conversely, the loops may also be “open”, with only one footpoint connected to the solar surface, the other end fading into the solar wind and are here referred to as plumes.

Many flux tubes may come together to form solar *prominences*. A prominence is a large (extending over thousands of km) loop of dense, chromospheric plasma, anchored in the photosphere, suspended in the sparse corona by magnetic fields. When viewed with high resolution telescopes, these may be resolved into separate threads, but due to interactions between these threads, the prominence may often be modelled as one unified structure. The magnetic field not only confers stability to prominences, but also provides thermal shielding, from the much hotter corona, since the thermal flux is channelled along the magnetic field lines². There are two basic geometries of magnetic field that may suspend the dense plasma: arcades and flux ropes. The flux rope model has the prominence intersecting field lines in closed loops; these are then surrounded by figure-of-eight shaped field lines, anchored below, with an X-point situated below the prominence (see Malherbe and Priest 1983). The arcade model has dense plasma sitting in “dipped” magnetic fields. Both these models are shown in Fig (1.4) and include contact discontinuities at the prominence edges, with inclined field lines.

²Thermal shielding and the stability provided by the magnetic fields are only effective in the case where magnetic field lines go around, rather than through the prominences itself (tangential rather than contact discontinuities.)

1.1.4 Eruptive Events

As well as long term stable structuring, the Sun can also exhibit sudden, eruptive events, such as *solar flares* and *coronal mass ejections*. Solar flares manifest as bright flashes, observed in e.g. X-ray, EUV or H_α and are present in all layers of the solar atmosphere. Flares produce huge bursts of electromagnetic radiation across all wavelengths of the electromagnetic spectrum, with most of the energy concentrated in X-ray frequencies. Coronal mass ejections (CMEs) often coincide with large flares and are a huge release of plasma from the solar corona. The ejected plasma is normally present as prominences, before being expelled into the solar wind. Magnetic fields accompany the ejected plasma, so, when CMEs are directed Earth-wards, the interaction of the CMEs' magnetic field with the Earth's produces geomagnetic storms.

These eruptive events are caused by the sudden release of magnetic energy, through *magnetic reconnection*. Magnetic reconnection is a non-ideal process, where the magnetic topology of the plasma is rearranged and magnetic energy is released, in the form of thermal energy and particle acceleration (instigating flares) and kinetic energy (forcing plasma outwards in the form of CMEs). These energy releases may also drive waves across the solar atmosphere, as well as contributing to coronal heating.

Another form of eruptive events are *spicules*, which are jets of chromospheric plasma, travelling upwards at speeds of around 20 km s^{-1} . Spicules have a width of approximately 500 km, and reach several thousands of km in height, before collapsing or dispersing, after approximately 10-15 minutes. Although it is possible that spicules are also driven by reconnection, like flares and CMEs, another theory is that spicules are formed as a result of pressure-driven oscillations at the surface of the Sun (Erdélyi and James, 2004).

1.1.5 Waves in the solar atmosphere

Waves and oscillations are ubiquitous phenomena in the solar atmosphere, and are very important to solar physics, both in the essential processes they carry out and from an observational point of view, probing the inner-workings of the Sun. In general, the energy for waves in the solar atmosphere comes from the convective motions at the bottom of the photosphere, but the waves themselves carry energy across different layers of the solar atmosphere. Waves can also dissipate their energy, causing plasma heating in the upper regions of the atmosphere (e.g. Einaudi et al. 1993, Erdélyi and Ballai 2007, Arregui 2015). This may, in part, help to explain the high coronal temperatures. As waves propagate through different regions, their properties may be altered and, in doing so, carry an imprint of the environment through which they have propagated. This idea is the foundation of *solar seismology* (covering helioseismology, in the solar interior, and atmospheric seismology), where physical parameters that may not be directly observed are inferred from the wave properties, such as amplitude, period, polarization, frequency, damping time and length, etc. This technique has been employed for some time in the solar interior, most notably to discover much of the information given in section (1.1.1). In more

recent years, with the improvements of space and ground-based telescopes, enabling more detailed observations, *magneto-seismology* has been developed and applied, to determine values of difficult to observe parameters in the outer solar atmosphere, such as magnetic field strength, its sub-resolution structure, the local density of the plasma, various transport coefficients, heating/cooling functions, etc. (see reviews by Arregui 2015, De Moortel and Nakariakov 2012, Mathioudakis et al. 2013, Arregui et al. 2018).

One of the most well-studied waves in the solar atmosphere is the kink wave, in the context of magnetic structures (filaments, spicules, prominences, coronal loops, etc). These are believed to be the result of the reaction of the flux tube to an external driver, such as a global wave or nearby release of energy (such as during a coronal mass ejection) and the magnetic structures themselves act as waveguides. The majority of these kink wave oscillations are observed to damp very quickly, due to a phenomenon known as resonant absorption. In addition, coronal loops, may support *decayless* kink waves, which appear as low amplitude transverse oscillations of coronal loops. These are thought to be due to resonance of flux tubes in the presence of continuous perturbations of the surrounding atmosphere (see Anfinogentov, S. et al. 2013). With flux tubes acting as a cylindrical waveguide, there are two major kinds of oscillation modes: *kink waves* and *sausage waves* (see Edwin and Roberts 1982). Sausage modes have zero azimuthal wavenumber, so are rotationally symmetric and manifest as a wave of oscillating radius of the tube. Kink waves, have an azimuthal wavenumber of one and perturb the centre of the tube, but maintain cross-sectional area. Higher order *fluting modes* also exist, which change the shape of the cross-section of the tube, but are more difficult to observe. Both kink and sausage modes have been observed in the solar atmosphere. Kink waves in coronal loops manifest as rapidly damping waves, propagating along the coronal loops and have been observed by several authors (e.g. Verwichte et al. 2005). The theory of kink waves in the solar atmosphere has also been studied by many authors (e.g. Aschwanden et al. 1999, Nakariakov and Roberts 1999 etc.) and observations have been used to estimate hard to observe parameters (see, e.g. Nakariakov et al. 1999, Andries et al. 2005, Verth et al. 2008). Sausage modes, though less easy to identify, have also been observed (see e.g. Aschwanden 2003, Erdélyi and Taroyan 2008, Dorotovič et al. 2014).

In addition to sausage and kink waves, flux tubes are able to support torsional waves known as “surface Alfvén waves” or “Alfvénic” waves, and identified as fast waves by Edwin and Roberts (1982). These are investigated in detail in Goossens et al. (2012) and are found to propagate at a phase-speed between the Alfvén speeds of the inner and outer plasmas and are driven predominantly by magnetic tension, with low compressibility effects, especially for the thin tube approximation. These waves are fundamental modes, with no radial modes, and the vorticity is located at the boundary, hence the name “Alfvénic”.

The strong magnetic fields within sunspots also act as waveguides, allowing the upward propagation of waves, and there are several well-known oscillations

connected with sunspots. Oscillations within the umbrae tend to be vertically propagating into the corona, with periods of 130-190 s (first identified in corona by DeForest and Gurman 1998), whereas in the penumbra, *running penumbral waves*, propagate horizontally outwards from the sunspot, with typical periods of 200-300 s (see e.g. Nye and Thomas 1974, Zirin and Stein 1972). A summary of observations of such oscillations may be found in (Lites et al. 1982 and Brynildsen et al. 2000). Running penumbral waves have, in fact, been shown to constitute a superposition of many waves, with varying periods and phase speed, see (Briskin and Zirin 1997 and Kobanov and Makarchik 2004). A detailed review of oscillations in sunspots and their atmospheres is provided by Khomenko and Collados (2015).

Prominences have also been observed to support an array of oscillations in filaments (see reviews by Ballester 2006, Oliver 2009). Longitudinal prominence thread oscillations have been studied theoretically, by modelling them as a single flux tube, surrounded by hot coronal plasma (Luna and Karpen, 2012), where gravity was found to provide a significant contribution to the dynamics and large amplitude oscillations on curved threads had gravity as the main restoring force. Observed transverse waves have been modelled as predominantly MHD waves (see review by Arregui et al. 2010). Observations of prominence oscillations also showed that the threads had relatively short lifetimes of approximately 5 minutes (Lin et al., 2009), which it has been suggested is due to the gravitational Rayleigh-Taylor instability (Terradas et al., 2012). The Rayleigh-Taylor instability in prominence threads will be revisited in Chapters 5 and 6.

All the above waves are strictly connected to the magnetic structure in which they propagate, therefore, they can very often be labelled as local waves. On the other hand, global waves are also able to propagate within the Sun, over very large distances. One of the most well-studied global modes are the *p*-modes (first discovered by Leighton 1960), which are acoustic oscillations, propagating in the photosphere. These oscillations are able to penetrate the solar interior and carry essential information back to the surface and, thus, these are an essential tool for helioseismologists. These oscillations are produced by the Sun's convective motion, continually disturbing the stable photosphere. Another form of global waves are those generated by a sudden energy release, such as a large flare or coronal mass ejection. These waves appear as circularly expanding shocks, rather like ripples on a pond after a stone is thrown in. In the chromosphere, these present as *Moreton waves* (Moreton and Ramsey, 1960) and propagate with super-Alfvénic speeds of 1000 - 2000 kms^{-1} . In the corona, *EIT waves* may be observed (named after the Extreme ultraviolet Imaging Telescope with which they are observed), which only propagate at speeds of a few hundred kms^{-1} (Thompson et al., 1999). Despite being instigated by the same events, it is still not clear how, or if, these waves are connected. Another form of large-scale waves are *transition region quakes* (TRQs), investigated by Scullion et al. (2011), where upward propagating spicules provoke oscillations of the transition region, rippling outwards from where the spicule strikes the transition region.

As we can see from this short review the solar atmosphere can host a rich variety of waves; practically, waves are observed in almost all magnetic features in the solar atmosphere. Local waves and oscillations are very much connected to the presence of the magnetic field, and these predominantly propagate along magnetic field lines or various magnetic structures, an aspect that will be investigated in detail in the present thesis. The main premise of the current work is the investigation of characteristics of waves and instabilities that appear at density interfaces and the effect of field inclination.

1.2 Outline of Thesis

The research presented in this thesis is centred around the effect of magnetic field inclination on both waves and instabilities at contact discontinuities in the solar atmosphere. To give the technical background necessary to investigate the effects of field inclination later in the thesis, Chapter 2 covers an introduction to some of the important concepts surrounding MHD waves and instabilities. This includes an introduction to the MHD equations, magneto-hydrodynamic waves, and continuity conditions for interfaces. A brief review of a study investigating surface waves at a tangential discontinuity is included for reference.

In Chapter 3, we explore the properties of waves that can propagate at a contact discontinuity interface. These properties are investigated as an eigenvalue problem, assuming linear perturbations, propagating along the interface, in a 2D, compressional plasma. A small angle approximation is introduced for the field inclination and a perturbation technique is used to find leaky wave solutions (i.e. propagating modes where energy disperses away from the interface) either side of the interface. A dispersion relation is then found, using boundary conditions for a contact discontinuity, and solved numerically, to find the phase-speed of waves.

Chapter 4 explores the initial value problem of waves at a contact discontinuity, for the incompressible case. Once again, the case for small inclination angle is considered and solutions are found analytically in terms of wavenumber for some initial velocity perturbation, centred at the interface. Three cases for this initial condition are considered and explicit solutions are found for each of these, in terms of time and spacial coordinates.

Chapter 5 gives some more background, pertinent to the following chapter, about gravitational instabilities in a plasma. Chapter 6 is devoted to the effect of magnetic field inclination on the magnetic Rayleigh-Taylor instability at the density interface. A similar technique as in Chapter 3 is used to study wave-like perturbations, in the linear MHD limit, to obtain the dispersion relation. Thanks to the simplification incompressibility affords, solutions to the dispersion relation are calculated analytically, for an arbitrary inclination angle. Using the expressions for the velocity, a proof of concept for an inversion technique is presented, where the orientation of the magnetic field is found for some observed prominence threads, providing an application of the theory to the diagnostics of magnetic field structure in the solar atmosphere.

CHAPTER 2

Physical and Mathematical Background

The present thesis deals with the properties of magnetohydrodynamic (MHD) waves and instabilities that are present at surfaces separating regions of different properties. The plasma dynamics will be described within the framework of MHD and the equations outlining the connection between various thermodynamic and electromagnetic parameters (together with the limit of their applicability) will be discussed below.

The surfaces along which waves and instabilities will propagate are modelled by discontinuities, and when we study the propagation of waves along these surfaces we will need to know how to connect solutions on both sides of the discontinuity. The magnetic field, that is present in the two regions, will play an important role, as its orientation will decide the nature of the discontinuity. In the present chapter we will derive the necessary conditions that allow us to connect the solutions at the separating surface and, as a result, to derive the dispersion relation of waves.

In order to better understand the implication of the magnetic field orientation with respect to the interface on wave propagation, we will need to review and understand the results obtained for the same problem when the magnetic field is parallel to the interface, a theory that has been developed almost four decades ago by Roberts (1981).

2.1 Introduction to MHD

As described in the Introduction, the solar plasma is a fluid made up of charged particles (positive and negative) that interact with electromagnetic fields. Although the plasma contains individual particles, collisions between these allow us to treat the ensemble as a single fluid, where particles have a collective motion. In order to mathematically model the dynamics in the solar atmosphere, we make use of *magnetohydrodynamics* (MHD), which describes the large-scale (macroscopic) changes of the magnetised plasma. The set of MHD equations may be obtained by combining the Navier-Stokes fluid dynamics equations, the equations of gas dynamics and Maxwell's equations of electrodynamics. The main attraction of the MHD model is that it provides an elegant dynamical theory. The MHD equations tell us how thermodynamic and (electro)magnetic variables evolve in time. Derivations of the MHD equations are not repeated

here, though may be found in many previous works, e.g. Priest (2014)

2.1.1 Assumptions of MHD

In MHD, as with fluid dynamics, the plasma is treated as a continuous medium. As such, MHD is valid provided the length-scales of the systems being studied are much greater than the small-scale plasma lengths; most notably the *mean free path* and the *ion gyroradius* (also known as Larmor radius). The mean free path gives the average distance between collisions, which is inversely proportional to the density of the plasma, so this is much longer in the corona than in the solar interior. The assumption that relevant length-scales are larger than the mean free path means that the plasma is collisionally dominated. The ion gyroradius is the radius of the circular motion of ions or electrons in the presence of a magnetic field, which is dependent on the magnetic field strength and so varies greatly in the solar atmosphere. In terms of time scales, we will focus on processes whose characteristic times are much longer than the collision times between particles, or the gyroperiod.

MHD also assumes that the plasma is continuous in terms of charge density. Since there is separation between the negatively charged electrons and positively charged ions, MHD is only valid when the Debye sphere, which gives a measure of the scale over which charge separation can occur, contains a high density of charged particles and length scales involved are much longer than the Debye radius. Further, it is assumed that the plasma is electrically neutral, i.e. the difference between the number density of positively and negatively charged particles is much less than the total number density.

Finally, we assume that plasma velocities are much less than the speed of light and thus relativistic effects need not be taken into account.

2.1.2 MHD equations

The set of MHD equations describe the evolution and coupling of fluid variables (pressure, density, velocity) and magnetic field. These have been derived by many authors (e.g. Priest (2014)), but are merely presented here, without derivation. As a matter of fact the equations we are going to present are no more than conservation laws valid for the fluid and the magnetic field.

The basic MHD equations, describing the dynamics of conducting fluids

are:

$$\text{Continuity: } \frac{\partial \rho}{\partial t} + \nabla \cdot (\rho \mathbf{v}) = 0, \quad (2.1)$$

$$\begin{aligned} \text{Momentum: } \rho \frac{\partial \mathbf{v}}{\partial t} + \rho(\mathbf{v} \cdot \nabla) \mathbf{v} = & -\nabla p + \frac{1}{\mu}(\nabla \times \mathbf{B}) \times \mathbf{B} + \rho \mathbf{g} \\ & + \rho \nu \left[\nabla^2 \mathbf{v} + \frac{1}{3} \nabla(\nabla \cdot \mathbf{v}) \right], \end{aligned} \quad (2.2)$$

$$\text{Energy equation: } \frac{\partial p}{\partial t} + \mathbf{v} \cdot \nabla p + \gamma p \nabla \cdot \mathbf{v} = \eta(\gamma - 1)|\mathbf{j}|^2 + H_\nu, \quad (2.3)$$

$$\text{Induction: } \frac{\partial \mathbf{B}}{\partial t} = \nabla \times (\mathbf{v} \times \mathbf{B}) + \eta \nabla^2 \mathbf{B}, \quad (2.4)$$

$$\text{Solenoidal Constraint: } \nabla \cdot \mathbf{B} = 0, \quad (2.5)$$

where ρ is the density, t is time, \mathbf{v} is the plasma velocity, p is the kinetic pressure, \mathbf{B} is the magnetic field strength, μ is the permeability of free space, \mathbf{g} is the constant gravitational acceleration, \mathbf{j} is the current, γ is the ratio of specific heats, ν is the kinematic viscosity coefficient, H_ν is viscous heating, and η is the magnetic diffusivity coefficient.

The continuity equation, Eq. (2.1) states that matter is neither created nor destroyed and plasma flow compensates for changes in density.

The momentum equation, Eq. (2.2) is the equation of motion and describes the motion of the plasma under the forces of gas (or kinetic) pressure, the *Lorentz force*, gravitational forces and viscous forces, given on the right-hand side of Eq. (2.2). The Lorentz force is the force exerted by the magnetic field on the plasma and may further be split into *magnetic tension* and *magnetic pressure*.

$$\frac{1}{\mu}(\nabla \times \mathbf{B}) \times \mathbf{B} = \frac{1}{\mu}(\mathbf{B} \cdot \nabla) \mathbf{B} - \frac{1}{2\mu} \nabla(\mathbf{B}^2) \quad (2.6)$$

Magnetic tension is given by the first term on the right-hand side of Eq. (2.6) and occurs wherever the magnetic field lines are curved. Magnetic pressure is given by the second term on the right-hand side of Eq. (2.6) and occurs wherever the field strength varies with position. The last term on the right-hand side of Eq. (2.2) describes “friction” of particles within the plasma. We should note here that the electric field does not appear explicitly in the above equations as this can be eliminated in favour of velocity and magnetic field. Furthermore, the electric field within a certain volume of plasma is always negligible in the rest frame of that volume.

The energy equation, Eq. (2.3) describes the balance of various forms of energy. The ratio of specific heats, γ , is 5/3 for a monotonic ideal gas (this value is connected to the number of degrees of freedom particles have in the plasma). In the derivation of the MHD equations, it was assumed that plasma follows the ideal gas laws and since we assumed it was fully ionised, it must also be monotonic. The first term on the right-hand side describes *Ohmic heating*, where the resistivity of the plasma causes heating when current passes through

it. The second term on the right-hand side is the viscous heating term, given by

$$H_\nu = \rho\mu \left[\frac{1}{2}e_{ij}e_{ij} - \frac{2}{3}(\nabla \cdot \mathbf{v})^2 \right],$$

where $e_{ij} = \partial v_i / \partial x_j + \partial v_j / \partial x_i$ is the rate of strain tensor. As we can see, both heating terms on the right hand side of the energy equation are connected to the heat produced by non-ideal effects and both appear as non-linear terms. Since our investigation deals with linear dynamics, both non-linear terms in the energy equation will be neglected and, therefore, the energy equation will describe adiabatic changes. Linearisation will be applied to all equations in the following section.

The induction equation, Eq. (2.4) explains the evolution of the magnetic field. The first term on the right hand side is the *convection* term, which describes how magnetic field lines are transported by plasma motions. The second term on the right hand side is the *diffusion* term, which describes how the magnetic field lines spread out in the plasma. The diffusion term is multiplied by the magnetic diffusivity, which is given by

$$\eta = \frac{1}{\mu\sigma},$$

where σ is the electric conductivity. If a plasma is perfectly conductive ($\sigma \rightarrow \infty$), the diffusion term disappears and magnetic field lines become *frozen-in* to the plasma, so that magnetic field lines move with the plasma.

The solenoidal constraint, Eq. (2.5), essentially states that there are no magnetic monopoles and magnetic field lines are always closed.

2.1.3 Ideal MHD Limit

While the MHD approximation has already assumed several simplifications to the physical context, the system of equations describing the evolution of the plasma is still overly complex to be solved analytically. We thus introduce the *ideal* MHD limit, which neglects the effects of diffusivity, viscosity and other dissipative processes, in general. However, there are several considerations that need to be taken into account in order to be able to neglect dissipative processes.

The *Reynolds number* is a dimensionless parameter, which quantifies the importance of viscosity, and is defined as the ratio of inertial to viscous forces, by

$$R_e = \frac{l_0 V_0}{\nu}, \quad (2.7)$$

where V_0 denotes a typical plasma speed and l_0 stands for a typical length scale. In much of the solar atmosphere, $R_e \gg 1$ and so inertial forces dominate over viscous forces. In the limit of vanishing viscosity, the *ideal* momentum equation simplifies to

$$\rho \frac{\partial \mathbf{v}}{\partial t} + \rho(\mathbf{v} \cdot \nabla)\mathbf{v} = -\nabla p + \frac{1}{\mu}(\nabla \times \mathbf{B}) \times \mathbf{B} + \rho \mathbf{g}. \quad (2.8)$$

The *magnetic Reynolds number* gives a measure of the coupling between the magnetic field and flow of the plasma. The magnetic Reynolds number is defined as

$$R_m = \frac{l_0 V_0}{\eta}. \quad (2.9)$$

If $R_m \ll 1$, the coupling is weak and diffusion of the magnetic field is a dominant process. If $R_m \gg 1$, the coupling is strong and the magnetic field lines can be described as being “tied-in” to the plasma, i.e. plasma lying along a magnetic field line will continue to lie along a magnetic field line, however the magnetic field may be distorted. In astrophysical plasmas, R_m is, in general, large and so diffusivity may be neglected. The induction equation simplifies to its ideal form as,

$$\frac{\partial \mathbf{B}}{\partial t} = \nabla \times (\mathbf{v} \times \mathbf{B}). \quad (2.10)$$

Finally when dissipative mechanisms are neglected the energy equation describes adiabatic processes, therefore the ideal energy equation used throughout the present thesis is

$$\frac{\partial p}{\partial t} + \mathbf{v} \cdot \nabla p + \gamma p \nabla \cdot \mathbf{v} = 0. \quad (2.11)$$

The above *ideal* equations, along with the equation of mass continuity, Eq. (2.1), and the solenoidal constraint, Eq. (2.5), given in the previous section, constitute a closed system of equations relating density, pressure, velocity and magnetic field. These equations give a good description of plasma dynamics in the solar atmosphere in most applications and will be used to describe the mathematical framework with which we have modelled phenomena studied in the present thesis.

2.1.4 Linearisation

In their original form, the MHD equations are highly non-linear and mathematical descriptions of dynamics in such plasmas is rather cumbersome. One elegant way to simplify the mathematical framework is to use the method of *linearisation*. This method assumes that all variables can be written as a sum of their equilibrium value and a small perturbation, i.e.

$$\begin{aligned} \rho(\mathbf{r}, t) &\rightarrow \rho_0(\mathbf{r}) + \rho(\mathbf{r}, t) \\ p(\mathbf{r}, t) &\rightarrow p_0(\mathbf{r}) + p(\mathbf{r}, t) \\ \mathbf{B}(\mathbf{r}, t) &\rightarrow \mathbf{B}_0(\mathbf{r}) + \mathbf{b}(\mathbf{r}, t), \end{aligned}$$

where quantities with subscript 0 refer to the background (equilibrium) state and those without denote the small perturbation of physical parameters. This notation will be used in all future chapters. In addition, we assume that the plasma is stationary in equilibrium, i.e. $\mathbf{v}_0 = 0$. As the perturbations are considered small compared to the equilibrium values, terms containing products of perturbed values can be considered very small and are therefore neglected.

By keeping linear terms of the perturbations, we maintain a reasonable approximation of plasma dynamics.

As a result, the linearised and ideal MHD equations are,

$$\frac{\partial \rho}{\partial t} + \nabla \cdot (\rho_0 \mathbf{v}) = 0, \quad (2.12)$$

$$\rho_0 \frac{\partial \mathbf{v}}{\partial t} = -\nabla p + \frac{1}{\mu} (\nabla \times \mathbf{B}_0) \times \mathbf{b} + \frac{1}{\mu} (\nabla \times \mathbf{b}) \times \mathbf{B}_0 + \rho \mathbf{g}, \quad (2.13)$$

$$\frac{\partial p}{\partial t} + \mathbf{v} \cdot \nabla p_0 = -\gamma p_0 \nabla \cdot \mathbf{v}, \quad (2.14)$$

$$\nabla \cdot \mathbf{b} = 0, \quad (2.15)$$

$$\frac{\partial \mathbf{b}}{\partial t} = \nabla \times (\mathbf{v} \times \mathbf{B}_0). \quad (2.16)$$

It is worth also introducing another essential plasma parameter, which will be used in later chapters. The *plasma- β* , is the ratio of plasma pressure to magnetic pressure and is defined as

$$\beta = \frac{2\mu p_0}{B_0^2} = \frac{2c_s^2}{\gamma v_A^2},$$

where c_s is the sound speed and v_A is the Alfvén speed, which are defined in the following section. This dimensionless parameter gives an indication of whether magnetic or pressure forces dominate. Accordingly, for low- β plasmas, the magnetic forces dominate (typical for the upper chromosphere and solar corona) and for high- β plasmas, kinetic pressure forces dominate (valid for photosphere and lower chromosphere).

2.2 MHD Waves

In a non-ionised, neutral fluid, a disturbance may produce a sound wave, which has a uniform propagation speed in a homogeneous environment. This is why if someone, for example, hits a drum, we hear this only once and the sound takes the same time to travel to us, regardless of the direction from the drum we are. However in an ionised plasma, there are at least three separate waves that are able to propagate, each with a different speed, dependent on the angle of propagation compared to the magnetic field orientation. These are known as the *fast*, *slow* and *Alfvén* waves. This means that in the solar atmosphere we would “hear” the drum twice, because of the magnetacoustic fast and slow waves, while the Alfvén wave could be seen, through magnetic field perturbations. As we will see later, Alfvén waves do not perturb density. These waves are already well understood in homogeneous media, but a brief derivation of properties of these three waves is repeated here, along with the sound wave, to introduce notation and techniques used in later chapters.

The MHD equations may be combined, by substituting $\partial \rho / \partial t$, $\partial p / \partial t$, and $\partial \mathbf{b} / \partial t$, obtained from Eqs. (2.12), (2.14), (2.16) into the time derivative of the

momentum equation, Eq. (2.13). This gives the three-dimensional *generalised equation*, in terms of \mathbf{v} as the only perturbed quantity

$$\rho_0 \frac{\partial^2 \mathbf{v}}{\partial t^2} = \nabla(\gamma p_0 \nabla \cdot \mathbf{v} + \mathbf{v} \cdot \nabla p_0) + \frac{1}{\mu} (\nabla \times \mathbf{B}_0) \times [\nabla \times (\mathbf{v} \times \mathbf{B}_0)] \quad (2.17)$$

$$+ \frac{1}{\mu} (\nabla \times [\nabla \times (\mathbf{v} \times \mathbf{B}_0)]) \times \mathbf{B}_0 - \nabla \cdot (\rho_0 \mathbf{v}) \mathbf{g}. \quad (2.18)$$

We seek wave-like solutions to the MHD equations, where all perturbed variables are written in the Fourier expanded form,

$$f(\mathbf{r}, t) = \hat{f} \exp[i(\mathbf{k} \cdot \mathbf{r} - \omega t)], \quad (2.19)$$

where \hat{f} is the amplitude of physical parameters, ω is the frequency of the waves, \mathbf{k} is the wavevector and \mathbf{r} is the vector describing the spatial position. Using this form, we may replace temporal and spatial derivatives as, $\nabla \rightarrow i\mathbf{k}$ and $\partial/\partial t \rightarrow -i\omega$. As a result, the generalised wave equation takes the form

$$\rho_0 \omega^2 \hat{\mathbf{v}} = \mathbf{k}(\gamma p_0 \mathbf{k} \cdot \hat{\mathbf{v}} + \hat{\mathbf{v}} \cdot \mathbf{k} p_0) + \frac{1}{\mu} (\mathbf{k} \times \mathbf{B}_0) \times [\mathbf{k} \times (\hat{\mathbf{v}} \times \mathbf{B}_0)] \quad (2.20)$$

$$+ \frac{1}{\mu} (\mathbf{k} \times [\mathbf{k} \times (\hat{\mathbf{v}} \times \mathbf{B}_0)]) \times \mathbf{B}_0 - \mathbf{k} \cdot (\rho_0 \hat{\mathbf{v}}) \mathbf{g}. \quad (2.21)$$

In a plasma with homogeneous equilibrium, the quantities, \mathbf{B}_0 , ρ_0 and p_0 , must all be constants, thus Eq.(2.21) simplifies to

$$\rho_0 \omega^2 \hat{\mathbf{v}} = \mathbf{k}(\gamma p_0 \mathbf{k} \cdot \hat{\mathbf{v}}) + \frac{1}{\mu} (\mathbf{k} \times [\mathbf{k} \times (\hat{\mathbf{v}} \times \mathbf{B}_0)]) \times \mathbf{B}_0 - \mathbf{k} \cdot (\rho_0 \hat{\mathbf{v}}) \mathbf{g}. \quad (2.22)$$

Depending on the dominant term on the right-hand side of the above equation, we can recover the types of waves that can propagate in plasmas.

2.2.1 Sound waves

When $\mathbf{g} = \mathbf{B}_0 = 0$, the only restoring force is the gradient of the kinetic pressure and Eq. (2.18) becomes,

$$\rho_0 \frac{\partial^2 \mathbf{v}}{\partial t^2} = \gamma p_0 \nabla(\nabla \cdot \mathbf{v}). \quad (2.23)$$

Substituting the form of \mathbf{v} given by Eq. (2.19), the above relation becomes

$$\omega^2 \hat{\mathbf{v}} = \frac{\gamma p_0}{\rho_0} \mathbf{k}(\mathbf{k} \cdot \hat{\mathbf{v}}). \quad (2.24)$$

Taking the scalar product with \mathbf{k} , assuming that $\mathbf{k} \cdot \hat{\mathbf{v}} \neq 0$, the *dispersion relation* for *sound* waves is

$$\omega^2 = \frac{\gamma p_0}{\rho_0} k^2 = c_s^2 k^2,$$

where $c_s = \sqrt{\gamma p_0 / \rho_0}$ is the sound speed, which is the propagation speed of sound waves. Strictly speaking, pure sound waves cannot propagate in magnetic plasmas, however the above quantities and concepts will be important when combined with the effects of magnetic fields.

2.2.2 Alfvén Waves

We next look at the opposite extreme, when waves are driven by magnetic tension alone and no kinetic pressure force acts. We once again require that the plasma is homogeneous, but also require that the plasma is *incompressible*, i.e. $\nabla \cdot \mathbf{v} = \mathbf{k} \cdot \mathbf{v} = 0$. With these conditions, Eq. (2.18) becomes

$$\rho_0 \frac{\partial^2 \mathbf{v}}{\partial t^2} = \frac{1}{\mu} (\nabla \times [\nabla \times (\mathbf{v} \times \mathbf{B}_0)]) \times \mathbf{B}_0. \quad (2.25)$$

Assuming the same exponential form of variables, Eq. (2.25) reduces to

$$\rho_0 \omega^2 \hat{\mathbf{v}} = \frac{1}{\mu} (\mathbf{k} \times [\mathbf{k} \times (\hat{\mathbf{v}} \times \mathbf{B}_0)]) \times \mathbf{B}_0. \quad (2.26)$$

From the outer vector product on the right-hand side of the above equation, it may be seen that the velocity perturbations must be perpendicular to \mathbf{B}_0 . This is expected, since the magnetic tension, the relevant restoring force for this case, acts perpendicular to the magnetic field. This also gives that $\mathbf{B}_0 \cdot \hat{\mathbf{v}} = 0$. Equation (2.26) may, thus, be expanded and written in terms of the angle between the direction of propagation, \mathbf{k} , and the equilibrium magnetic field, \mathbf{B}_0 , denoted by θ_B . Once again employing the incompressibility criterion, this simplifies to the dispersion relation for incompressible *Alfvén waves*,

$$\rho_0 \omega^2 \hat{\mathbf{v}} = \frac{1}{\mu} B_0^2 k^2 \cos^2 \theta_B \hat{\mathbf{v}}. \quad (2.27)$$

This equation has the non-trivial solutions,

$$\omega = \pm k \cos \theta_B \sqrt{\frac{B_0^2}{\mu \rho_0}}, \quad (2.28)$$

which, in the direction of the magnetic field, propagate at the *Alfvén speed*, defined as

$$v_A = \sqrt{\frac{B_0^2}{\mu \rho_0}}.$$

Alfvén waves are transverse wave, where the velocity perturbations are normal to the direction of propagation and these waves do not perturb the density. When Alfvén waves occur in a cylindrical geometry, they present as purely azimuthal perturbations and are known as *torsional Alfvén waves*.

2.2.3 Magnetoacoustic waves

Next we come to consider the combined effects of magnetic and kinetic forces in a homogeneous plasma. When both restoring forces are taken into account, the combined momentum equation is

$$\rho_0 \frac{\partial^2 \mathbf{v}}{\partial t^2} = \nabla(\gamma p_0 \nabla \cdot \mathbf{v}) + \frac{1}{\mu} (\nabla \times [\nabla \times (\mathbf{v} \times \mathbf{B}_0)]) \times \mathbf{B}_0. \quad (2.29)$$

Using the exponential form of perturbations, the above equation becomes

$$\rho_0 \omega^2 \hat{\mathbf{v}} = \mathbf{k}(\gamma p_0 \mathbf{k} \cdot \hat{\mathbf{v}}) + \frac{1}{\mu}(\mathbf{k} \times [\mathbf{k} \times (\hat{\mathbf{v}} \times \mathbf{B}_0)]) \times \mathbf{B}_0. \quad (2.30)$$

Now that we have defined the sound and Alfvén speeds, we may introduce these into the above equation, by using a vector, with magnitude of the Alfvén speed, directed in the same direction as the magnetic field, $v_A \hat{\mathbf{B}}_0$, where $\hat{\mathbf{B}}_0$ is the unit vector directed along the equilibrium magnetic field. Using vector identities, Eq. (2.30) yields

$$[\omega^2 - v_A^2 (\mathbf{k} \cdot \hat{\mathbf{B}}_0)^2] \hat{\mathbf{v}} = \left[(c_s^2 + v_A^2) (\mathbf{k} \cdot \hat{\mathbf{v}}) - v_A^2 (\mathbf{k} \cdot \hat{\mathbf{B}}_0) (\hat{\mathbf{B}}_0 \cdot \hat{\mathbf{v}}) \right] \mathbf{k} - v_A^2 (\mathbf{k} \cdot \hat{\mathbf{B}}_0) (\mathbf{k} \cdot \hat{\mathbf{v}}) \hat{\mathbf{B}}_0 \quad (2.31)$$

This equation may be written in terms of the angle between the propagation direction and the direction of the magnetic field, θ_B , as

$$\begin{aligned} [\omega^2 - k^2 v_A^2 \cos^2 \theta_B] \hat{\mathbf{v}} &= \left[(c_s^2 + v_A^2) (\mathbf{k} \cdot \hat{\mathbf{v}}) - v_A^2 k \cos \theta_B (\hat{\mathbf{B}}_0 \cdot \hat{\mathbf{v}}) \right] \mathbf{k} \\ &\quad - k v_A^2 \cos \theta_B (\mathbf{k} \cdot \hat{\mathbf{v}}) \hat{\mathbf{B}}_0. \end{aligned} \quad (2.32)$$

Without loss of generality, we consider magnetic field lines directed in the z -direction. Hence, Eq. (2.32) may further be simplified to give

$$[\omega^2 - k^2 v_A^2 \cos^2 \theta_B] \hat{\mathbf{v}} = \left[(c_s^2 + v_A^2) (\mathbf{k} \cdot \hat{\mathbf{v}}) - v_A^2 k v_z \cos \theta_B \right] \mathbf{k} - k v_A^2 \cos \theta_B (\mathbf{k} \cdot \hat{\mathbf{v}}) \hat{\mathbf{z}}. \quad (2.33)$$

When $\mathbf{k} \cdot \hat{\mathbf{v}} = 0$, this reduces to the incompressible Alfvén wave investigated in the previous section. For the compressible case, we make take the scalar product of the above equation with \mathbf{k} and $\hat{\mathbf{B}}_0$ to achieve,

$$[\omega^2 - k^2 (c_s^2 + v_A^2)] (\mathbf{k} \cdot \mathbf{v}) = -k^3 v_A^2 \cos \theta_B (\hat{\mathbf{B}}_0 \cdot \mathbf{v}), \quad (2.34)$$

and

$$k \cos \theta_B c_s^2 (\mathbf{k} \cdot \mathbf{v}) = \omega^2 (\hat{\mathbf{B}}_0 \cdot \mathbf{v}). \quad (2.35)$$

By eliminating $\mathbf{k} \cdot \mathbf{v}$ and $\hat{\mathbf{B}}_0 \cdot \mathbf{v}$ from the above relations, we obtain the dispersion relation for compressible MHD waves:

$$\omega^4 - \omega^2 k^2 (c_s^2 + v_A^2) + c_s^2 v_A^2 k^4 \cos^2 \theta_B = 0. \quad (2.36)$$

This bi-quadratic equation has solutions

$$\omega = \pm \frac{k}{2} \left[(c_s^2 + v_A^2) \pm \sqrt{c_s^4 + v_A^4 - 2c_s^2 v_A^2 \cos 2\theta} \right]^{1/2}, \quad (2.37)$$

which constitute the dispersion relation of the forward and backward propagating *fast* (“+” solutions) and *slow* (“-” solutions) *magnetoacoustic waves*.

The relative propagation speeds of the fast, slow and Alfvén waves, and their propagation characteristics relative to the ambient magnetic field, may be seen clearly in the *polar diagram* (see Fig 2.1). The slow wave is caused by destructive interference of kinetic and magnetic forces, while the fast mode is caused by the constructive interference, as such they have speeds either side of the Alfvén mode. Both the slow and Alfvén waves propagate fastest in the direction of (or anti-parallel to) the magnetic field and have zero velocity perpendicular to it. The fast wave conversely propagates fastest perpendicular to the magnetic field.

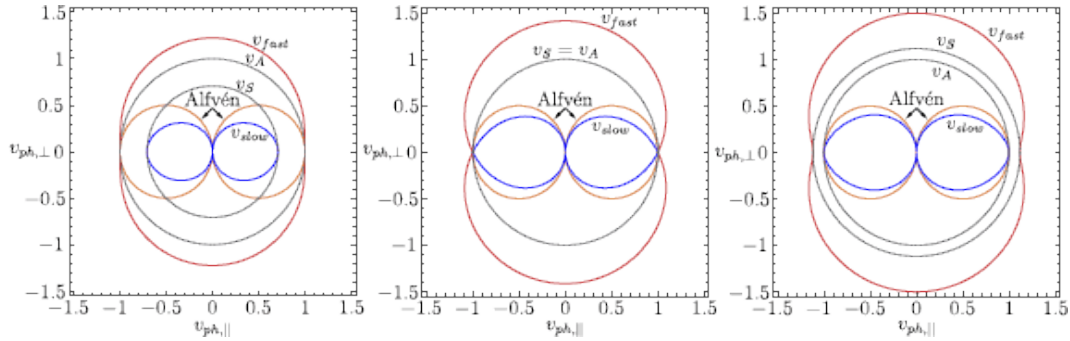


Figure 2.1: Velocities of Alfvén, fast (v_{fast}) and slow (v_{slow}) waves in a homogeneous plasma, for a magnetic field, directed in the horizontal direction. Here, the sound speed is denoted v_s . The relevant velocities are shown for the three cases: sound speed slower than Alfvén speed (left), Alfvén and sound speeds equal (middle), and sound speed greater than Alfvén speed (right). Credit: Jess et al. (2015)

2.3 Discontinuities and Jump Conditions

Waves in a homogeneous plasma are well-understood, but much of the present work is concerned with waves propagating along an interface between plasmas with different properties. Such interfaces constitute discontinuities, where physical parameters can change abruptly from one side of the interface to the other. When discontinuities in any plasma quantities are present, it is essential to know which quantities must be continuous under the given circumstances. These are most commonly known as the *jump conditions* across the interface. The jump conditions serve as boundary conditions when quantities are matched at the interface.

For a fluid, the continuity conditions across a shock are given by the Rankine-Hugoniot conditions:

$$\rho_1 u_1 = \rho_2 u_2, \quad (2.38)$$

$$\rho_1 u_1^2 + p_1 = \rho_2 u_2^2 + p_2, \quad (2.39)$$

$$2h_1 + u_1^2 = 2h_2 + u_2^2, \quad (2.40)$$

where the subscripts refer to the variables either side of the shock, $u_{1,2}$ are the velocities perpendicular to the shock and $h_{1,2}$ are the specific enthalpies. These equations give conservation of mass, momentum and energy. A discontinuity is a specific case of a shock where there is no flow across the shock. Thus, the continuity conditions for a fluid interface are achieved by the added condition that

$$u_1 = u_2.$$

When a plasma rather than a non-magnetic fluid, is considered, the jump conditions become more complex and several different situations, relating to different magnetic field alignments must be considered. An intuitive derivation of the jump conditions in a plasma is given by Goedbloed and Poedts (2004),

by considering a plasma interface as a shock, where the velocity through the shock front is zero, and key ideas are repeated here.

It is convenient for the derivation of continuity conditions to write the ideal MHD equations in conservative form as

Conservation of Mass:

$$\frac{\partial \rho}{\partial t} + \nabla \cdot (\rho \mathbf{v}) = 0, \quad (2.41)$$

Conservation of Momentum:

$$\frac{\partial}{\partial t}(\rho \mathbf{v}) + \nabla \cdot [\rho \mathbf{v} \mathbf{v} + (p^2 + \frac{1}{2} B^2) \mathbf{I} - \mathbf{B} \mathbf{B}] = \rho \mathbf{g}, \quad (2.42)$$

Conservation of Energy Density:

$$\frac{\partial}{\partial t} \left(\frac{1}{2} \rho v^2 + \rho e + \frac{1}{2} B^2 \right) + \nabla \cdot \left[\left(\frac{1}{2} \rho v^2 + \rho e + \frac{1}{2} B^2 \right) \mathbf{v} - \mathbf{v} \cdot \mathbf{B} \mathbf{B} \right] = \rho \mathbf{v} \cdot \mathbf{g}, \quad (2.43)$$

Conservation of Magnetic Flux:

$$\frac{\partial \mathbf{B}}{\partial t} + \nabla \cdot (\mathbf{v} \mathbf{B} - \mathbf{B} \mathbf{v}) = 0. \quad (2.44)$$

Here we used the same notation for physical parameters as in Eqs. (2.1) - (2.5) and these equations are *not* linearised. In addition, e denotes internal energy, which will be used instead of pressure, p , through the use of the relation, $p = (\gamma - 1)\rho e$. These equations are once again supplemented by the solenoidal constraint.

Considering a shock travelling with speed u , in the direction \mathbf{n} , normal to the shock front, the subscripts $-$ and $+$ are used to denote the values of quantities on either side of the shock, we can define a jump in a quantity f as $\llbracket f \rrbracket = f_- - f_+$ ¹. The integral across the interface introduces the substitutions

$$\frac{\partial f}{\partial t} \rightarrow -u \llbracket f \rrbracket, \quad \nabla f \rightarrow \mathbf{n} \llbracket f \rrbracket.$$

Hence, integrating the system of MHD equations, given by Eqs. (2.41) - (2.44) across the shock results in the jump conditions:

$$-u \llbracket \rho \rrbracket + \mathbf{n} \cdot \llbracket \rho \mathbf{v} \rrbracket = 0, \quad (2.45)$$

$$-u \llbracket \rho \mathbf{v} \rrbracket + \mathbf{n} \cdot \left[\llbracket \rho \mathbf{v} \mathbf{v} + (p^2 + \frac{1}{2} B^2) \mathbf{I} - \mathbf{B} \mathbf{B} \rrbracket \right] = 0, \quad (2.46)$$

$$-u \left[\llbracket \frac{1}{2} \rho v^2 + \rho e + \frac{1}{2} B^2 \rrbracket \right] + \mathbf{n} \cdot \left[\llbracket (\frac{1}{2} \rho v^2 + \rho e + \frac{1}{2} B^2) \mathbf{v} - \mathbf{v} \cdot \mathbf{B} \mathbf{B} \rrbracket \right] = 0, \quad (2.47)$$

$$-u \llbracket \mathbf{B} \rrbracket + \mathbf{n} \cdot \llbracket \mathbf{v} \mathbf{B} - \mathbf{B} \mathbf{v} \rrbracket = 0, \quad \mathbf{n} \cdot \llbracket \mathbf{B} \rrbracket = 0. \quad (2.48)$$

For convenience, these relations are transformed into the frame in which the shock is stationary and velocities are rewritten using $\mathbf{v}' = \mathbf{v} - u\mathbf{n}$, to give

¹If we were to consider flow in the opposite direction, i.e. $u \rightarrow -u$, this would also necessitate considering the difference of the variables across the interface in the opposite orientation, so $\llbracket f \rrbracket \rightarrow -\llbracket f \rrbracket$ and thus the jump conditions would be unchanged.

the continuity conditions:

$$\text{Mass continuity: } \llbracket \rho v'_n \rrbracket = 0, \quad (2.49)$$

$$\text{Continuity of Normal Momentum: } \llbracket \rho v_n'^2 + p + \frac{1}{2} B_t^2 \rrbracket = 0, \quad (2.50)$$

$$\text{Continuity of Tangential Momentum: } \rho v'_n \llbracket \mathbf{v}'_t \rrbracket = B_n \llbracket \mathbf{B}_t \rrbracket, \quad (2.51)$$

$$\text{Energy Continuity: } \rho v'_n \llbracket \frac{1}{2} (v_n'^2 + v_t'^2) + \frac{1}{\rho} \left(\frac{\gamma}{\gamma - 1} p + B_t^2 \right) \rrbracket = B_n \llbracket \mathbf{v}'_t \cdot \mathbf{B}_t \rrbracket, \quad (2.52)$$

$$\text{Continuity of Normal Flux: } \llbracket B_n \rrbracket = 0, \quad (2.53)$$

$$\text{Continuity of Tangential Flux: } \rho v'_n \llbracket \frac{\mathbf{B}_t}{\rho} \rrbracket = B_n \llbracket \mathbf{v}'_t \rrbracket, \quad (2.54)$$

where subscript n refers to quantities normal to the shock front and subscript t refers to quantities tangential to the shock front.

An interface between two plasma regions with different properties is equivalent to a shock front, where there is no flow across the discontinuity, i.e. $v'_n = 0$. Substituting this into the above equations, the jump conditions across an interface simplify to:

$$\text{Continuity of Total Pressure: } \llbracket p + \frac{1}{2} B_t^2 \rrbracket = 0, \quad (2.55)$$

$$\text{Continuity of Tangential Momentum: } B_n \llbracket \mathbf{B}_t \rrbracket = 0, \quad (2.56)$$

$$\text{Energy Continuity: } B_n \llbracket \mathbf{v}'_t \cdot \mathbf{B}_t \rrbracket = 0, \quad (2.57)$$

$$\text{Continuity of Normal Flux: } \llbracket B_n \rrbracket = 0, \quad (2.58)$$

$$\text{Continuity of Tangential Flux: } B_n \llbracket \mathbf{v}'_t \rrbracket = 0. \quad (2.59)$$

There are two distinct kinds of discontinuities, with distinct jump conditions: *tangential discontinuities*, where the magnetic field is parallel to the interface and *contact discontinuities*, where the magnetic field intersects the interface.

For a tangential discontinuity, where $B_n = 0$, all above conditions are inherently satisfied except Eq. (2.55). The necessary boundary conditions are thus the continuity of *total pressure*,

$$\llbracket P_T \rrbracket = \llbracket p + \frac{1}{2} B_t^2 \rrbracket = 0,$$

and the continuity of normal velocity, $v'_n = 0$, which was the condition for considering an interface, rather than a genuine shock.

For a contact discontinuity, $B_n \neq 0$, so Eq. (2.56) gives the condition that $\llbracket \mathbf{B}_t \rrbracket = 0$. This, in turn, along with Eq. (2.55), results in the condition that $\llbracket p \rrbracket = 0$ and, with Eq. (2.59), it results in the condition that $\llbracket \mathbf{v}'_t \rrbracket = 0$.

In summary, the boundary conditions for a contact discontinuity are much more restrictive than those for a tangential discontinuity. Now, the kinetic

pressure, normal and tangential components of velocity, and normal and tangential components of the magnetic field are all continuous and the only quantity that is allowed to have a jump is the density.

Linearising these jump conditions, we obtain that the continuity conditions at discontinuities are:

1. **Tangential Discontinuity:** ($B_n = 0$)

$$[[v_n]] = 0, \quad [[p + \mathbf{b} \cdot \mathbf{B}_0]] = 0, \quad (2.60)$$

2. **Contact Discontinuity:** ($B_n \neq 0$)

$$[[v_n]] = 0, \quad [[\mathbf{v}_t]] = 0, \quad [[b_n]] = 0, \quad \left[\left[\sqrt{\mathbf{B}_{0t} \cdot \mathbf{b}_{0t}} \right] \right] = 0, \quad [[p]] = 0. \quad (2.61)$$

The literature of waves at tangential discontinuities is vast (e.g. Roberts 1981*a*, Jain and Roberts 1991, Joarder and Nakariakov 2006, Mather and Erdélyi 2016, Zsámberger et al. 2018 etc.), while little has been done in the case of contact discontinuities. Thus the novelty of our work lies with our focus on contact discontinuities.

There is also a third kind of MHD discontinuity, the *rotational discontinuity*. These occur where density, pressure and the normal components of magnetic field strength and velocity are unchanged across the interface, however the tangential components of magnetic field and velocity rotate across the interface. Thus the magnitude of magnetic field strength and velocity remains continuous, while the orientation changes. Rotational discontinuities have been proposed to occur in the fast solar wind (see e.g. Levy et al. 1964) and were first observed by Paschmann et al. (1979).

2.3.1 Jump conditions in the presence of gravity

For almost all of the linearised conditions, the jump across the unperturbed interface at equilibrium is the same as across the perturbed interface. Since the position of the unperturbed interface is defined at the outset of any problems investigated, the jump $[[f]]$ is most useful when defined as the difference either side of where the interface is positioned at equilibrium. However, when gravity is taken into account, the condition for pressure continuity must be amended. This is relatively straightforward, but will be re-derived using the method described by Ruderman et al. (2014).

For a homogeneous background magnetic field, the background pressure balance becomes

$$\frac{\partial p_0}{\partial z} = -g\rho_0.$$

When a horizontal interface located at $z = z_0$ is perturbed, its variation can be described by the equation $z = z_0 + h(x, t)$, where h is the small perturbation of the interface, in the z -direction. A Taylor expansion of linearised pressure

at the interface gives

$$\begin{aligned} p(z_0 + h) &\approx p(z_0) + h \frac{\partial p_0}{\partial z} \Big|_{z=z_0} + O(h^2) \\ &\approx p(z_0) - gh\rho_0(z_0) + O(h^2). \end{aligned} \quad (2.62)$$

This condition allows us to write that for the case when gravity is present, the continuity of pressure across the interface, becomes, in terms of the jump across the unperturbed interface,

$$\llbracket p - g\rho_0 h \rrbracket = 0, \quad \text{across } z = z_0. \quad (2.63)$$

Noting that $\partial h / \partial t = v_z$, we may take the time derivative of this condition (this is possible as we consider the time independent solutions). Taking the time derivative of Eq. (2.63) gives

$$\left[\left[\frac{\partial p}{\partial t} - g\rho_0 v_z \right] \right] = 0, \quad \text{across } z = z_0, \quad (2.64)$$

and so continuity of total pressure across the interface is satisfied when

$$\left[\left[\frac{\partial p}{\partial t} - g\rho_0 v_z + \mathbf{B}_0 \cdot \frac{\partial \mathbf{b}}{\partial t} \right] \right] = 0, \quad \text{across } z = z_0. \quad (2.65)$$

These jump conditions will be used throughout the thesis, to determine the dispersion relation of waves and the generation of instabilities.

2.4 MHD Waves Propagating Along an Interface

In a series of papers published more than 30 years ago, Roberts laid the foundation of MHD waves propagating in a magnetically structured atmosphere (Roberts 1981*a*, Roberts 1981*b*, Edwin and Roberts 1982). While considering several different geometries, these all begin with the linear, ideal MHD equations and use analytical techniques to find a dispersion relation and associated solutions, for thin and thick structures. The first paper, ‘‘Surface Waves at a Magnetic Interface’’ (Roberts, 1981*a*) has a particular pertinence to the research presented in the current work, since the background plasma configuration is the same; a single interface separating two regions of different properties. Due to these similarities, the key techniques and results from the paper will now be explored and used later as reference.

In the equilibrium state, the plasma is arranged into two homogeneous plasma regions, separated by a sharp interface at $z = 0$. The equilibrium homogeneous magnetic field is parallel to the interface, i.e. $\mathbf{B}_0 = B_0 \hat{\mathbf{x}}$. As a result, the equilibrium density and magnetic field take the simple form,

$$\rho_0(z) = \begin{cases} \rho_-, & z < 0, \\ \rho_+, & z > 0, \end{cases}$$

$$B_0(z) = \begin{cases} B_-, & z < 0, \\ B_+, & z > 0, \end{cases}$$

where the indices, \pm , refer to the regions corresponding to $z > 0$ and $z < 0$, respectively.

Assuming that all perturbations are of the form $f = \hat{f}(z) \exp[i(k_x x + k_y y - \omega t)]$, the MHD equations may be reduced to a single equation

$$\frac{d}{dz} \left[\frac{\rho_0(z) (k_x^2 v_A^2(z) - \omega^2)}{m_0^2(z) + k_y^2} \frac{d\hat{v}_z}{dz} \right] - \rho_0(z) (k_x^2 v_A^2(z) - \omega^2) \hat{v}_z = 0, \quad (2.66)$$

where m_0 is the magnetoacoustic parameter defined as

$$m_0^2(z) = \frac{(k_x^2 c_s^2(z) - \omega^2) (k_x^2 v_A^2(z) - \omega^2)}{(c_s^2(z) + v_A^2(z)) (k_x^2 c_T^2(z) - \omega^2)}. \quad (2.67)$$

This parameter acts as an effective wavenumber in the z -direction, giving a measure of how quickly the wave amplitude decays away from the interface. In the above expression, v_A is the Alfvén speed, c_s is the sound speed, and, c_T is the cusp (or tube) speed, defined as

$$c_T^2(z) = \frac{c_s^2(z) v_A^2(z)}{c_s^2(z) + v_A^2(z)}.$$

Either side of the interface, where the plasma is homogeneous, this equation simplifies to

$$(k^2 v_A^2 - \omega^2) \left(\frac{d^2 \hat{v}_z}{dz^2} - (m_0^2 + k_y^2) \hat{v}_z \right) = 0. \quad (2.68)$$

For simplicity let us assume that the motion is independent of the y -direction, so we choose $k_y = 0$ and $k_x = k$. Hence, *evanescent* surface wave solutions, which decay away from the interface, are given by

$$\hat{v}_z(z) = \begin{cases} \alpha_- \exp[m_- z], & z < 0, \\ \alpha_+ \exp[-m_+ z], & z > 0, \end{cases} \quad (2.69)$$

where the expressions of m_- and m_+ are given by similar relations as Eq. (2.67). Solutions will be surface waves, evanescent away from the interface, if m_- and m_+ are both real quantities. Therefore, physical solutions will not exist if

$$\max(c_s^2, v_A^2) < \frac{\omega^2}{k^2}, \quad \text{or} \quad c_T^2 < \frac{\omega^2}{k^2} < \min(c_s^2, v_A^2), \quad (2.70)$$

for the plasma parameters both sides of the interface.

Since the equilibrium magnetic field is parallel to the interface, we are dealing with a tangential discontinuity, where we require that the normal component of velocity, v_z and total pressure, P_T are continuous across the interface, $z = 0$. Continuity of \hat{v}_z , using the solution (2.69) implies that $\alpha_- = \alpha_+$. Using the MHD equations, the total pressure perturbation may be written in terms of \hat{v}_z as,

$$\hat{P}_T = \frac{i\rho_0}{\omega} (c_s^2 + v_A^2) \frac{k^2 c_T^2 - \omega^2}{k^2 c_s^2 - \omega^2} \frac{d\hat{v}_z}{dz}. \quad (2.71)$$

Substituting the solution (2.69) into the continuity of \hat{P}_T , we obtain the *dispersion relation* for surface waves at a single magnetic interface

$$\rho_- (k^2 v_{A-}^2 - \omega^2) m_+ + \rho_+ (k^2 v_{A+}^2 - \omega^2) m_- = 0. \quad (2.72)$$

In order to compare the solutions of the above dispersion relation, obtained for the tangential discontinuity, to solutions for contact discontinuities in later chapters, we consider the case with a constant and identical background magnetic field either side of the interface, so we take $B_0 = B_- = B_+$. In this case, it follows that $\rho_- v_{A-}^2 = \rho_+ v_{A+}^2$. Let us introduce the density ratio

$$d = \frac{\rho_-}{\rho_+} = \frac{v_{A+}^2}{v_{A-}^2},$$

which allows us to write the dispersion relation in terms of fewer variables. We also introduce the plasma- β parameter and the dimensionless phase-speed, to allow us to write the dispersion relation in dimensionless form, with \tilde{c}_{ph} depending only on d and β ,

$$\beta = \frac{c_-^2}{v_{A-}^2} = \frac{c_+^2}{v_{A+}^2}, \quad \tilde{c}_{ph} = \frac{\omega}{k v_{A+}}.$$

The dimensionless dispersion relation is now written as

$$d(d - \tilde{c}_{ph}^2) \tilde{m}_+ + (1 - \tilde{c}_{ph}^2) \tilde{m}_- = 0, \quad (2.73)$$

where the dimensionless magnetoacoustic parameters become

$$\tilde{m}_-^2 = \frac{m_-^2}{k^2} = \frac{(d\beta - \tilde{c}_{ph}^2)(d - \tilde{c}_{ph}^2)}{d(\beta + 1)(\tilde{c}_{T-}^2 - \tilde{c}_{ph}^2)}, \quad \tilde{m}_+^2 = \frac{m_+^2}{k^2} = \frac{(\beta - \tilde{c}_{ph}^2)(1 - \tilde{c}_{ph}^2)}{(\beta + 1)(\tilde{c}_{T+}^2 - \tilde{c}_{ph}^2)}, \quad (2.74)$$

and the tube speeds in units of Alfvén speed in the upper plasma region are

$$\tilde{c}_{T-}^2 = \frac{c_{T-}^2}{v_{A+}^2} = \frac{d\beta}{\beta + 1}, \quad \tilde{c}_{T+}^2 = \frac{c_{T+}^2}{v_{A+}^2} = \frac{\beta}{\beta + 1}.$$

Further we see that no solutions exist in the regions where any of the following criteria (derived from Eq. 2.70) are satisfied,

$$\begin{aligned} \tilde{c}_{T-} < \tilde{c}_{ph} < \min(d, d\beta), & \quad \tilde{c}_{ph} > \max(d, d\beta), \\ \tilde{c}_{T+} < \tilde{c}_{ph} < \min(1, \beta), & \quad \tilde{c}_{ph} > \max(1, \beta). \end{aligned} \quad (2.75)$$

In what follows, the dispersion relation (2.73) will be solved numerically for a wide range of parameters.

2.4.1 Numerical Solutions of The Dispersion Relation

The dimensionless phase speed may now be studied in terms of the two variables d and β , by solving Eq. (2.73). Although Eq. (2.73) may seem simple at first glance, since \tilde{m}_\pm are themselves square roots of functions of \tilde{c}_{ph} , it is

not currently written as a rational function. Of course, we could square both sides of the equation and solve the resulting polynomial, however, this would introduce spurious roots and it may not be clear which correspond to physical solutions. Since the algebraic expressions for the solutions to the polynomial are not straightforward, this method shows no immediate advantage. We thus choose to solve the dispersion relation numerically from the outset. For all cases, the solutions are shown to have speeds between the two Alfvén speeds, but, more importantly, the obtained phase speeds are always greater than the lower cusp speed, which suggests all propagating surface modes in this 2D model are fast modes.

The solutions of the dimensionless dispersion relation are plotted for two values of plasma- β ($\beta = 0.1$ and $\beta = 10$), for varying density ratio in Figs. (2.2a) and (2.2b). Only positive solutions, corresponding to forward propagating waves, are shown, since solutions are symmetric. Regions where solutions would not be evanescent are shaded with grey, to show that no physical surface wave solutions exist in these regions.

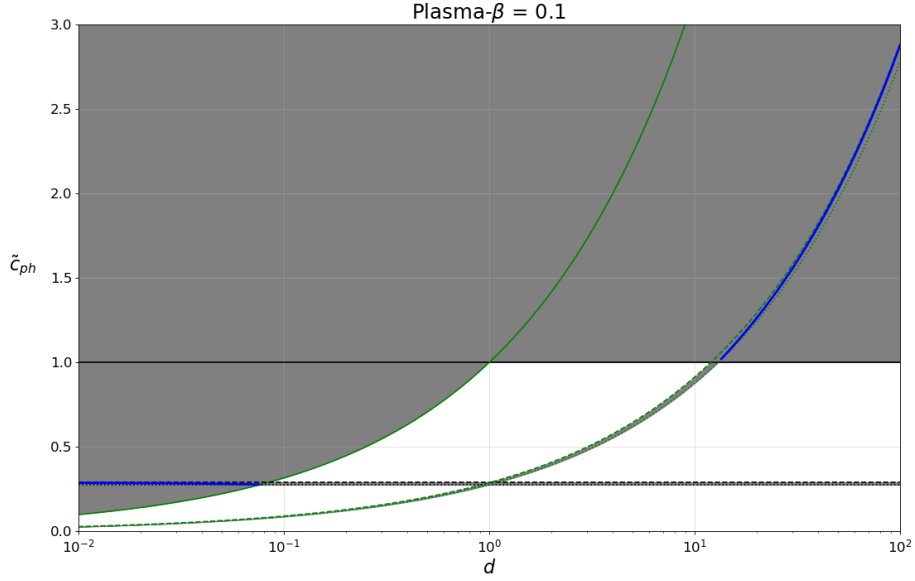
Solutions for low plasma- β , where kinetic forces dominate, are shown in Fig. (2.2a). The solution for low values of d is between the cusp and sound speed of the lower plasma region while for high values of d solutions are obtained between the cusp and sound speed of the upper plasma region. However, it is clear that these solutions fall entirely within the regions where solutions are not evanescent, so there are no physical solutions for $\beta = 0.1$. This confirms the statement in Roberts (1981a) that there are no surface-waves in the low-beta regime, when only considering propagations parallel to the magnetic field.

Solutions for high plasma- β (dynamics dominated by magnetic forces) are shown in Fig. (2.2b). The solution for $d < 1$ is between the Alfvén and sound speed of the upper plasma region, appearing to tend towards v_{A+} as $d \rightarrow 0$. For $d > 1$ the solution is between the Alfvén and sound speed of the lower plasma region. As $d \rightarrow \infty$, the curve of solutions appears to saturate to a value between these two speeds.

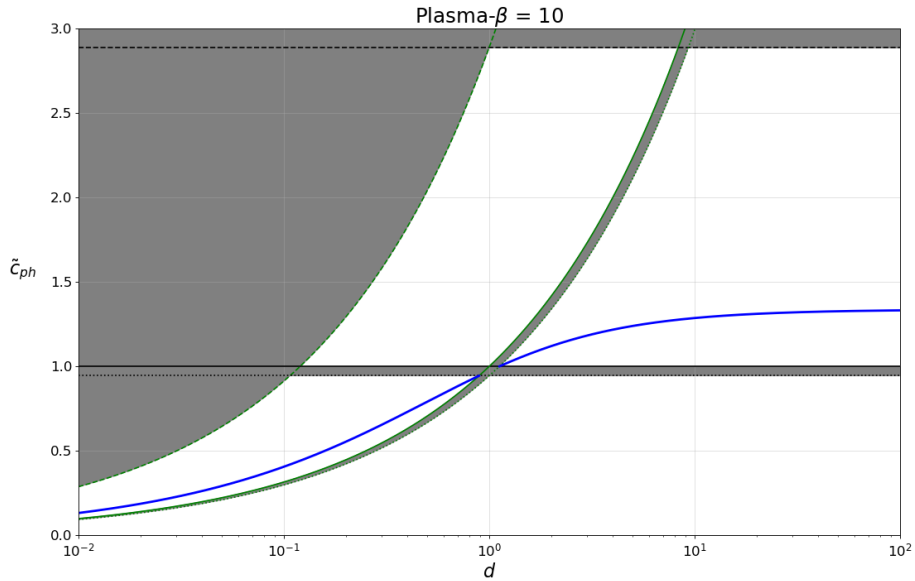
In Figs. (2.3a) and (2.3b), we plot solutions for several values of density ratio and with plasma- β varying over a range of four orders of magnitude. Solutions for $\tilde{c}_{ph} = \omega/kv_{A+}$, where the density ratio is $d = d_0$, are identical to solutions for $\bar{c}_{ph} = \omega/kv_{A-}$ where the density ratio is $d = 1/d_0$. As such, we will only show solutions for $d < 1$, corresponding to a denser plasma above.

Figure (2.3a) shows two separate families of solutions. For lower β values the phase-speed is between c_T and c_s , tending to c_s , with increasing β . For low plasma- β values, solutions are not evanescent, this confirms the results shown in Figure (2.2a). However, for higher plasma- β values, solutions are evanescent and the phase speed of waves is between v_{A+} and c_+ , beginning where these speeds intersect and tending towards some fixed value as $\beta \rightarrow \infty$. This value may be found by using an asymptotic expansion, with respect to β of the dispersion relation, which to highest order is

$$d(d - \tilde{c}_{ph}^2) - \tilde{c}_{ph}^2 + 1 + O(\beta^{-1}) = 0.$$

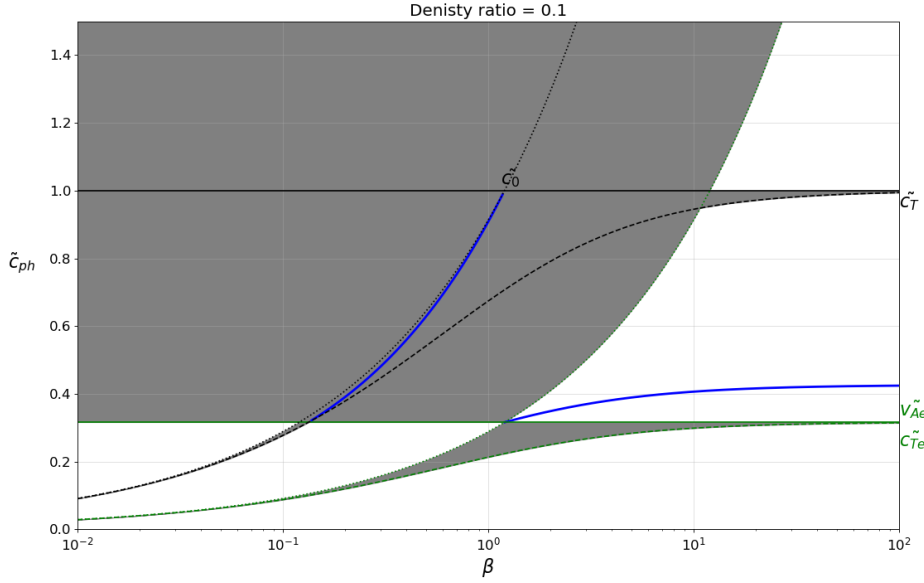


(a) $\beta = 0.1$

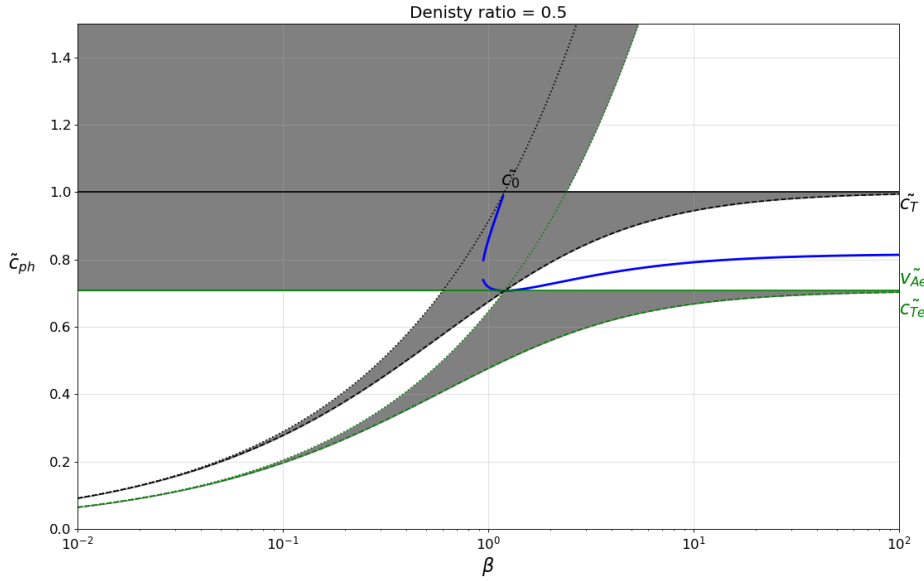


(b) $\beta = 10$

Figure 2.2: Solutions of the dispersion relation of waves propagating along an interface in the tangential discontinuity case, for $\beta = 0.1$ (above) and $\beta = 10$ (below), for varying density ratio. Solutions are shown with solid blue lines. Critical speeds above the interface are shown in green and below the interface are shown in black. The Alfvén speeds are shown with solid lines, the sound speeds are shown with dotted lines and the cusp speeds are shown with a dashed line.



(a) $d = 0.1$



(b) $d = 0.5$

Figure 2.3: Solutions of the dispersion relation of waves propagating along an interface in the tangential discontinuity case, for $d = 0.1$ (above) and $d = 0.5$ (below), for varying plasma- β . Solutions are shown with solid blue lines. Critical speeds above the interface are shown in green and below the interface are shown in black. The Alfvén speeds are shown with solid lines, the sound speeds are shown with dotted lines and the cusp speeds are shown with a dashed line.

The solutions to this equation are

$$\tilde{c}_{ph}^2 = \frac{d^2 + 1}{d + 1},$$

which matches well with what may be seen in Figs (2.3a) - (2.3b). For $d = 0.5$ (Figure 2.3b), the two separate curves of solutions almost connect. This suggests the possibility of *mode conversion*, if modes with negative m_- or m_+ were allowed. However, this cannot be a possibility for surface waves.

2.4.2 Symmetry

For the present configuration, we would expect to obtain the same solutions, regardless of the arrangement of the two plasma layers. For our original system we supposed the density ratio was $d = D$ and the dimensionless phase-speed was $\tilde{c}_{ph} = W$. If the orientation of the system were “flipped”, with ρ_- now the density of the upper plasma and ρ_+ denoting the density of the lower plasma, we would consider the density ratio to be $d = \rho_+/\rho_- = v_{A-}^2/v_{A+}^2 = 1/D$. The dimensionless phase-speed was defined in terms of the lower plasma, so for the “flipped” case, the dimensionless phase-speed becomes

$$\tilde{c}_{ph} = \frac{\omega}{kv_{A+}} = \frac{\omega}{kv_{A+}} \frac{v_{A-}}{v_{A+}} = \frac{W}{\sqrt{D}}.$$

We introduce these new expressions for density ratio and dimensionless phase-speed into the expressions for the effective wavenumber in dimensionless form, (Eq. 2.74). From this we find that

$$\tilde{m}_-^2 \left(d = \frac{1}{D} \right) = \tilde{m}_+^2 (d = D), \quad \tilde{m}_+^2 \left(d = \frac{1}{D} \right) = \tilde{m}_-^2 (d = D).$$

Next, we input these expressions into the dispersion relation, Eq. (2.73), and obtain

$$\frac{1}{D^2}(1 - W^2)\tilde{m}_-(d = D) + (1 - W^2/D)\tilde{m}_+(d = D) = 0.$$

Multiplying this equation through by D^2 we see that the dispersion relation is identical to that found for our original configuration. Thus, as expected, the nature of the waves is unchanged by the orientation of the equilibrium configuration.

However, Fig. (2.2) appears not to be symmetric in terms of comparing d with $1/d$. This is simply due to the fact that solutions are given in terms of the dimensionless phase-speed, which, as explained above, must be modified when considering a different orientation.

2.5 Summary and Conclusions

The present chapter was devoted to the introduction of the mathematical and physical framework of the thesis. In particular we presented the MHD

equations and described their limitations. In order to make these equations mathematically tractable, we used the linear and ideal limit, i.e. we focus on small amplitude waves, where no energy sinks or sources are considered. We also presented the fundamental properties of MHD waves, as these will be used in later chapters. We have described, in detail, the jump conditions we must impose when connecting solutions at discontinuities. From this we have seen that the orientation of the magnetic field, with respect to the interface, will determine the nature of the discontinuity.

As a reference case for our investigation, we reviewed the study by Roberts (1981*a*), analysing the properties of surface waves propagating along a density interface in the presence of a background magnetic field parallel to the interface.

It has been shown that a density interface, with such a tangential discontinuity, may support stable surface waves for high plasma- β values. These solutions have real frequency, suggesting that the amplitude of the surface waves is constant over time. For any given density ratio and plasma- β , there is only ever one physical solution.

The phase speeds of all solutions lie between the Alfvén speeds for the upper and lower plasma regions, hence all solutions have phase speed above the lower cusp speed, c_T and so cannot be identified as slow modes. Thus, we conclude that only fast surface waves propagate in this environment. Due to the phase-speed between the two Alfvén speeds, these modes bear some similarity to the so-called surface Alfvén modes (see Section 1.1.5), though lack the torsional component.

These results have many applications in the solar atmosphere, including modelling short length-scale waves at the edges of flux tubes, prominences and inter-granular lanes. We will later compare these results to those for the contact discontinuity.

CHAPTER 3

Propagation of Leaky MHD Waves at Discontinuities with Tilted Magnetic Field

Although there have been many studies focused on waves at a tangential discontinuities (see Section 1.1.5), there have been few theoretical studies looking into situations where the magnetic field is inclined to the direction of wave propagation and fewer still considering waves at contact discontinuities. However there are several examples of structures in the solar atmosphere with inclined magnetic fields, where contact discontinuities would be an appropriate model. These include sunspot penumbrae, where running penumbral waves propagate at an angle to the magnetic field lines. In regions above sunspot penumbrae, there are also oblique fields, with vertically propagating waves (see e.g. Schunker and Cally 2006). On large length scales the transition region may even be modelled as a contact discontinuity, with magnetic field lines intersecting a sharp density gradient. Waves along the transition region have been studied by (e.g. Scullion et al. 2011). These provide a few concrete examples in the solar atmosphere where the following study of waves propagating along contact discontinuities would provide important information on solar dynamics.

We will, in particular, investigate *leaky waves*, where energy propagates away from the interface and leads to wave attenuation. These have been studied in a theoretical sense, in flux tubes, by Cally (1986) and Ruderman and Roberts (2006) and have been observed in coronal loops, using TRACE, by Cally (2003).

Inspired by the seminal work by Roberts (1981*a*), on MHD waves at a tangential discontinuity (summarised in the previous chapter), the present chapter uses an eigenmode analysis to investigate the effect of magnetic field inclination across the interface. Following on from the time-independent study covered in this chapter, Chapter 4 will use a time dependent analysis to study these waves in further detail, to model how the waves evolve from an initial perturbation.

This chapter is based on the following refereed journal article:

- Vickers, E., Ballai, I., Erdélyi, R. (2018); Propagation of Leaky MHD Waves at Discontinuities with Tilted Magnetic Field, *Solar Phys.*, Volume 293, Issue 10

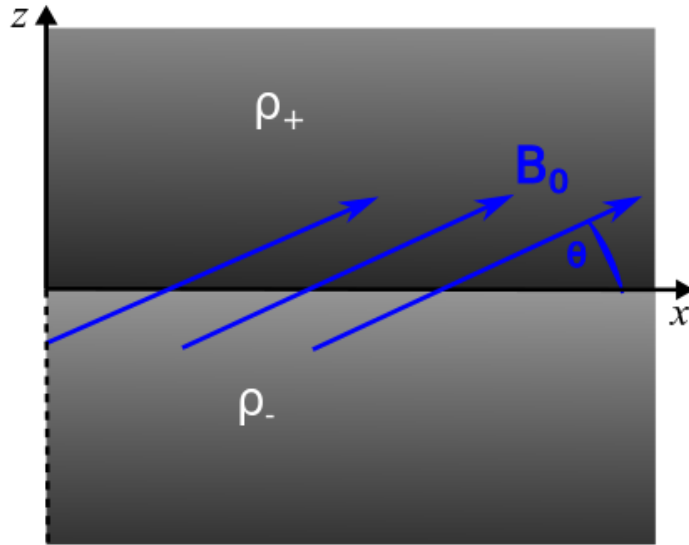


Figure 3.1: The plasma is structured into two semi-infinite regions of constant density and gas pressure, with a sharp interface at $z = 0$. A constant magnetic field crosses the interface and it is inclined at an angle θ to the interface.

The background equilibrium will, once again, be a discontinuity in density and temperature, aligned with $z = 0$, with homogeneous plasma either side of this discontinuity. The novelty of our research resides in considering a constant magnetic field that permeates the plasma, at an angle, θ to the discontinuity in the (x, z) plane and has the form $\mathbf{B}_0 = B_0(\cos \theta, 0, \sin \theta)$. Without loss of generality we may assume $0 < \theta \leq \pi$. In our working model, with a tilted magnetic field, the restoring force will be the tangential component of the Lorentz force, with magnetic tension acting on any displacement transversal to the field and magnetic pressure acting on any displacement that changes the magnetic field strength. The effect of gravity is neglected, and we restrict ourselves to the study of the two-dimensional dynamics, with no y -component of perturbations. A schematic representation of the equilibrium configuration is shown in Figure (3.1).

The system considered now has a component of the magnetic field intersecting the interface and, as such, the interface is a *contact* discontinuity. The continuity conditions are thus (see section (2.3)),

$$[[v_{\perp}]] = 0, \quad [[v_{\parallel}]] = 0, \quad [[b_{\perp}]] = 0, \quad [[b_{\parallel}]] = 0, \quad [[p]] = 0.$$

The dynamics of MHD waves in this system will be described within the framework of linearised, ideal magnetohydrodynamics (MHD), using the equations (2.12)-(2.16), given in the previous chapter.

3.1 Governing Equation

In general, the propagation of waves can be studied with the help of their dispersion relation, i.e. the relation between the frequency of waves and the

wavenumber, in terms of characteristic speeds and quantities specific to the medium in which they propagate. First, general solutions are found for the plasma regions either side of the interface, and the dispersion relation may then be obtained by matching the solutions in the two regions, at the interface at $z = 0$, using the jump conditions given above.

The mathematical procedure we employ in the present study would classify our task as an eigenvalue problem. However, when comparing to an initial value problem investigation, there are differences between a standard eigenvalue problem and the problem concerning leaky waves. As pointed out by Ruderman and Roberts (2006), while standard eigenvalue solutions correspond to the asymptotic behaviour of the time-dependent solutions, the leaky mode solutions are instead intermediate asymptotics, where the time-scale is greater than the period of the wave, but less than the attenuation time. This will be revisited in Chapter 4.

The system of ideal, linearised MHD equations for this environment may be written in terms of their components as

$$\frac{\partial \rho}{\partial t} + \rho_0 \left(\frac{\partial v_x}{\partial x} + \frac{\partial v_z}{\partial z} \right) = 0, \quad (3.1)$$

$$\rho_0 \frac{\partial v_x}{\partial t} = -\frac{\partial p}{\partial x} + \frac{1}{\mu} B_0 \sin \theta \left(\frac{\partial b_x}{\partial z} - \frac{\partial b_z}{\partial x} \right), \quad (3.2)$$

$$\rho_0 \frac{\partial v_z}{\partial t} = -\frac{\partial p}{\partial z} + \frac{1}{\mu} B_0 \cos \theta \left(\frac{\partial b_z}{\partial x} - \frac{\partial b_x}{\partial z} \right), \quad (3.3)$$

$$\frac{\partial p}{\partial t} = c_s^2 \frac{\partial \rho}{\partial t}, \quad (3.4)$$

$$\frac{\partial b_x}{\partial x} + \frac{\partial b_z}{\partial z} = 0, \quad (3.5)$$

$$\frac{\partial b_x}{\partial t} = B_0 \left(\sin \theta \frac{\partial v_x}{\partial z} - \cos \theta \frac{\partial v_z}{\partial x} \right), \quad (3.6)$$

$$\frac{\partial b_z}{\partial t} = B_0 \left(\cos \theta \frac{\partial v_z}{\partial x} - \sin \theta \frac{\partial v_x}{\partial z} \right). \quad (3.7)$$

By differentiating the x - and z -components of the momentum equation, (3.2) and (3.3), with respect to time and using the energy, continuity and induction equations (3.1), (3.4), (3.6), (3.7), we obtain two simultaneous, differential equations for the horizontal and vertical velocity perturbations,

$$\begin{aligned} \frac{\partial^2 v_x}{\partial t^2} &= (v_A^2 \sin^2 \theta + c_s^2) \frac{\partial^2 v_x}{\partial x^2} + v_A^2 \sin^2 \theta \frac{\partial^2 v_x}{\partial z^2} \\ &\quad - v_A^2 \sin \theta \cos \theta \frac{\partial^2 v_z}{\partial x^2} + c_s^2 \frac{\partial^2 v_z}{\partial x \partial z} - v_A^2 \sin \theta \cos \theta \frac{\partial^2 v_z}{\partial z^2}, \end{aligned} \quad (3.8)$$

$$\begin{aligned} \frac{\partial^2 v_z}{\partial t^2} &= -v_A^2 \sin \theta \cos \theta \frac{\partial^2 v_x}{\partial x^2} + c_s^2 \frac{\partial^2 v_x}{\partial x \partial z} - v_A^2 \sin \theta \cos \theta \frac{\partial^2 v_x}{\partial z^2} \\ &\quad + v_A^2 \cos^2 \theta \frac{\partial^2 v_z}{\partial x^2} + (v_A^2 \cos^2 \theta + c_s^2) \frac{\partial^2 v_z}{\partial z^2}, \end{aligned} \quad (3.9)$$

where the Alfvén speed was defined in Chapter 2.

We assume that all of the perturbed quantities will reach a steady state and oscillate with frequency, ω , and real wave-number, k . Therefore, we take any perturbations to be of the form $f = \hat{f}(z) \exp[i(kx - \omega t)]$, where \hat{f} is the amplitude of perturbations that depends on z . Applying this ansatz to the above system of equations, we arrive at the system of coupled differential equations for a homogeneous medium,

$$\begin{aligned} & [\omega^2 - k^2(v_A^2 \sin^2 \theta + c_s^2)]\hat{v}_x + v_A^2 \sin^2 \theta \frac{d^2 \hat{v}_x}{dz^2} \\ & + k^2 v_A^2 \sin \theta \cos \theta \hat{v}_z + ikc_s^2 \frac{d\hat{v}_z}{dz} - v_A^2 \sin \theta \cos \theta \frac{d^2 \hat{v}_z}{dz^2} = 0, \end{aligned} \quad (3.10)$$

$$\begin{aligned} & k^2 v_A^2 \sin \theta \cos \theta \hat{v}_x + ikc_s^2 \frac{d\hat{v}_x}{dz} - v_A^2 \sin \theta \cos \theta \frac{d^2 \hat{v}_x}{dz^2} \\ & + (\omega^2 - k^2 v_A^2 \cos^2 \theta)\hat{v}_z + (v_A^2 \cos^2 \theta + c_s^2) \frac{d^2 \hat{v}_z}{dz^2} = 0. \end{aligned} \quad (3.11)$$

Since all coefficients in this system of equations are constants, we can eliminate the component of velocity parallel to the interface, \hat{v}_x to obtain a single fourth-order differential equation, for the normal component of velocity perturbation, \hat{v}_z ,

$$\begin{aligned} & c_s^2 v_A^2 \sin^2 \theta \frac{d^4 \hat{v}_z}{dz^4} + 2ikc_s^2 v_A^2 \cos \theta \sin \theta \frac{d^3 \hat{v}_z}{dz^3} + [\omega^2(c_s^2 + v_A^2) - k^2 c_s^2 v_A^2] \frac{d^2 \hat{v}_z}{dz^2} \\ & - 2ik^3 c_s^2 v_A^2 \cos \theta \sin \theta \frac{d\hat{v}_z}{dz} + [\omega^4 - \omega^2 k^2 (c_s^2 + v_A^2) + k^4 c_s^2 v_A^2 \cos^2 \theta] \hat{v}_z = 0. \end{aligned} \quad (3.12)$$

If the inclination of the magnetic field is omitted (i.e. $\theta = 0$), we recover the governing equation for compressional waves for the tangential case, derived by Roberts (1981*a*) (see Section 2.4). The solution of the above equation will be of the form $\hat{v}_z \sim \exp[\Gamma z]$, where Γ are the roots of the characteristic equation,

$$\begin{aligned} & c_s^2 v_A^2 \sin^2 \theta \Gamma^4 + 2ikc_s^2 v_A^2 \cos \theta \sin \theta \Gamma^3 + [\omega^2(c_s^2 + v_A^2) - k^2 c_s^2 v_A^2] \Gamma^2 \\ & - 2ik^3 c_s^2 v_A^2 \cos \theta \sin \theta \Gamma + [\omega^4 - \omega^2 k^2 (c_s^2 + v_A^2) + k^4 c_s^2 v_A^2 \cos^2 \theta] = 0. \end{aligned} \quad (3.13)$$

The values of Γ will be used to determine the dispersion relation for the waves propagating along the interface. We note that this equation describes dynamics for both plasma regimes, above and below the interface, with appropriate characteristic speeds substituted in.

We will show by contradiction that in order to obtain propagating solutions, Γ must be complex. Let us assume that Γ is real, then the left-hand side of Equation (3.13) is a complex analytical function which may therefore be split into real and imaginary parts as

$$u(\omega, k) + iv(\omega, k) = 0, \quad (3.14)$$

where u and v are the real functions,

$$u(\omega, k) = c_s^2 v_A^2 \sin^2 \theta \Gamma^4 + [\omega^2(c_s^2 + v_A^2) - k^2 c_s^2 v_A^2] \Gamma^2$$

$$+[\omega^4 - \omega^2 k^2 (c_s^2 + v_A^2) + k^4 c_s^2 v_A^2 \cos^2 \theta],$$

$$v(\omega, k) = \Gamma [2k c_s^2 v_A^2 \sin \theta \cos \theta \Gamma^2 - 2k^3 c_s^2 v_A^2 \cos \theta \sin \theta].$$

In order for Equation 3.14 to be satisfied, we require that *both* functions $u(\omega, k)$ and $v(\omega, k)$, are equal to zero simultaneously. Setting $v(\omega, k) = 0$ gives the solutions $\Gamma = 0, \pm k$. The solutions $\Gamma = 0$ is not a solution to $u(\omega, k) = 0$. Substituting $\Gamma = \pm k$ into Eq. (??) returns a trivial solution for ω . This proves that, in order for the wave to propagate, Γ must be a complex quantity. The imaginary part of Γ represents an oscillatory component to the variation of \hat{v}_z with respect to the transverse coordinate, z . This will in turn give complex solutions for frequency, which will introduce energy flow into the system, either towards or away from the interface, depending on the sign of ω . Since no energy source is specified, this only makes physical sense if energy flow is away from the interface. These *leaky wave* solutions correspond to the case where the group speed is positive above the interface and negative below and the effect of lateral energy leakage is an attenuation of the waves.

3.2 Solving The Governing Equation - A perturbation Technique

While an explicit solution to the fourth order governing equation could be found, these solutions for Γ would be wildly complicated expressions. Therefore, in order to give a solution with which we can make analytical progress, we assume that the angle between the magnetic field lines and the interface is small and so the inclination induces only a small change to the waves' properties in each homogeneous semi-infinite volume, compared to the case with parallel magnetic field. This allows us to make approximations in θ , letting $\cos \theta \approx 1$ and $\sin \theta \approx \theta$.

The governing equation for the quantity Γ , in the case of small values of inclination angle, is given by

$$c_s^2 v_A^2 \theta^2 \Gamma^4 + 2ik c_s^2 v_A^2 \theta \Gamma^3 + [\omega^2 (c_s^2 + v_A^2) - k^2 c_s^2 v_A^2] \Gamma^2 - 2ik^3 c_s^2 v_A^2 \theta \Gamma + A = 0, \quad (3.15)$$

where

$$A = \omega^4 - \omega^2 k^2 (c_s^2 + v_A^2) + k^4 c_s^2 v_A^2.$$

In order to physically account for the transition of perturbed quantities from one side of the interface to the other, we consider a thin boundary layer (embracing the interface), in which the transition takes place, with width less than 2θ .

Despite the small angle, even the first term of Eq. (3.15) is comparable to the other terms, since it is multiplied by the highest derivative of \hat{v}_z , which may be large. Let us now apply the method of *dominant balance* to find the roots of the fourth order polynomial. This involves rescaling the equation and simplifying it to an approximate form, by neglecting terms corresponding to a higher order of θ , while ensuring this approximate form still includes the highest derivative term.

First, since some terms are smaller than others, they could not possibly be part of the dominant balance and may be ignored. We seek solutions in the form of an asymptotic power series in θ ,

$$\Gamma = \Gamma_0 + \theta\Gamma_1 + \theta^2\Gamma_2 + \dots \quad (3.16)$$

To leading order (i.e. terms proportional to $\mathcal{O}(1)$), we obtain that

$$[\omega^2(c_s^2 + v_A^2) - k^2c_s^2v_A^2]\Gamma_0^2 - A = 0, \quad (3.17)$$

which means that

$$\Gamma_0 = \pm m, \quad (3.18)$$

where

$$m = \left[\frac{(\omega^2 - k^2v_A^2)(\omega^2 - k^2c_s^2)}{(c_s^2 + v_A^2)(\omega^2 - k^2c_T^2)} \right]^{1/2}.$$

This quantity, m , coincides with the *effective wave-number* determined for magnetoacoustic modes obtained by Roberts (1981*a*) in the case of tangential discontinuity and given by Eq. (2.67), if we assume that m is real when ω is real. This is expected, since this is equivalent to the limit $\theta \rightarrow 0$. However, in the case of leaky modes, ω is complex and so too is m , introducing an oscillatory behaviour in the z -direction. A similar expression can be derived for both plasma regions, for the appropriate values of c_s and v_A . For simplicity, we will introduce the subscripts $+$ and $-$, to refer to parameters in the plasmas above and below the interface, respectively. Hence, in the $z < 0$ region we will use m_- , whereas in the upper region ($z > 0$), we will use m_+ . Here, the signs of m_- and m_+ should be chosen in such a way that the real parts of m_- and m_+ are positive. We choose the signs of Γ_0 , above and below the interface, such that these match the solutions for the case of the parallel magnetic field, i.e. physical solutions are given by

$$\Gamma_0 = \begin{cases} m_-, & \text{if } z < 0, \\ -m_+, & \text{if } z > 0. \end{cases}$$

Eq. (3.15) is a fourth-order polynomial and the remaining two roots must still be found. This can be done by rescaling the problem. For some unknown exponent, Q (to be determined), let us set,

$$\Gamma = \theta^Q y, \quad (3.19)$$

where y is bounded and also bounded away from zero as $\theta \rightarrow 0$. Thus Eq. (3.15) becomes (after dividing by $c_s^2v_A^2$)

$$\theta^{(4Q+2)}y^4 + 2ik\theta^{(3Q+1)}y^3 + \frac{1}{c_T^2}(\omega^2 - k^2c_T^2)\theta^{2Q}y^2 - 2ik^3\theta^{(Q+1)}y + A' = 0, \quad (3.20)$$

where $A' = A/c_s^2v_A^2$. We will now find the correct value of Q by using the principle of dominant balance, so that the rescaled equation is consistent as $\theta \rightarrow 0$, if at least two terms correspond to the same power of θ (this is called

balance). In addition, the balance is *dominant* in the sense that every term not involved in the balance corresponds to a higher power of θ , and therefore must be smaller than the balancing terms.

It can be shown that, when balancing the first three terms, the balance will occur for $Q = -1$ and the balancing terms are proportional to $\mathcal{O}(\theta^{-2})$ while the other terms are $\sim \mathcal{O}(1)$. With this value of Q , we obtain that

$$\theta^{-2}y^4 + 2ik\theta^{-2}y^3 + \frac{1}{c_T^2}(\omega^2 - k^2c_T^2)\theta^{-2}y^2 - 2ik^3y + A' = 0. \quad (3.21)$$

Multiplying the above equation by $\xi = \theta^2$, we have

$$y^4 + 2iky^3 + \frac{1}{c_T^2}(\omega^2 - k^2c_T^2)y^2 - 2ik^3\xi y + A'\xi = 0. \quad (3.22)$$

Now, we write y also in the form of an asymptotic series in terms of ξ as

$$y = y_0 + y_1\xi + y_2\xi^2 + \dots$$

In the leading order, we obtain

$$y_0^2(y_0^2 + 2iky_0 + \frac{1}{c_T^2}(\omega^2 - k^2c_T^2)) = 0, \quad (3.23)$$

that has 4 roots for y_0 , i.e.

$$y_{0A} = y_{0B} = 0, \quad y_{0(C,D)} = -\frac{i}{c_T}(kc_T \mp \omega)$$

The $y_0 = 0$ solutions contradict our assumptions that y is bounded to a non-zero value as $\theta \rightarrow 0$ and must be disregarded, so the remaining two solutions will be

$$y_{0(C,D)} = -\frac{i}{c_T}(kc_T \mp \omega). \quad (3.24)$$

Returning now to the original variables, the four roots of the polynomial in Γ are (in the leading order)

$$\begin{aligned} \Gamma_A &= m + \mathcal{O}(\theta); & \Gamma_B &= -m + \mathcal{O}(\theta); \\ \Gamma_C &= \theta^{-1}y_{0C} + \mathcal{O}(\theta); & \Gamma_D &= \theta^{-1}y_{0D} + \mathcal{O}(\theta). \end{aligned}$$

Higher-order terms in θ are neglected, as they are small compared to the leading order terms.

In order for the sharp density gradients in e.g. sunspot penumbra and prominences, to be considered as contact *discontinuities*, we require that the length-scales of the waves in the direction perpendicular to the interface to be large compared to the scale-height of the density change, i.e. small effective wavenumbers. Unfortunately, we see that $y \sim \theta^{-1}$ and thus the length scales in the z -direction are small. This renders our discussion of contact discontinuities largely unphysical, except for the cases of *very* sharp density gradients. However, this work is a useful starting point to understand the implications of inclined magnetic fields and will have relevancy when variable density gradient, rather than a sharp interface, is considered, in future work.

Let us briefly discuss the form and sign of the last two roots. The key ingredient in both expressions is $y_{0(C,D)} = -\frac{i}{c_T}(kc_T \mp \omega)$. Since we are dealing with an interface with inclined magnetic field, we expect that modes will be leaky and the frequency of waves can be written as $\omega = \omega_r + i\omega_i$. Introducing this expression into the form of $y_{0(C,D)}$ we obtain that

$$y_{0C} = -\frac{\omega_i}{c_T} + \frac{i}{c_T}(\omega_r - kc_T); \quad y_{0D} = \frac{\omega_i}{c_T} - \frac{i}{c_T}(\omega_r + kc_T). \quad (3.25)$$

Since attenuation of waves due to leakage corresponds to $\omega_i < 0$, Equation (3.25) shows that $\Re(y_{0C}) > 0$, while $\Re(y_{0D}) < 0$. To ensure that the group speed is positive above the interface and negative below it, the physically acceptable solutions for y_{0C} and y_{0D} must have the corresponding sign. Hence, for the $z < 0$ region we are going to use y_{0D} , while in the region above the interface we will need to use a similar root as y_{0C} but written for the corresponding characteristic speeds.

Using the same subscripts as above, we write y_{0D} , below the interface, as y_- and y_{0C} above the interface as y_+ . Therefore, keeping terms of exponents with the lowest order of θ , the expression of \hat{v}_z in the lower ($z < 0$) region is

$$\hat{v}_{z-} = F_- e^{m-z} + G_- e^{\theta^{-1}y_- z}. \quad (3.26)$$

The corresponding expression for v_z , in the upper ($z > 0$) region becomes

$$\hat{v}_{z+} = F_+ e^{-m+z} + G_+ e^{\theta^{-1}y_+ z}, \quad (3.27)$$

where the characteristic speeds for the relevant plasma are used to determine m_{\pm} and y_{\pm} in that region and F_{\pm} and G_{\pm} are constants.

3.3 Dispersion Relation of Waves Along Discontinuities

Since four constants are involved in the two expressions of \hat{v}_z , *four* boundary conditions will be needed to find the values of those constants and determine the dispersion relation. We are dealing with a contact discontinuity, therefore we require continuity of both components of velocity, \hat{v}_x and \hat{v}_z , the kinetic pressure, \hat{p} , and both components of the magnetic field, \hat{b}_x and \hat{b}_z . In this equilibrium, continuity of b_z is implied by the continuity of \mathbf{v} , so we have the correct number of boundary conditions to find all unknown coefficients.

Using the expression for \hat{v}_x and \hat{v}_z , given by Eqs. (3.10), we can find that \hat{v}_x may also be written in terms of the same exponentials as \hat{v}_z , i.e.

$$\hat{v}_{x\pm} = f_{\pm} F_{\pm} \exp(\mp m_{\pm} z) + g_{\pm} G_{\pm} \exp(y_{\pm} z),$$

where the expressions for f_{\pm} and g_{\pm} are given by

$$f_{\pm} = \frac{\theta v_{A_{\pm}}^2 (m_{\pm}^2 - k^2) \mp ikc_{0\pm}^2 m_{\pm}}{\omega^2 - k^2 c_{0\pm}^2}, \quad g_{\pm} = \frac{1}{\theta} \frac{v_{A_{\pm}}^2 y_{\pm}^2 - \theta kc_{0\pm}^2 y_{\pm}}{(\omega^2 - k^2 c_{0\pm}^2)} = \frac{1}{\theta} g'_{\pm}. \quad (3.28)$$

The condition that the vertical component of velocity, \hat{v}_z , is continuous across the boundary results in

$$F_- + G_- = F_+ + G_+. \quad (3.29)$$

Continuity of the parallel component of velocity, \hat{v}_x , results in

$$\theta f_- F_- + g'_- G_- = \theta f_+ F_+ + g'_+ G_+. \quad (3.30)$$

The condition that the parallel component of the magnetic field, b_x , is continuous, gives

$$-\theta m_- F_- + (g'_- - 1)y_- G_- = \theta m_+ F_+ + (g'_+ - 1)y_+ G_+, \quad (3.31)$$

to first order of θ . Finally, pressure balance across the interface gives

$$\begin{aligned} & \rho_- c_{0-}^2 [\theta(ikf_- + m_-)F_- + (ikg'_- + y_-)G_-] \\ &= \rho_+ c_{0+}^2 [\theta(ikf_+ - m_+)F_+ + (ikg'_+ + y_+)G_+]. \end{aligned} \quad (3.32)$$

Due to the particular choice of discontinuity, $\rho_-/\rho_+ = c_{0+}^2/c_{0-}^2$, so multipliers cancel in this equation.

These conditions may be written together as a matrix equation,

$$\mathbf{M} \begin{bmatrix} F_- \\ G_- \\ F_+ \\ G_+ \end{bmatrix} = 0,$$

where,

$$\mathbf{M} = \begin{bmatrix} 1 & 1 & -1 & -1 \\ \theta f_- & g'_- & -\theta f_+ & -g'_+ \\ -\theta m_- & (g'_- - 1)y_- & -\theta m_+ & -(g'_+ - 1)y_+ \\ \theta(ikf_- + m_-) & ikg'_- + y_- & -\theta(ikf_+ - m_+) & -(ikg'_+ + y_+) \end{bmatrix}.$$

We seek eigen-mode solutions, by solving the *dispersion relation*, which is given by the equation

$$\det(\mathbf{M}) = 0. \quad (3.33)$$

3.3.1 Dispersion Relation in Dimensionless Form

Written in the present form, the dispersion relation is dependent on the densities, Alfvén speeds and sound speeds relating to the two plasmas either side of the interface, as well as the wavenumber and frequency of the waves themselves. However, the two key dimensionless parameters that can affect the characteristics of waves are the ratio between the densities of the two plasma regions ($d = \rho_-/\rho_+$) and the modified plasma- β , which gives a ratio between kinetic and magnetic forces and is defined as $\bar{\beta} = c_s^2/v_A^2 = \bar{\beta}$, which is the same in both plasma regions. This clearly reduces the complexity of the problem,

which is why we write the dispersion relation in terms of these two parameters and we determine the equations in their dimensionless form. We introduce the phase speed, relative to the Alfvén speed of the lower plasma, as $\tilde{c}_{ph} = c_{ph}/v_{A-} = \omega/kv_{A-}$. Due to the particular form of the magnetic field, we see that $d = c_{0+}^2/c_{0-}^2 = v_{A+}^2/v_{A-}^2$ and hence $\beta_- = \beta_+ = \beta$.

The effective wave-numbers in dimensionless form are

$$\frac{m_-^2}{k^2} = \frac{(\bar{\beta} - \tilde{c}_{ph}^2)(1 - \tilde{c}_{ph}^2)}{\bar{\beta} - (\bar{\beta} + 1)\tilde{c}_{ph}^2}, \quad \frac{m_+^2}{k^2} = \frac{(d\bar{\beta} - \tilde{c}_{ph}^2)(d - \tilde{c}_{ph}^2)}{d^2\bar{\beta} - d(\bar{\beta} + 1)\tilde{c}_{ph}^2},$$

and

$$\frac{y_-}{k} = -i - i\tilde{c}_{ph}\sqrt{\frac{\bar{\beta} + 1}{\bar{\beta}}}, \quad \frac{y_+}{k} = -i + i\tilde{c}_{ph}\sqrt{\frac{\bar{\beta} + 1}{d\bar{\beta}}}.$$

The ratios between tangential and transversal components of velocity are given in dimensionless form by

$$f_- = \frac{\theta(m_-^2/k^2 - 1) + i\bar{\beta}m_-/k}{\tilde{c}_{ph}^2 - \bar{\beta}}, \quad f_+ = \frac{\theta d(m_+^2/k^2 - 1) - id\bar{\beta}m_+/2k}{\tilde{c}_{ph}^2 - d\bar{\beta}},$$

$$g'_- = \frac{y_-^2/k^2 - \theta\bar{\beta}y_-/k}{\tilde{c}_{ph}^2 - \bar{\beta}}, \quad g'_+ = \frac{dy_+^2/k^2 - \theta d\bar{\beta}y_+/k}{\tilde{c}_{ph}^2 - d\bar{\beta}}.$$

In this new, dimensionless, form, the dispersion relation is now given by the equation

$$\det(\mathbf{M}') = 0. \quad (3.34)$$

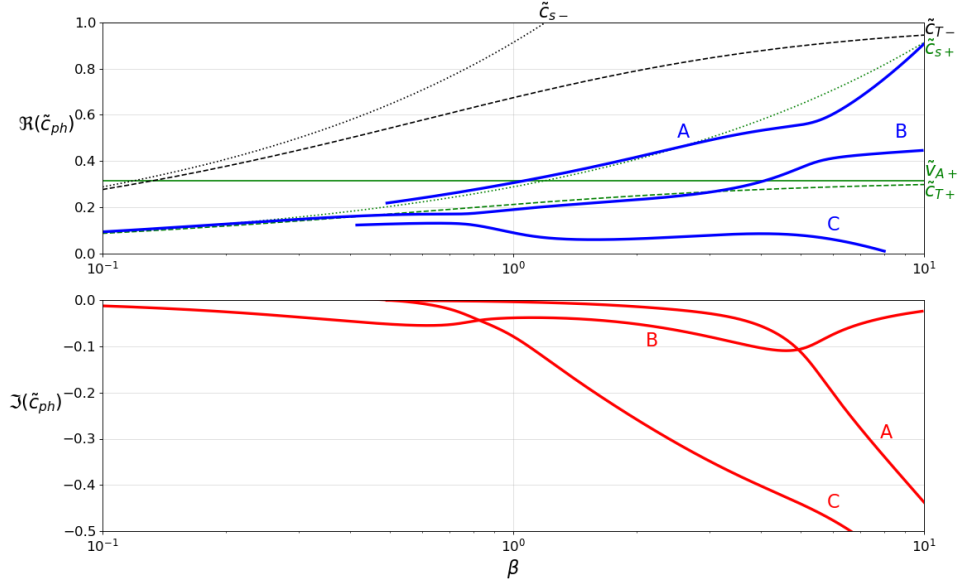
where,

$$\mathbf{M}' = \begin{bmatrix} 1 & 1 & -1 & -1 \\ \theta f_- & g'_- & -\theta f_+ & -g'_+ \\ -\theta \frac{m_-}{k} & (g'_- - 1)\frac{y_-}{k} & -\theta \frac{m_+}{k} & -(g'_+ - 1)\frac{y_+}{k} \\ \theta (if_- + \frac{m_-}{k}) & ig'_- + \frac{y_-}{k} & -\theta (if_+ - \frac{m_+}{k}) & -(ig'_+ + \frac{y_+}{k}) \end{bmatrix}.$$

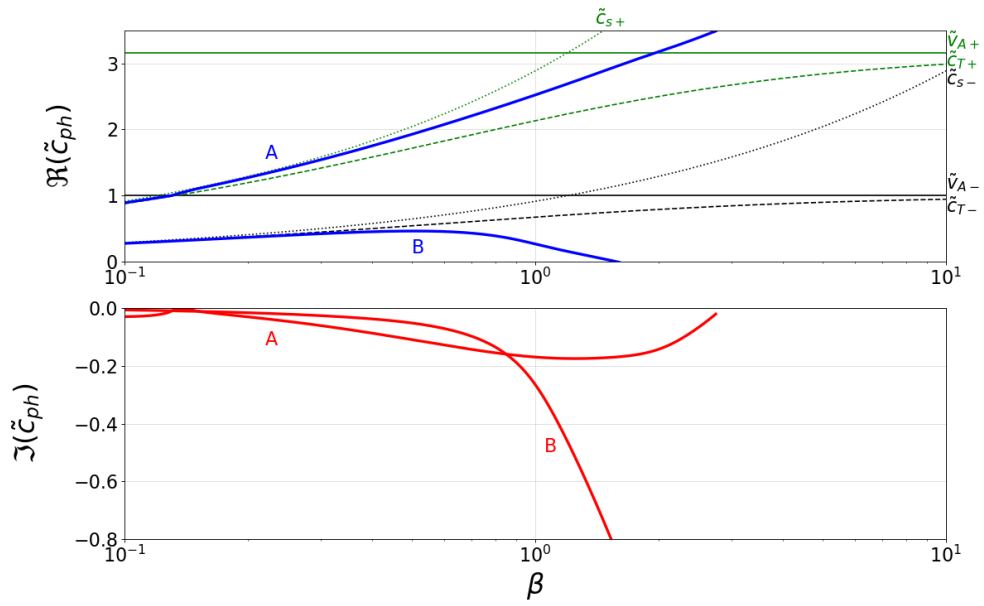
3.4 Numerical Solutions and Discussion of Results

In what follows, we solve the dispersion relation in dimensionless form (Equation 3.34) numerically, for varying density ratio and plasma- β . For simplicity, we choose to plot only forward propagating waves. Only the physical, attenuating modes are shown.

First, we plot the dispersion curves of forward propagating waves for a fixed density ratio. In Figure (3.2), we set $d = 0.1$ (upper panel) and $d = 10$ (lower panel) and allow the plasma- β to vary over two orders of magnitude, covering the spectrum of possible values in the solar atmosphere plasma. When the plasma above the interface is heavier (here $d = 0.1$), the dispersion relation allows the propagation of three modes. Mode (A), is present as an attenuating mode for larger values of plasma- β ($\beta > 0.6$), with phase-speed close to the



(a) $d = 0.1$



(b) $d = 10$

Figure 3.2: The variation of the dimensionless phase-speed of the waves, \tilde{c}_{ph} , propagating along the interface in terms of the plasma- β , for two values of density ratio. The real part is plotted in the *upper panel* and the imaginary part in the *lower panel*. The characteristic speeds are also shown for reference, using *thin lines*: the Alfvén (*solid line*), sound (*dotted line*) and cusp speeds (*dashed line*) for the regions above (*green lines*) and below the interface (*black lines*).

sound speed of the upper plasma, c_{s+} . The imaginary part of the solution increases in magnitude for higher values of plasma- β , so that for $\beta = 10$, the period is approximately half of the attenuation time. Since the phase speed is higher than the Alfvén speed in the upper region, this mode must be a highly attenuated fast mode. Its propagation speed increases with plasma- β .

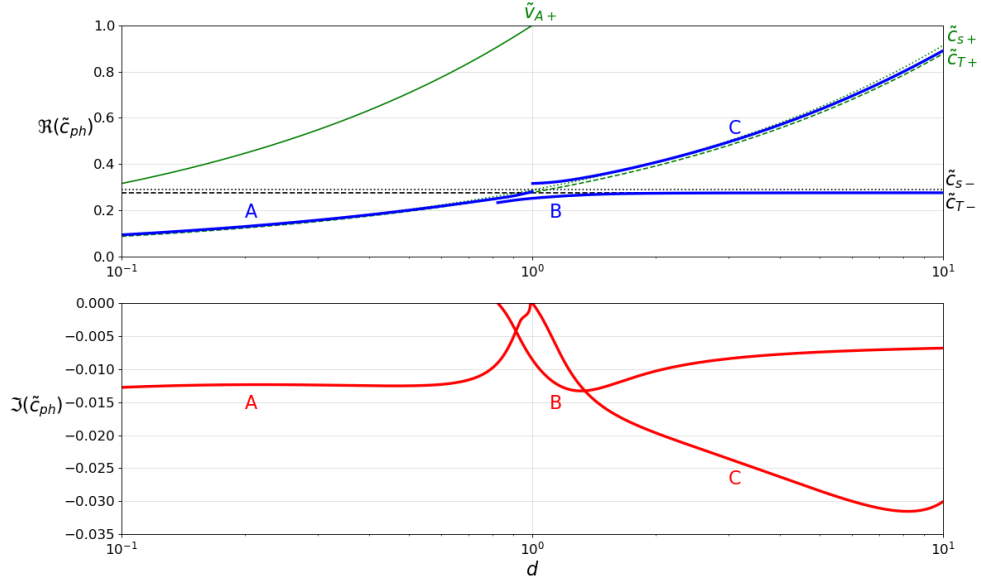
Mode (B) is present for the entire range of plasma- β and the phase-speed is, for most of the range, close to the cusp-speed of the plasma in the upper region, c_{T+} , increasing to a speed between the two cusp-speeds for high plasma- β . For $\beta \rightarrow 0$, we find that mode (B) also tends to zero, meaning that we are dealing with a slow wave. The imaginary part of the solution stays fairly steady, between 0 and -0.1 (or between one tenth and one quarter of the real part), so these waves show a rather weak attenuation. Although dissimilar for low- β values, the real part of this mode tends towards the real solution for the tangential case, shown in Figure (2.3a).

Mode (C), is only attenuating for $\beta > 0.5$, since for lower values of plasma- β , solutions do not satisfy the conditions set for the imaginary part of the frequency (they do not “leak-out”). For $\beta > 1$, the phase-speed of this mode decreases, with increasing plasma- β , while the imaginary part increases in magnitude greatly, so that, for $\beta > 1$, the period of the wave is greater than the attenuation time, meaning that the expected life-time of these modes is rather short. This mode should be labelled as a slow mode, as it is slower than either cusp speeds, however, it shows a rather peculiar behaviour. Its phase speed does not increase with plasma- β , a feature characteristic for slow waves. Due to their high attenuation, modes (A) and (C) are unlikely to be observable, due to having an attenuation time much shorter than the wave period, especially in the high-beta regime.

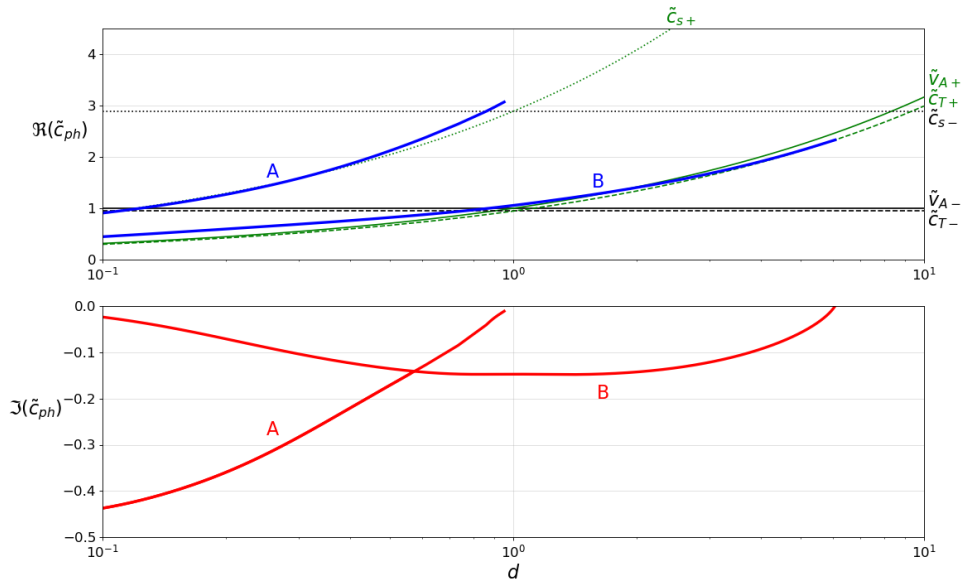
In Figure (3.2b), we show solutions to the dispersion relation for $d = 10$ and we can see two modes of propagation. Mode (A) has a phase speed between the sound and cusp speeds in the upper plasma region, though is only present for $\beta < 3$, since for higher plasma- β the mode is no longer a leaky mode. For low values of plasma- β , mode (A) tends to zero, so this is clearly a slow mode. In the region corresponding to $\beta < 1$, the attenuation of this mode is very small, however, the attenuation rate increases with the value of plasma- β . At a value of $\beta = 2$ the attenuation of the mode decreases again.

Mode (B), similar to the mode (C) in Figure (3.2a), has phase speed close to the lowest value of the cusp-speeds for lower plasma- β and its phase speed decreases to zero around $\beta = 1$. Again, based on its propagation speed we label this mode as a typical slow mode, however, it has the same peculiar behaviour with respect to plasma- β . This mode, again, is highly attenuated, especially for $\beta > 1$. It is possible that these highly attenuated modes are in fact a manifestation along the interface of waves propagating along the magnetic field lines.

Figure (3.3) shows the variation of the solutions of the dispersion relation with density ratio, for low and high values of plasma- β . In Figure (3.3a), we set $\beta = 0.1$ (a typical solar upper solar atmospheric condition) and the numerical investigation of the dispersion relation reveals the existence of three modes



(a) $\beta = 0.1$



(b) $\beta = 10$

Figure 3.3: The variation of the dimensionless phase-speed of the waves, \tilde{c}_{ph} propagating along the interface in terms of the density ratio, for two values of plasma- β . The real part is plotted in the *upper panel* and the imaginary part in the *lower panel*. The characteristic speeds are also shown for reference, using *thin lines*: the Alfvén (*solid line*), sound (*dotted line*) and cusp speeds (*dashed line*) for the regions above (*green lines*) and below the interface (*black lines*).

(two for any given d), all with relatively small imaginary part, meaning these modes are weakly attenuated. Mode (A) has phase speed below the cusp and sound speeds of the plasma in the lower region and a small imaginary part, which decreases in magnitude towards $d = 1$, at which point the imaginary part becomes zero. Mode (B) is a physical solution for $d > 0.8$ and has phase speed very close to the cusp speed of the lower plasma region. Although the dimensionless phase speed of these two modes are very similar in the region where $d = 1$, they have a rather distinctive imaginary part. Mode (C) exists for $d > 1$ and has phase-speed close to both the sound and cusp speeds of the upper plasma and this mode shows the largest attenuation among all possible modes. The real part of this solution is very similar to the numerical, but non-physical, solution for $d > 1$, for the tangential case, shown in Figure (2.2a). However, modes (A) and (C) have no counterpart in the tangential case; this exemplifies that the range of physical solutions for leaky waves is not so strict as for evanescent surface waves, for the tangential case. The $d = 1$ value corresponds to the situation when the difference between the two regions disappear and there is no interface. This situation was earlier studied by Cally and Schunker (2006) and the dispersion relation for MHD waves in this context, for small inclination angle between the wave vector and the magnetic field, may be easily solved to give that the $c_{ph} \approx c_{s-}$ or v_{A-} . This agrees with the value of mode (C) at this point and explains the decrease in attenuation of modes (A) and (C), towards $d = 1$.

In Figure (3.3b), we plot the variation of the dimensionless phase speed of waves for a given value of plasma- β (here taken to be 10) and we let the density ratio of the two regions vary. This regime of parameters is more relevant to photospheric conditions. We can see that the interface enables the propagation of two surface modes. Comparing these solutions to the ones obtained for low coronal conditions (i.e. $\beta < 1$) it is obvious that under photospheric conditions these modes have a much stronger attenuation; the leakage of waves is more accentuated in plasmas with $\beta > 1$. Mode (A) has phase speed very close to the sound speed of the upper plasma region and an imaginary part to the solutions with fairly large amplitude, which decreases towards zero, with increasing density ratio. Given its propagation speed, this mode is a fast MHD mode. This mode does not exist when the plasmas in the upper region becomes heavier. In this case, mode (A) does not satisfy the condition imposed on the imaginary part of its frequency. Mode (B) shows a rather interesting characteristics as its propagation speed is sub-Alfvénic for $d < 1$ (the Alfvén speed in the lower region is taken as reference), and it becomes super-Alfvénic for $d > 1$. For the entire domain of its definition, the propagation speed of waves stays close to the sound speed c_{s-} . Given the lower phase-speed, as well as a smaller degree of attenuation, we suggest that mode (B) is a slow MHD mode. The sub-Alfvénic part, for $d < 1$ is comparable to the $d < 1$ solution for the tangential case, shown in Figure (2.2b), though the real part of solutions for the tangential and contact discontinuity cases differ greatly for $d > 1$.

In Figure (3.4), we show the height dependence of the vertical velocity, for each solution, corresponding to the eigenvalues found in Figures (3.2) and

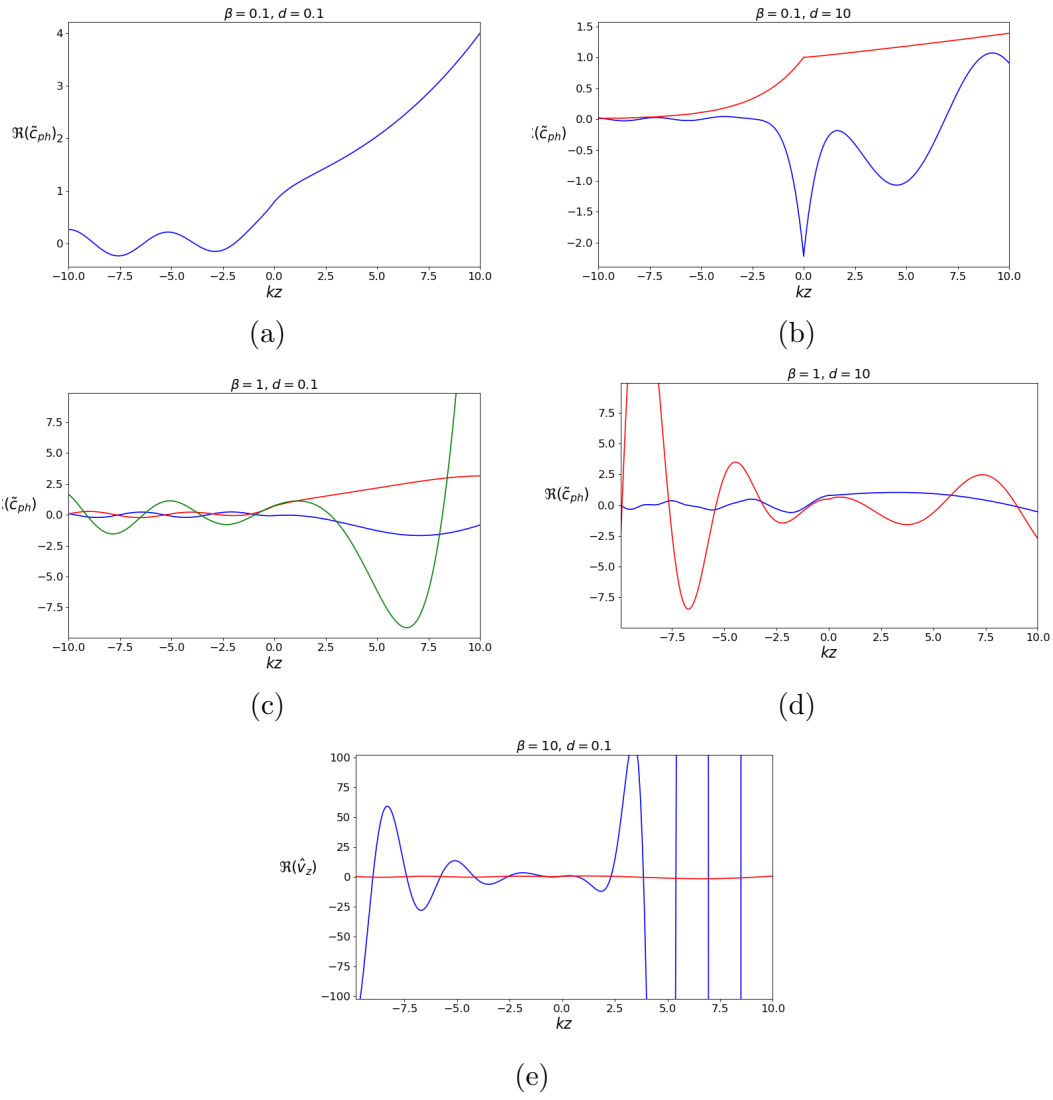


Figure 3.4: Height dependence of eigenfunctions, corresponding to the eigenvalues found in Figures (3.2) and (3.3), proportional to the value G_+ .

(3.3). These velocities cannot be found explicitly, and are instead given in terms of G_+ . We see that, as expected for a leaky wave, all solutions increase in amplitude away from the interface in an oscillatory fashion.

These figures clearly show that there are qualitative differences between surface waves at the contact discontinuity, studied in the present chapter, and surface waves at the tangential discontinuity, presented in Section 2.4. We have already noted that the present case has complex solutions, unlike the purely real solutions for the tangential case. Another noteworthy difference is that there are no explicit real frequency regions where solutions are not physical, unlike the grey shaded regions shown in Figures (2.2a) - (2.3b). However, the imaginary part of the frequency must instead be negative, for physical solutions to be possible, though this is a less strict condition, than the condition for the tangential case that ω and both m_{\pm} are real. The less strict condition, as well as the higher order of the dispersion relation, admits more possible modes than the tangential case. Thus, more modes are able to propagate for a given plasma- β and density ratio; up to three simultaneous modes, in some cases.

3.5 Symmetry

Let us explore the symmetries of this system. With the introduction of inclination of the magnetic field, the symmetry between forward and backward propagating modes is broken and so these need to be considered separately.

We first consider when the magnetic field is anti-parallel to the original orientation. This may equally be considered as the case where the inclination of the magnetic field with respect to the positive x -direction is given by $\phi = \pi + \theta$. As a result, the sine and cosine of ϕ become $\cos \phi = -\cos \theta$ and $\sin \phi = -\sin \theta$. Inserting these results into the original governing equation, Eq. (3.12), we find that the relation is unchanged and, thus, the solutions are not altered.

When the system is viewed from different angles, however, the orientation-dependent variables are altered, despite the inherent physics of the system remaining unchanged. One such invariant orientation is illustrated in Figure (3.5).

We will now write these orientation-dependent variables, in terms of d , θ and k , and thus find these in terms of the values for the original orientation, where $d = D$, $\theta = \Theta$, $k = K$ and $\tilde{c}_{ph} = W$. We consider a vertical rotation of the system by 180° . Here $d = 1/D$, so the positive z -direction is reversed and the direction of propagation also reversed, i.e. $k = -K$. However the angle of inclination is unchanged. As found in Section (2.4.2), the dimensionless phase-speed for the case $d = 1/D$ is,

$$\tilde{c}_{ph}^2 \left(d = \frac{1}{D} \right) = \frac{W^2}{D}$$

The expressions for m_{\pm}^2 are identical to those defined for the tangential case, though swapping definitions,

$$\tilde{m}_-^2 \left(d = \frac{1}{D} \right) = \tilde{m}_+^2 (d = D), \quad \tilde{m}_+^2 \left(d = \frac{1}{D} \right) = \tilde{m}_-^2 (d = D).$$



(a) Case 1: original orientation
 $d = D, \theta = \Theta, \mathbf{k} = K\hat{\mathbf{x}}$

(b) Case 2: rotation of 180°
 $d = \frac{1}{D}, \theta = \Theta, \mathbf{k} = -K\hat{\mathbf{x}}$

Figure 3.5: The invariant orientations of the equilibrium system.

Due to the inversion of the vertical direction, we still require that the exponents to be positive below the interface and negative above, i.e.

$$\tilde{m}_- \left(d = \frac{1}{D} \right) = -\tilde{m}_+ (d = D), \quad \tilde{m}_+ \left(d = \frac{1}{D} \right) = -\tilde{m}_- (d = D).$$

Inserting these expressions for m_\pm into the expressions for f_\pm , we find that

$$\tilde{f}_- \left(d = \frac{1}{D}, k = -K \right) = f_+ (d = D, k = K) \quad (3.35)$$

$$\tilde{f}_+ \left(d = \frac{1}{D}, k = -K \right) = f_- (d = D, k = K). \quad (3.36)$$

Next, we consider the new forms of y_\pm . Let us introduce a slightly different definition: $y_\pm = \pm Y_\pm$, so

$$Y_- = i \frac{\omega}{c_T} - ik = y_-, \quad Y_+ = i \frac{\omega}{c_T} + ik = y_-.$$

Introducing \mathbf{k} in terms of our original wavevector, we see that

$$Y_- (k = -K) = -Y_+ (k = K), \quad z < 0, \quad (3.37)$$

$$Y_+ (k = -K) = -Y_- (k = K), \quad z > 0. \quad (3.38)$$

Again, we must non-dimensionalise these expressions and so we obtain that

$$\tilde{Y}_- \left(d = \frac{1}{D}, k = -K \right) = -\tilde{Y}_+ (d = D, k = K), \quad z < 0, \quad (3.39)$$

$$\tilde{Y}_+ \left(d = \frac{1}{D}, k = -K \right) = -\tilde{Y}_- (d = D, k = K), \quad z > 0. \quad (3.40)$$

The new forms of Y_\pm , in turn, give that g_\pm for this case are equivalent to g_\mp for the original case. Thus, the dispersion relation will simply give a negative expression from that found previously, which must have all of the same solutions.

We have, thus, confirmed that the same system, viewed from another orientation will indeed give the same solutions, when following the technique outlined in the present work. Therefore, the mathematical results confirm the physical behaviour, even when the assumptions used above are applied.

3.6 Conclusions

This chapter considered the problem of MHD waves propagating along an interface, in the presence of an inclined magnetic field, in a two-dimensional configuration. For a small-angle approximation, the dispersion relation was derived analytically, by employing the method of dominant balance. The effective wavenumbers are shown to be complex, so wave amplitude decays away from the interface in an oscillatory pattern. The complex effective wavenumbers, in turn, give rise to complex solutions for the frequency of the waves, which would give amplification or attenuation. However, since no outside energy source exists in this situation, only solutions with negative imaginary part are permitted physically. These solutions correspond to MHD waves where amplitude decays due to lateral energy leakage, towards $|z| \rightarrow \infty$.

Solutions to the dispersion relation, for varying density ratio and plasma- β , were found numerically. The solutions found all have negative imaginary component, showing that the introduction of magnetic field inclination introduces energy flow to the system, compared to the case with parallel magnetic field and so even a small angle between the interface and the magnetic field produces a qualitative change in the modes which may propagate. Thus, a contact discontinuity in density and temperature, in the presence of an inclined constant magnetic field, may support the propagation of surface leaky waves. However, quantities averaged over a thin boundary layer do tend towards the solutions for a tangential discontinuity, as the inclination angle tends towards zero, so the contact and tangential discontinuity solutions are qualitatively comparable.

Furthermore, it was found that, with an oblique field, more leaky modes are permitted over a wider range of variables, than the surface mode solutions to the tangential case. For the tangential case, there are no solutions for low values of plasma- β , whereas leaky modes persist at the contact discontinuity for all values of β . For the tangential case, each pair of values of plasma- β and density ratio resulted in only one solution; the fast surface mode. However for the case of the contact discontinuity, there are two propagating modes for most values of the variables, corresponding to the fast and slow magnetoacoustic modes. For low values of density ratio, there is even a third mode which may propagate, which is identified as a second slow-mode.

These results may have considerable applications to the study of waves in the solar atmosphere. In particular, the penumbra of sunspots have been shown to have highly inclined magnetic field lines and, at high-resolutions, *running penumbral waves* were detected (*e.g.* Giovanelli 1972, Zirin and Stein 1972). Understanding that the outer edge of the sunspot may support leaky waves, more readily than trapped waves, could give a different explanation to

any observed damping of running penumbral waves. While, inside the sunspot, the sharp density variation is horizontal, in the outer edge of the penumbra and the outer canopy, the sharp density gradient is vertical. It has been shown (in *e.g.* Jess et al. 2013) that field inclination (from the horizontal) in the penumbra is $0 - 60^\circ$, but also that the field inclination in the magnetic canopy is $0 - 35^\circ$. Hence, small-angle approximation may have relevance to a much wider range of applications, especially across the solar transition region, where the density variation is sudden. This study may also be of particular use for the investigation of transition region quakes (TRQs) (Scullion et al., 2011), since these waves have large vertical length scales, so the transition region may be viewed as a single interface. When considering TRQs as surface waves propagating along an density discontinuity, the fact that interfaces with inclined fields can only support leaky waves, may help to explain how energy is transferred into the solar corona, through wave leakage.

CHAPTER 4

Time-Dependent Analysis of Waves at a Contact Discontinuity

The previous chapter was dedicated to the eigenvalue problem, for waves propagating along contact discontinuities. The imaginary part of the frequency gave us key information of how the amplitude of the waves changed over time. One of the findings of that study was that, once the background magnetic field crosses the density interface (i.e. waves propagate along a contact discontinuity), waves will undergo an attenuation of their amplitude due to lateral leakage, and this leakage can be rather important for explaining wave attenuation in various solar physics applications. However, to gain a better understanding of the temporal evolution, an *initial value problem* technique must be employed. For standard surface wave solutions, the eigenvalue solutions correspond to the asymptotic behaviour of time-dependent solutions, i.e. the value that solutions tend towards after long time-scales. For *leaky* wave solutions, however, the eigenvalue solutions instead correspond to *intermediate asymptotics*, where the time-scale is much greater than the period of the wave, but less than the attenuation time. The initial value problem of waves at a contact discontinuity is going to be addressed using the technique of Laplace transforms.

The previous chapter has already given motivation for studying waves at a contact discontinuity, as well as many physical applications. However, the assumption that a leaky wave would reach a steady state (in the sense that solutions $\sim e^{-i\omega t}$) may not be valid for every case, so the *evolving* solutions need also be considered. Additionally, time-dependent solutions give a clear description of the features and dynamics of waves at contact discontinuities, which are more readily compared to observations, than the time-independent solutions.

The equilibrium considered in this chapter is similar to that previously considered in a Cartesian coordinate system; a constant magnetic field of the

This chapter is based on the following refereed journal article:

- Ruderman, M.S., Vickers, E., Ballai, I., Erdélyi, R. (2018); Propagation of Leaky Surface Waves on Contact Magnetohydrodynamic Discontinuities in Incompressible Plasmas, *Physics of Plasmas*, Volume 25, Issue 12

form $\mathbf{B}_0 = B_0(\cos \theta, 0, \sin \theta)$ permeates a density interface, situated at $z = 0$, separating two homogeneous plasma regions of different densities. As specified previously, we neglect gravitational effects and the equilibrium (unperturbed) state is static. For simplicity, we consider that the two plasma regions are incompressible. We will, once again, consider perturbations only in the (x, z) -plane, independent of y . The components of velocity and magnetic field perturbation are denoted by $\mathbf{v} = (v_x, 0, v_z)$ and $\mathbf{b} = (b_x, 0, b_z)$, with v_y and b_y assumed to be zero.

4.1 Governing equations

The system of linearised, ideal MHD equations (see Eqs. 2.12 - 2.16) for the incompressible plasma, therefore becomes

$$\rho_0 \frac{\partial \mathbf{v}}{\partial t} = -\nabla p + \frac{1}{\mu_0}(\mathbf{B}_0 \cdot \nabla)\mathbf{b} - \frac{1}{\mu_0}\nabla(\mathbf{b} \cdot \mathbf{B}_0) \quad (4.1)$$

$$\frac{\partial \mathbf{b}}{\partial t} = (\mathbf{B}_0 \cdot \nabla)\mathbf{v} \quad (4.2)$$

$$\nabla \cdot \mathbf{b} = 0, \quad (2.15)$$

where all variables were defined in Chapter 2 and the incompressibility condition, $\nabla \cdot \mathbf{v} = 0$ is also taken into account. The perturbation to the total pressure may also be introduced, which is defined as

$$P_T = p + \frac{1}{\mu_0}\mathbf{b} \cdot \mathbf{B}_0.$$

This allows us to rewrite Eq. (4.1) much more simply in terms of the total pressure, as

$$\rho_0 \frac{\partial \mathbf{v}}{\partial t} = -\nabla P_T + \frac{1}{\mu_0}(\mathbf{B}_0 \cdot \nabla)\mathbf{b}. \quad (4.3)$$

Taking the divergence of this equation, together with the incompressibility and solenoidal conditions allows us to obtain a simple relation for the total pressure:

$$\nabla^2 P_T = 0. \quad (4.4)$$

Since we consider the time-dependent case, the ansatz, $f \sim \hat{f} \exp[i(kx - \omega t)]$ used previously, is no longer useful. However, we still consider solutions to be oscillatory along the interface (in the x -direction), so we now consider the perturbations of all quantities proportional to $\exp(ikx)$, where k is a real and positive constant. As a result, the system of equations, including Eq. (4.4), reduces to

$$\rho_0 \frac{\partial v_z}{\partial t} = -\frac{\partial P_T}{\partial z} + \frac{B_0}{\mu_0} \left(\frac{\partial b_z}{\partial z} \sin \theta + ikb_z \cos \theta \right), \quad (4.5)$$

$$\frac{\partial v_z}{\partial z} + ikv_x = 0, \quad (4.6)$$

$$\frac{\partial b_z}{\partial t} = B_0 \left(\frac{\partial v_z}{\partial z} \sin \theta + ikv_z \cos \theta \right), \quad (4.7)$$

$$\frac{\partial b_z}{\partial z} + ikb_x = 0, \quad (4.8)$$

$$\frac{\partial^2 P_T}{\partial z^2} - k^2 P_T = 0. \quad (4.9)$$

In order to make analytical progress, while keeping information about time dependence, we introduce the Laplace transform with respect to time,

$$\hat{f}(z, \omega) = \int_0^\infty f(z, t) e^{i\omega t} dt, \quad (4.10)$$

which is defined in the upper half of the complex ω -plane. Applying the Laplace transform to Eqs. (4.5)–(4.9) yields the following system of equations:

$$i\omega \hat{v}_z = \frac{1}{\rho_0} \frac{\partial \hat{P}_T}{\partial z} - \frac{v_A^2}{B_0} \left(\frac{\partial \hat{b}_z}{\partial z} \sin \theta + ik \hat{b}_z \cos \theta \right) - v_{z0}, \quad (4.11)$$

$$\frac{\partial \hat{v}_z}{\partial z} + ik \hat{v}_x = 0, \quad (4.12)$$

$$i\omega \hat{b}_z = -B_0 \left(\frac{\partial \hat{v}_z}{\partial z} \sin \theta + ik \hat{v}_z \cos \theta \right) - b_{z0}, \quad (4.13)$$

$$\frac{\partial \hat{b}_z}{\partial z} + ik \hat{b}_x = 0, \quad (4.14)$$

$$\frac{\partial^2 \hat{P}_T}{\partial z^2} - k^2 \hat{P}_T = 0, \quad (4.15)$$

where $v_{z0}(z) = v_z(z, t = 0)$ and $b_{z0}(z) = b_z(z, t = 0)$ are the initial values of the z -components of the velocity and magnetic field perturbation. Note that $\rho_- v_{A-}^2 = \rho_+ v_{A+}^2$, where the subscripts - and + indicate that the quantity is calculated in the regions $z < 0$ and $z > 0$, respectively.

Equation (4.15) can be easily solved and has solutions of the form $\hat{P}_T \sim e^{\pm kz}$. Supposing that the total pressure perturbation vanishes as $|z| \rightarrow \infty$ and it is continuous across $z = 0$, the physical solutions of Eq. (4.15) can be written as

$$\hat{P}_T = A(\omega) \begin{cases} e^{kz}, & z < 0, \\ e^{-kz}, & z > 0, \end{cases} \quad (4.16)$$

where $A(\omega)$ is an arbitrary function, that will be determined later, with the help of the jump conditions across the interface

Eliminating \hat{b}_z from Eqs. (4.11) and (4.13) yields

$$\begin{aligned} v_A^2 \frac{\partial^2 \hat{v}_z}{\partial z^2} \sin^2 \theta + ikv_A^2 \frac{\partial \hat{v}_z}{\partial z} \sin 2\theta + (\omega^2 - k^2 v_A^2 \cos^2 \theta) \hat{v}_z \\ = i\omega v_{z0} - v_A^2 F(z) - \frac{i\omega}{\rho_0} \frac{d\hat{P}_T}{dz}, \end{aligned} \quad (4.17)$$

where the function $F(z)$ is defined entirely in terms of the initial value of the z -component of the magnetic field perturbation as

$$F(z) = \frac{1}{B_0} \left(\frac{\partial b_{z0}}{\partial z} \sin \theta + ikb_{z0} \cos \theta \right). \quad (4.18)$$

To simplify the analysis we consider that there is no initial perturbation to the vertical magnetic field, i.e. $b_{z0}(z) = 0$, so $F(z) = 0$. From this, along with the expression for P_T (Eq. 4.16), we obtain a governing equation for \hat{v}_z

$$v_{A\pm}^2 \frac{\partial^2 \hat{v}_z}{\partial z^2} \sin^2 \theta + ikv_{A\pm}^2 \frac{\partial \hat{v}_z}{\partial z} \sin 2\theta + (\omega^2 - k^2 v_{A\pm}^2 \cos^2 \theta) \hat{v}_z = i\omega v_{z0} \pm ik\omega \frac{1}{\rho_{\pm}} A(\omega) e^{\pm kz}. \quad (4.19)$$

We aim to solve this equation, using the method of variation of parameters. Firstly we find the general solution to the homogeneous equation corresponding to (4.19) i.e. we are setting the right hand side to zero. This gives

$$\hat{v}_{z,g} = Be^{i\lambda_+ z} + Ce^{i\lambda_- z} = By_1 + Cy_2,$$

where the effective wavenumbers are given by

$$\lambda_{\pm} = \frac{-kv_A \cos \theta \pm \omega}{v_A \sin \theta} \quad (4.20)$$

and the coefficients B and C are complex amplitudes, yet to be determined. The method of variation of parameters states that an equation of the form

$$\frac{d^2 y}{dz^2} + p(z) \frac{dy}{dz} + q(z)y = g(z)$$

has a solutions of the form

$$y = u_1(z)y_1(z) + u_2(z)y_2(z),$$

where y_1 and y_2 are solutions of the homogeneous equation (in this case $e^{i\lambda_{\pm} z}$) and u_1 and u_2 are given by

$$u_1 = - \int \frac{y_2 g}{W(y_1, y_2)} dz + c_1, \quad u_2 = \int \frac{y_1 g}{W(y_1, y_2)} dz + c_2.$$

Here c_1 and c_2 are constants to be determined and $W(y_1, y_2)$ is the Wronskian, which may be written as,

$$W(y_1, y_2) = i(\lambda_- - \lambda_+) e^{i(\lambda_- + \lambda_+)z}.$$

We are hence able to find that

$$\begin{aligned} u_1 &= \frac{1}{2v_A \sin \theta} \left[c_+ + \int_0^z v_{z0}(z') e^{-\lambda_+ z'} dz' + \int_0^z -\frac{k}{\rho_{\pm}} A(\omega) e^{(-i\lambda_+ \pm k)z'} dz' \right] \\ &= \alpha_+ + \beta_+ + \gamma_+ \end{aligned} \quad (4.21)$$

and

$$\begin{aligned} u_2 &= -\frac{1}{2v_A \sin \theta} \left[c_- + \int_0^z v_{z0}(z') e^{-\lambda_- z'} dz' + \int_0^z -\frac{k}{\rho_{\pm}} A(\omega) e^{(-i\lambda_- \pm k)z'} dz' \right] \\ &= -(\alpha_- + \beta_- + \gamma_-). \end{aligned} \quad (4.22)$$

With the help of these quantities we write the z -component of the velocities as

$$\begin{aligned}\hat{v}_z &= y_A + y_B + y_C \\ &= (\alpha_+ e^{i\lambda_+ z} - \alpha_- e^{i\lambda_- z}) + (\beta_+ e^{i\lambda_+ z} - \beta_- e^{i\lambda_- z}) + (\gamma_+ e^{i\lambda_+ z} - \gamma_- e^{i\lambda_- z})\end{aligned}$$

where, more explicitly,

$$y_A = \frac{1}{2v_A \sin \theta} (c_+ e^{i\lambda_+ z} + c_- e^{i\lambda_- z}), \quad (4.23)$$

$$y_B = \frac{1}{2v_A \sin \theta} \int_0^z v_{z0}(z') \left[e^{i\lambda_+(z-z')} - e^{i\lambda_-(z-z')} \right] dz', \quad (4.24)$$

$$\begin{aligned}y_C &= \frac{\rho_{\pm}}{2kv_{A\pm} \sin \theta} A(\omega) \left[\frac{e^{\pm kz} - e^{i\lambda_+ z}}{\pm k - i\lambda_+} - \frac{e^{\pm kz} - e^{i\lambda_- z}}{\pm k - i\lambda_-} \right] \\ &= \frac{ik\omega}{\rho} A(\omega) e^{\pm kz} \frac{1}{(\omega^2 - k^2 v_A^2 e^{\mp 2i\theta})} + D_+ e^{i\lambda_+ z} + D_- e^{i\lambda_- z}.\end{aligned} \quad (4.25)$$

Combining c_{\pm} and D_{\pm} into the arbitrary constants A_{\pm} , we finally have an expression for the vertical velocity,

$$\begin{aligned}\hat{v}_z &= B e^{i\lambda_+ z} + C e^{i\lambda_- z} + \frac{1}{2v_A \sin \theta} \int_0^z v_{z0}(z') \left[e^{i\lambda_+(z-z')} - e^{i\lambda_-(z-z')} \right] dz' \\ &\mp \frac{ik\omega A(\omega) e^{\pm kz}}{\rho(\omega^2 - k^2 v_A^2 e^{\mp 2i\theta})}\end{aligned} \quad (4.26)$$

We will use \pm subscripts to denote quantities above and below the interface, respectively.

Since we assume that ω is in the upper part of the ω -plane, it follows that $\Re(i\lambda_+) < 0$ and $\Re(i\lambda_-) > 0$. The integral in the above expression can be calculated once the profile of the initial velocity is specified, something we will address later in this Chapter. We should also specify that the frequencies we are going to deal with will be such that the resonance will never occur, i.e. the denominator of the last term will never reach zero (or values near zero).

Now, we use the condition that $\hat{v}_z \rightarrow 0$ as $|z| \rightarrow \infty$, i.e. vertical wave amplitudes do not increase far from the interface. For simplicity, we assumed that $v_{z0}(z)$ has finite support, meaning that there is always such a z_m value that satisfies $v_{z0}(z) = 0$ for $|z| \geq z_m$. This condition guarantees the convergence of the integral in Eq. (4.26). When $z < 0$ the asymptotic behaviour of \hat{v}_z for large $|z|$ is given by

$$\hat{v}_z \sim e^{i\lambda_1 z} \left(B_- - \frac{1}{2v_{A-} \sin \theta} \int_{-\infty}^0 v_{z0}(z') e^{-i\lambda_1 z} dz \right), \quad (4.27)$$

where $\lambda_{1\pm}$ refers to the effective wavenumbers of the lower plasma and $\lambda_{2\pm}$ refers to the upper plasma. So the condition that $\hat{v}_z \rightarrow 0$ for $z \rightarrow -\infty$ (i.e. that the velocities are bounded far from the interface) in turn implies

$$B_- = \frac{1}{2v_{A-} \sin \theta} \int_{-\infty}^0 v_{z0}(z') e^{-i\lambda_1 z} dz, \quad (4.28)$$

and so the expression for \hat{v}_z in the lower plasma region is

$$\begin{aligned} \hat{v}_{z-} = & e^{i\lambda_1 - z} \left(C_- - \frac{1}{2v_{A-} \sin \theta} \int_0^z v_{z0} e^{-i\lambda_1 - z'} dz' \right) \\ & + \frac{ik\omega A e^{kz}}{\rho_-(\omega^2 - k^2 v_{A-}^2 e^{-2i\theta})} + \frac{e^{i\lambda_1 + z'}}{2v_{A-} \sin \theta} \int_{-\infty}^z v_{z0}(z') e^{-i\lambda_1 + z'} dz'. \end{aligned} \quad (4.29)$$

In a similar fashion, when $z > 0$, the condition that $\hat{v}_z \rightarrow 0$ for $z \rightarrow \infty$ is

$$C_+ = \frac{1}{2v_{21} \sin \theta} \int_0^\infty v_{z0}(z') e^{-i\lambda_2 - z} dz, \quad (4.30)$$

so the expression for \hat{v}_z in the upper plasma region becomes

$$\begin{aligned} \hat{v}_{z+} = & e^{i\lambda_2 + z} \left(B_+ - \frac{1}{2v_{A+} \sin \theta} \int_0^z v_{z0} e^{-i\lambda_2 + z'} dz' \right) \\ & + \frac{ik\omega A(\omega) e^{-kz}}{\rho_+(\omega^2 - k^2 v_{A+}^2 e^{-2i\theta})} + \frac{e^{i\lambda_2 - z'}}{2v_{A+} \sin \theta} \int_z^\infty v_{z0}(z') e^{-i\lambda_2 - z'} dz'. \end{aligned} \quad (4.31)$$

Again, the expressions of the integrals will be known once particular forms for v_{z0} are chosen.

4.2 Joining solutions at the interface

In order to determine the temporal evolution of various components of velocity, we will need to join the solutions determined for each region at the interface. The necessary continuity conditions at the contact discontinuity were derived in Chapter 2, here we are going to use these relations with no further proof. We are dealing with a contact discontinuity, therefore the continuity conditions across the interface are once again

$$[[\mathbf{v}]] = 0, \quad [[\mathbf{b}]] = 0, \quad [[p]] = 0. \quad (4.32)$$

Since the magnetic field is continuous across the interface, the final condition is equivalent to

$$[[P_T]] = 0. \quad (4.33)$$

Combining this jump condition with Eq. (4.16), we obtain that $A(\omega)$ is also a continuous function across $z = 0$. Using the incompressibility condition, we see that

$$\hat{v}_x = -\frac{i}{k} \frac{\partial \hat{v}_z}{\partial z}. \quad (4.34)$$

Hence, the condition of continuity of \hat{v}_x is given by

$$\left[\left[\frac{\partial \hat{v}_z}{\partial z} \right] \right] = 0. \quad (4.35)$$

Next, we are going to use the continuity of the two components of the magnetic field perturbation. First, from equation (4.13), continuity of b_z is equivalent to

$$\left[\left[\frac{\partial \hat{v}_z}{\partial z} \sin \theta + ik \hat{v}_z \cos \theta \right] \right] = 0. \quad (4.36)$$

Using this result, along with the solenoidal constraint, the condition that b_x is continuous becomes

$$\left[\left[\frac{\partial^2 \hat{v}_z}{\partial z^2} \sin \theta + ik \frac{\partial \hat{v}_z}{\partial z} \cos \theta \right] \right] = 0. \quad (4.37)$$

By simplifying Eqs. (4.36) and (4.37), the remaining continuity conditions are thus (in terms of \hat{v}_z)

$$[[\hat{v}_z]] = 0, \quad \left[\left[\frac{\partial \hat{v}_z}{\partial z} \right] \right] = 0, \quad \left[\left[\frac{\partial^2 \hat{v}_z}{\partial z^2} \sin \theta + ik \frac{\partial \hat{v}_z}{\partial z} \cos \theta \right] \right] = 0. \quad (4.38)$$

Using the solutions for \hat{v}_z , given by equations (4.29) and (4.31), the jump condition $[[\hat{v}_z]] = 0$ results in

$$\begin{aligned} B_+ + \frac{ik\omega A(\omega)}{\rho_+(\omega^2 - k^2 v_{A+}^2 e^{2i\theta})} + \frac{1}{2v_{A+} \sin \theta} \int_0^\infty v_{z0}(z) e^{-i\lambda_2 - z} dz \\ = C_- - \frac{ik\omega A(\omega)}{\rho_-(\omega^2 - k^2 v_{A-}^2 e^{-2i\theta})} + \frac{1}{2v_{A-} \sin \theta} \int_{-\infty}^0 v_{z0}(z) e^{-i\lambda_1 + z} dz. \end{aligned} \quad (4.39)$$

Furthermore, the second jump condition, derived from continuity of v_x translates into

$$\begin{aligned} \lambda_{2+} B_+ - \frac{k^2 \omega A(\omega)}{\rho_+(\omega^2 - k^2 v_{A+}^2 e^{2i\theta})} + \frac{\lambda_{2-}}{2v_{A+} \sin \theta} \int_0^\infty v_{z0}(z) e^{-i\lambda_2 - z} dz \\ = \lambda_{1-} C_- - \frac{k^2 \omega A(\omega)}{\rho_-(\omega^2 - k^2 v_{A-}^2 e^{-2i\theta})} + \frac{\lambda_{1+}}{2v_{A-} \sin \theta} \int_{-\infty}^0 v_{z0}(z) e^{-i\lambda_1 + z} dz. \end{aligned} \quad (4.40)$$

Equations (4.39) and (4.40) constitute a system of linear algebraic equations for B_+ and C_- . Solving this system we obtain expressions for these unknowns,

$$\begin{aligned} C_- = \frac{kA(\omega)v_{A-}v_{A+} \sin \theta}{v_{A-} + v_{A+}} \left(\frac{i\lambda_{2+} + k}{\rho_+(\omega^2 - k^2 v_{A+}^2 e^{2i\theta})} + \frac{i\lambda_{2+} - k}{\rho_-(\omega^2 - k^2 v_{A-}^2 e^{-2i\theta})} \right) \\ + \frac{1}{(v_{A-} + v_{A+}) \sin \theta} \left(\frac{v_{A-}}{v_{A+}} \int_0^\infty v_{z0}(z) e^{-i\lambda_2 - z} dz \right. \\ \left. + \frac{v_{A+} - v_{A-}}{2v_{A-}} \int_{-\infty}^0 v_{z0}(z) e^{-i\lambda_1 + z} dz \right), \end{aligned} \quad (4.41)$$

$$\begin{aligned} B_+ = \frac{kA(\omega)v_{A-}v_{A+} \sin \theta}{v_{A-} + v_{A+}} \left(\frac{i\lambda_{1-} + k}{\rho_+(\omega^2 - k^2 v_{A+}^2 e^{2i\theta})} + \frac{i\lambda_{1-} - k}{\rho_-(\omega^2 - k^2 v_{A-}^2 e^{-2i\theta})} \right) \\ + \frac{1}{(v_{A+} + v_{A-}) \sin \theta} \left(\frac{v_{A+}}{v_{A-}} \int_{-\infty}^0 v_{z0}(z) e^{-i\lambda_1 + z} dz \right. \\ \left. + \frac{v_{A-} - v_{A+}}{2v_{A+}} \int_0^\infty v_{z0}(z) e^{-i\lambda_2 - z} dz \right). \end{aligned} \quad (4.42)$$

The final jump condition, $\llbracket \hat{b}_x \rrbracket = 0$, gives

$$\begin{aligned}
& \frac{\lambda_{1-}C_-}{v_{A-}} + \frac{\lambda_{2+}B_+}{v_{A+}} + k^3 A(\omega) \left(\frac{e^{-i\theta}}{\rho_-(\omega^2 - k^2 v_{A-}^2 e^{-2i\theta})} - \frac{e^{i\theta}}{\rho_+(\omega^2 - k^2 v_{A+}^2 e^{2i\theta})} \right) \\
&= \frac{1}{2 \sin \theta} \left(\frac{\lambda_{1+}}{v_{A-}^2} \int_{-\infty}^0 v_{z0}(z) e^{-i\lambda_{1+}z} dz + \frac{\lambda_{2-}}{v_{A+}^2} \int_0^{\infty} v_{z0}(z) e^{-i\lambda_{2-}z} dz \right) \\
&- \frac{iv_{z0}(0)}{\sin \theta} \left(\frac{1}{v_{A+}^2} - \frac{1}{v_{A-}^2} \right). \tag{4.43}
\end{aligned}$$

After a lengthy but straightforward calculation, using Eqs. (4.41) and (4.42), we can isolate the coefficient function $A(\omega)$ and its expression is given by

$$A(\omega) = \frac{H(\omega)G(\omega)}{kD(\omega)}, \tag{4.44}$$

where

$$D(\omega) = (\rho_- + \rho_+)\omega^2 + 2ik\omega(\rho_-v_{A-} + \rho_+v_{A+}) \sin \theta - 2\rho_-v_{A-}^2k^2, \tag{4.45}$$

$$H(\omega) = \rho_- \rho_+ (v_{A+} - v_{A-}) (\omega - kv_{A-} e^{-i\theta}) (\omega + kv_{A+} e^{i\theta}), \tag{4.46}$$

$$\begin{aligned}
G(\omega) &= \frac{i\omega}{\sin \theta} \left(\int_{-\infty}^0 \frac{v_{z0}(z)}{v_{A-}^2} e^{-i\lambda_{1+}z} dz + \int_0^{\infty} \frac{v_{z0}(z)}{v_{A+}^2} e^{-i\lambda_{2-}z} dz \right) \\
&+ v_{z0}(z=0) \left(\frac{1}{v_{A-}} + \frac{1}{v_{A+}} \right). \tag{4.47}
\end{aligned}$$

The function $D(\omega)$ will play an important role in our analysis, as the singularities, relating to its zeros will help determine the time dependent solutions. The zeros occur at $\omega_{\pm} = \pm\omega_r + i\omega_i$, where

$$\omega_r = \frac{\rho_-^{1/2} k v_{A-}}{\rho_- + \rho_+} \sqrt{\left(\rho_-^{1/2} - \rho_+^{1/2}\right)^2 + \left(\rho_-^{1/2} + \rho_+^{1/2}\right)^2 \cos^2 \theta}, \tag{4.48}$$

$$\omega_i = -\frac{k(\rho_-v_{A-} + \rho_+v_{A+}) \sin \theta}{\rho_- + \rho_+}. \tag{4.49}$$

4.3 Finding time-dependent solutions

By inserting the solutions for A_{\pm} and $A(\omega)$, given by Eqs. (4.40), (4.41) and (4.44), into the expressions for \hat{v}_z , (4.29) and (4.31), we have obtained the Laplace transform for the vertical velocity. With the help of this form we can find the Laplace transforms for the other perturbed quantities. The temporal evolution of perturbations will be found, by performing an inverse Laplace Transform for particular types of drivers.

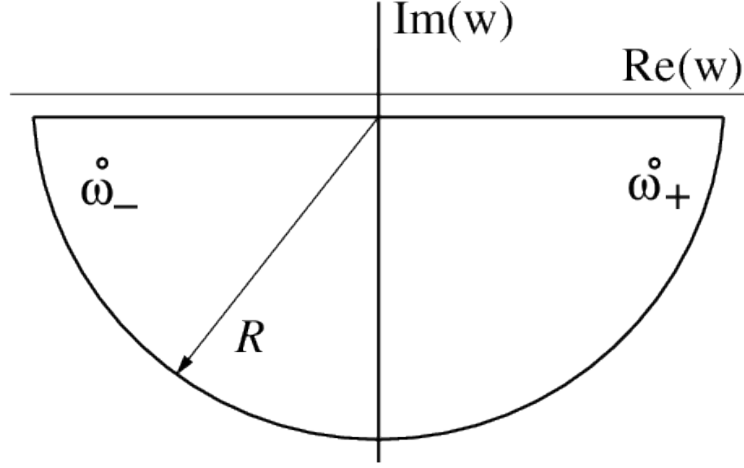


Figure 4.1: A sketch of the contour in the complex ω -plane used to perform inverse Laplace transforms of perturbations. (Taken from Ruderman, Vickers, Ballai and Erdélyi (2018))

The time-dependent velocity, v_z is thus given by the inverse Laplace transform,

$$v_z = \int_{i\zeta - \infty}^{i\zeta + \infty} \hat{v}_z e^{-i\omega t} d\omega, \quad (4.50)$$

where the integration path, ζ is chosen in such a way that the integration line is above all singularities of the integrand.

In order to calculate the above integral we consider the closed contour in the complex plane, as shown in figure (4.1). Accordingly, the contour is made up of the straight line from $\omega = i\zeta - R$, to $\omega = i\zeta + R$ and the half circle, C of radius R , joining these two points. The radius of the semi-circle, R is chosen to be large enough that the zeros of $D(\omega)$, which give the poles of $A(\omega)$, are within the contour. By performing integration over the contour and considering the simple poles at ω_{\pm} , we obtain that

$$\left(\int_C + \int_{i\zeta - R}^{i\zeta + R} \right) \hat{v}_z e^{-i\omega t} d\omega = -2\pi i \left[\text{res}_{\omega_-} (\hat{v}_z e^{-i\omega t}) + \text{res}_{\omega_+} (\hat{v}_z e^{-i\omega t}) \right], \quad (4.51)$$

where $\text{res}_{\omega_{\pm}}$ are the residues at the poles, ω_{\pm} , given by the the formula,

$$\text{res}_{\omega_{\pm}} = \lim_{\omega \rightarrow \omega_{\pm}} [(\omega - \omega_{\pm}) \hat{v}_z e^{-i\omega t}]. \quad (4.52)$$

By considering the integral over the half-circle, it may be shown that, as $R \rightarrow \infty$, the integral along the semi-circle vanishes, i.e.

$$\int_C \hat{v}_z e^{-i\omega t} d\omega \rightarrow 0. \quad (4.53)$$

Thus, the integral, (4.50) is given by $-2\pi i$ times the sum of the two residues, given above. When the residues are calculated explicitly, the vertical compo-

nents of the velocity are found (in Appendix A) to be

$$v_z(t, z) = e^{\omega_i t} \left\{ e^{-i\omega_r t} \left[U_{1+} e^{kz} + W_{1+} \exp \left(\frac{[\omega_i - i(kv_{A-} \cos \theta + \omega_r)]z}{v_{A-} \sin \theta} \right) \right] - e^{i\omega_r t} \left[U_{1-} e^{kz} + W_{1-} \exp \left(\frac{[\omega_i - i(kv_{A-} \cos \theta - \omega_r)]z}{v_{A-} \sin \theta} \right) \right] \right\} \quad (4.54)$$

for $z < 0$, and

$$v_z(t, z) = e^{\omega_i t} \left\{ e^{-i\omega_r t} \left[U_{2+} e^{-kz} - W_{2+} \exp \left(-\frac{[\omega_i + i(kv_{A+} \cos \theta - \omega_r)]z}{v_{A+} \sin \theta} \right) \right] - e^{i\omega_r t} \left[U_{2-} e^{-kz} - W_{2-} \exp \left(-\frac{[\omega_i + i(kv_{A+} \cos \theta + \omega_r)]z}{v_{A+} \sin \theta} \right) \right] \right\}, \quad (4.55)$$

for $z > 0$, where $U_{1,2\pm}$ and $W_{1,2\pm}$ are given by the expressions,

$$U_{1\pm} = \frac{\rho_+ \omega_{\pm} G(\omega_{\pm})(v_{A-} - v_{A+})(\omega_{\pm} + kv_{A+} e^{i\theta})}{2\omega_r(\rho_- + \rho_+)(\omega_{\pm} + kv_{A-} e^{-i\theta})}, \quad (4.56)$$

$$U_{2\pm} = \frac{\rho_- \omega_{\pm} G(\omega_{\pm})(v_{A+} - v_{A-})(\omega_{\pm} - kv_{A-} e^{-i\theta})}{2\omega_r(\rho_- + \rho_+)(\omega_{\pm} - kv_{A+} e^{i\theta})}, \quad (4.57)$$

$$W_{1\pm} = \frac{G(\omega_{\pm})v_{A-}(v_{A+} - v_{A-})}{2\omega_r(\rho_- + \rho_+)(v_{A-} + v_{A+})(\omega_{\pm} + kv_{A-} e^{-i\theta})} \times [(\rho_- + \rho_+) \omega_{\pm}^2 + 2ik\omega_{\pm} \rho_+ v_{A+} \sin \theta - 2k^2 \rho v_A^2 e^{-i\theta} \cos \theta], \quad (4.58)$$

$$W_{2\pm} = \frac{G(\omega_{\pm})v_{A+}(v_{A+} - v_{A-})}{2\omega_r(\rho_- + \rho_+)(v_{A-} + v_{A+})(\omega_{\pm} - kv_{A+} e^{i\theta})} \times [(\rho_- + \rho_+) \omega_{\pm}^2 + 2ik\omega_{\pm} \rho_- v_{A-} \sin \theta - 2k^2 \rho v_A^2 e^{i\theta} \cos \theta]. \quad (4.59)$$

The horizontal component of the velocity, v_x , can also be found by using the incompressibility condition, (4.6), with the determined expressions for v_z , (Eqs. 4.54 and 4.55). These solutions are clearly in Fourier form, as were the results for the previous chapter. This confirms that our assumption in the previous chapter, that solutions would be proportional to $e^{-i\omega t}$, was valid.

The given solutions are not valid, unless the resultant waves have been allowed a sufficiently large period of time to transit outwardly from the interface. Hence, an MHD wave in a given position may only be valid at time, t , which exceeds the time taken to reach that position, t_m . Similarly, the solutions at some arbitrary value of time, t , will only exist in the region encompassing the interface, $|z| < z_m$. This is explicitly given by the conditions,

$$0 < z \leq tv_{A+} \sin \theta, \quad \text{or} \quad -tv_{A-} \sin \theta \leq z < 0. \quad (4.60)$$

The above relations are identical to the conditions imposed for y_B , given in Eq. (4.24) to be convergent.

4.4 Small Inclination Angle Approximation

In order to more easily make comparisons with the previous chapter, we now consider the case of a small inclination angle, $\theta \ll 1$, so that the magnetic field is close to horizontal. In this approximation (as in the previous chapter), we take $\sin \theta \approx \theta$ and $\cos \theta \approx 1$. Then, it follows from Eqs. (4.48) and (4.49) that a linear approximation in θ of the zeros of $D(\omega)$ results in

$$\omega_r = kC_k + \mathcal{O}(\theta^2), \quad \omega_i = -k\theta\Gamma + \mathcal{O}(\theta^3), \quad (4.61)$$

where

$$C_k^2 = \frac{2\rho v_A^2}{\rho_- + \rho_+}, \quad \Gamma = \frac{\rho_- v_{A-} + \rho_+ v_{A+}}{\rho_- + \rho_+}. \quad (4.62)$$

It is clear that the phase speed of waves is independent on the inclination of the magnetic field (in the leading order), however, the attenuation rate is proportional to the inclination angle. Furthermore, in this small-inclination angle limit, the expressions for $U_{1,2\pm}$ and $W_{1,2\pm}$ reduce to

$$U_{1\pm} = U_{2\pm} = \pm \frac{1}{2} v_{z0}(0) + \mathcal{O}(\theta), \quad (4.63)$$

$$W_{1\pm} = W_{2\mp} = \frac{i\theta v_{z0}(0) C_k (v_{A+} - v_{A-})}{2(C_k \mp v_{A-})(C_k \pm v_{A+})} + \mathcal{O}(\theta^2). \quad (4.64)$$

Using the above expressions, the small angle approximations for the vertical velocity in leading order is thus

$$v_z(t, z) = e^{\omega_i t} v_{z0}(0) \cos(kC_k t) \begin{cases} e^{kz}, & z < 0, \\ e^{-kz}, & z > 0. \end{cases} \quad (4.65)$$

Using the incompressibility condition we can find that the expression of the x -component of the velocity, v_x , can be found to be

$$v_x(z, t) = \tilde{v}_x(z, t) + \bar{v}_x(z, t), \quad (4.66)$$

where

$$\tilde{v}_x(z, t) = ie^{\omega_i t} v_{z0}(0) \cos(kC_k t) \begin{cases} e^{kz}, & z < 0, \\ -e^{-kz}, & z > 0, \end{cases} \quad (4.67)$$

and

$$\bar{v}_x(z, t) = \frac{i}{2} e^{\omega_i t} v_{z0}(0) C_k (v_{A+} - v_{A-}) \begin{cases} u_-, & z < 0, \\ u_+, & z > 0, \end{cases} \quad (4.68)$$

where the expressions for u_{\pm} , in the solution for \bar{v}_x above, are given by

$$u_- = \frac{1}{v_{A-}} \exp \left[-kz \left(\frac{\Gamma}{v_{A-}} + \frac{i}{\theta} \right) \right] \times \left(\frac{\exp[-ikC_k(t + z/\theta v_{A-})]}{C_k + v_{A+}} + \frac{\exp[ikC_k(t + z/\theta v_{A-})]}{C_k - v_{A+}} \right), \quad (4.69)$$

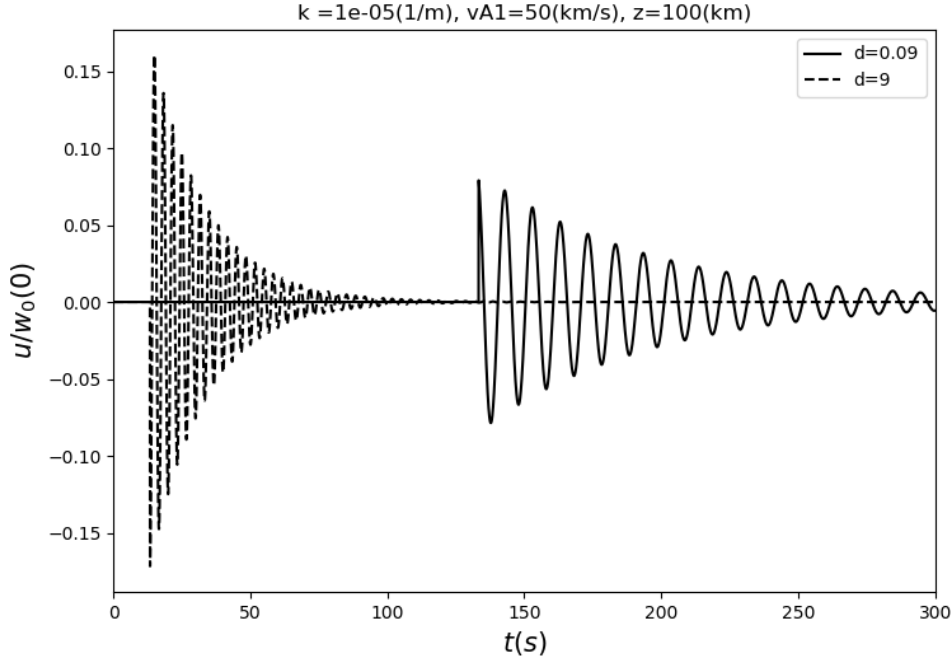


Figure 4.2: The variation of the real part of horizontal velocity, v_x , with respect to time, 100 km above the interface, for two values of density ratio, $d = 0.09, 9$. The inclination angle is take to be $\theta = 5^\circ$

$$u_+ = \frac{1}{v_{A+}} \exp \left[kz \left(\frac{\Gamma}{v_{A+}} - \frac{i}{\theta} \right) \right] \times \left(\frac{\exp [-ikC_k(t - z/\theta v_{A+})]}{C_k - v_{A-}} + \frac{\exp [ikC_k(t - z/\theta v_{A+})]}{C_k + v_{A-}} \right). \quad (4.70)$$

Similar expressions may be found for the magnetic field perturbations, by using Equations (4.7 and 4.8).

Solutions obtained for v_x over time are shown in Figure 4.2. For $t < t_m$, solutions are not plotted, as the physical velocity is unknown, since the present analysis is only valid for $t > t_m$. As expected, we see that waves decay over time, due to the lateral energy leakage. The time taken for the waves to attenuate to e^{-1} of the original amplitude is

$$t_d = -1/\omega_i = \frac{1}{\theta k v_{A-}} \frac{d+1}{d + \sqrt{d}}. \quad (4.71)$$

This gives a quicker decay rate for greater Alfvén speed, as well as for greater inclination angle, θ . This emphasises once again that the attenuation of the waves is due to the inclination of the magnetic field. However, the decay rate is slower for higher values of d , which means that the attenuation is much more pronounced if the magnetic field is tilted towards the denser plasma, than if the field is tilted towards the less dense plasma. This implies that MHD waves in this system have a preferential propagation direction. In other words, given the wavenumber and decay rate of a wave in a system with known Alfvén speed

	$d = 10$	$d = 0.1$
$v_{A-} = 100 \text{ km s}^{-1}$	$t_d = 9.6 \text{ s}$	$t_d = 30.3$
$v_{A-} = 50 \text{ km s}^{-1}$	$t_d = 19.2 \text{ s}$	$t_d = 60.5$
$v_{A-} = 10 \text{ km s}^{-1}$	$t_d = 96 \text{ s}$	$t_d = 303 \text{ s}$

Table 4.1: The attenuation times for different values of Alfvén speed, for an inclination angle of $\theta = 5^\circ$ and a typical wavenumber of 10^{-5} m^{-1} .

and density ratio, it would be possible to infer the orientation as well as the magnitude of field inclination.

Some values of attenuation time for different Alfvén speeds are shown in Table (4.1). We see that that for chromospheric Alfvén speeds, attenuation times may be less than 10s. These values show that the lateral wave leakage due to the inclination of magnetic field can be a very effective way to damp waves; particularly when Alfvén speeds are high.

4.5 Comparison to Tangential Solutions

In order to fully understand the implication of wave propagation at contact discontinuity, we now compare the expressions for the leaky modes, found above, with the expressions for surface waves propagating along a tangential discontinuity. In what follows, we use the subscript ‘ t ’ to indicate quantities corresponding to the surface MHD wave on the tangential discontinuity. By taking the limit $\theta \rightarrow 0$ in Eq.(4.19), we can find that the tangential solution for the Laplace transformed vertical velocity is

$$\hat{v}_{zt} = \frac{1}{\omega^2 - k^2 v_{At\pm}^2} \left[i\omega v_{z0} \pm ik\omega \frac{A}{\rho_{\pm}} \right]. \quad (4.72)$$

By applying the condition of continuity of v_z , the remaining jump condition for a tangential discontinuity, we find that

$$A_t(\omega) = \frac{k v_{z0} \rho_+ \rho_- (v_{A-}^2 - v_{A+}^2)}{(\rho_+ + \rho_-) \omega^2 - 2\rho_- v_{A-}^2 k^2}. \quad (4.73)$$

By using the same contour integration introduced previously, it may be shown that

$$v_{zt} = \lim_{\theta \rightarrow 0} v_z, \quad v_{xt} = \lim_{\theta \rightarrow 0} \tilde{v}_x, \quad (4.74)$$

Since $\tilde{v}_x \not\rightarrow 0$ we conclude that $v_x \not\rightarrow v_{xt}$ as $\theta \rightarrow 0$. Hence, only v_z tends to the corresponding quantity in a tangential discontinuity, while v_x does not. This implies that there is no continuous transition from the leaky mode on the contact discontinuity to the surface wave on the tangential discontinuity.

When $\theta \ll 1$ the z -dependence of v_x is highly spatially oscillatory, with the oscillation wavelengths equal to

$$L_{1+} = \frac{2\pi\theta v_{A-}}{k(C_k + v_{A-})}, \quad L_{1-} = \frac{2\pi\theta v_{A-}}{k|C_k - v_{A-}|} \quad (4.75)$$

for $z < 0$, and

$$L_{2+} = \frac{2\pi\theta v_{A+}}{k(C_k + v_{A+})}, \quad L_{2-} = \frac{2\pi\theta v_{A+}}{k|C_k - v_{A+}|} \quad (4.76)$$

for $z > 0$. These wavelengths tend towards zero, as $\theta \rightarrow 0$, making the solutions hugely oscillatory and so difficult to compare directly to the tangential solution.

We will now introduce a different definition of continuous transition, in terms of an average value of a function $f(z)$, introduced in Ruderman, Vickers, Ballai and Erdélyi (2018), and defined to be

$$\langle f \rangle = \frac{k}{2\sqrt{\theta}} \int_{z-\theta^{1/2}/k}^{z+\theta^{1/2}/k} f(z') dz'. \quad (4.77)$$

This describes an average over a small transitional layer, with width proportional to $\sqrt{\theta}$. The choice of the averaging interval, equal to $k^{-1}\theta^{1/2}$, is somewhat arbitrary. Instead of $\theta^{1/2}$, we can choose any quantity that is much smaller than unity and much larger than θ , when $\theta \ll 1$. Applying this averaging technique to v_x , we find, to lowest order of θ ,

$$\langle \tilde{v}_x \rangle = ie^{\omega_i t} v_{z0}(0) \cos(kC_k t) \begin{cases} e^{kz}, & kz < -\theta^{1/2}, \\ -\theta^{-1/2}kz, & k|z| \leq \theta^{1/2}, \\ -e^{-kz}, & kz > \theta^{1/2}, \end{cases} \quad (4.78)$$

$$\langle \bar{v}_x \rangle = \frac{1}{4}\theta^{1/2}e^{-\gamma t}v_{z0}(0)C_k(v_{A+} - v_{A-}) \begin{cases} \Upsilon_1, & kz < -\theta^{1/2}, \\ \Upsilon_t, & k|z| \leq \theta^{1/2}, \\ \Upsilon_2, & kz > \theta^{1/2}. \end{cases} \quad (4.79)$$

This gives the average horizontal velocity over a small height. The quantities Υ_1 , Υ_2 , and Υ_t are found, through long but straightforward calculations, and are given in the Appendix B.

It follows from Eq.(4.79) that, for any value of z , $\langle \bar{v}_x \rangle \rightarrow 0$ as $\theta \rightarrow 0$. However, it also follows from the expressions for Υ_1 and Υ_2 that $\max_z |\langle \bar{v}_x \rangle| \rightarrow \infty$ as $|z| \rightarrow \infty$, while θ is fixed. Hence, the convergence of $\langle \bar{v}_x \rangle$ to zero is non-uniform with respect to z .

From Eq. (4.78) we can also see that $\langle \tilde{v}_x \rangle = \tilde{v}_x = v_{xt}$ for $kz \geq \theta^{1/2}$. Hence,

$$\langle v_x \rangle = \langle \tilde{v}_x \rangle + \langle \bar{v}_x \rangle \rightarrow v_{xt}, \quad \text{as } \theta \rightarrow 0$$

and $z \neq 0$. Summarising, we can state that the difference between $\langle v_x \rangle$ and v_{xt} is of the order of $\theta^{1/2}$ except for a transitional layer, surrounding the interface, of thickness of the order of $\theta^{1/2}$ when $\theta \ll 1$ and z is sufficiently small. It follows from the expressions for Υ_1 and Υ_2 that the latter condition is equivalent to $k|z| \ll 1$. Hence, $\langle v_x \rangle \approx v_{xt}$ for $\theta^{1/2} \ll k|z| \ll 1$.

In Figure (4.3), we compare v_x , $\langle v_x \rangle$ and v_{xt} with respect to distance from the interface, z , displaying both the real and imaginary parts of the solutions. We see how the averaged velocity $\langle v_x \rangle$, approximately connects the solutions for the tangential discontinuity, across a boundary layer of width $2\sqrt{\theta}$, while

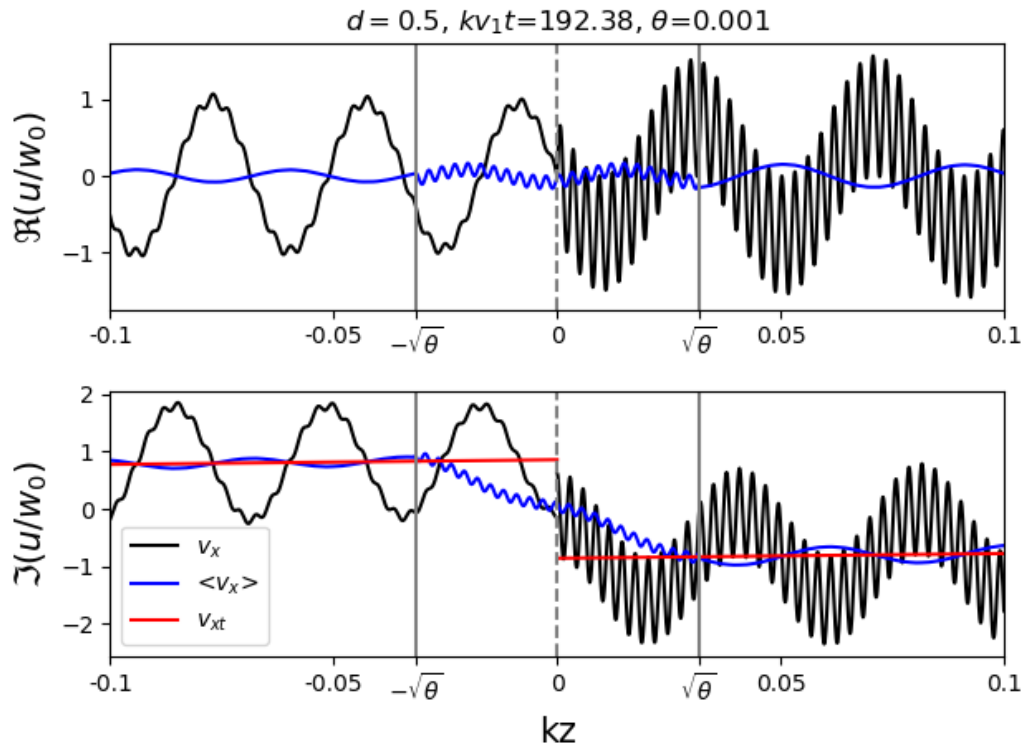


Figure 4.3: The real and imaginary parts of the velocity, v_x , the tangential solution for the velocity, u_t and the averaged velocity, $\langle v_x \rangle$, with respect to dimensionless height, kz , across the interface, for $\theta = 0.001$, $d = 0.5$ and kv_1t being the value for the 25th peak.

also giving an approximation of the velocity, v_x . For this value of θ , the average value over the boundary layer is highly oscillatory within the boundary layer, but the magnitude of these oscillations is proportional to $\theta^{1/2}/k$, so a smaller θ would lead to a more linear solution, across a smaller boundary region and would thus be comparable to the tangential solution.

4.6 x -dependent solutions

In order to find how solutions vary in the direction of the wave propagation, we must perform inverse Fourier transforms of the velocities. Since the velocity $\mathbf{v}(x, z, t)$ must be real, we know that $\mathbf{v}(-k, z, t) = \mathbf{v}^*(k, z, t)$, where f^* denotes the complex conjugate of f . By splitting the integral into positive and negative ranges for k , we may rewrite the inverse Fourier transform as

$$v(x, z, t) = \frac{1}{2\pi} \int_0^\infty [e^{ikx}v(k, z, t) + e^{-ikx}v^*(k, z, t)] dk. \quad (4.80)$$

Inserting the expressions for $v_z(k, z, t)$ from Eq. (4.65) into the above integral we find,

$$v_z(x, z, t) = \frac{1}{\pi} \int_0^\infty v_{z0}(k)e^{-k(|z|+\theta\Gamma t)} \cos(kC_k t) \cos(kx) dk. \quad (4.81)$$

The above equation can be used together with particular initial conditions to find the temporal evaluation of the wave along the x -axis. A similar calculation may be performed to obtain the x -dependent form of the horizontal component of velocity, v_x , but these calculations are not presented here.

4.6.1 Delta-function driver

We first use an initial solution in the form of a delta-function, $v_{z0}(x) = \pi a \delta(x)$, where a is a positive constant with the dimension of the velocity. The delta function can be thought of as the limit of a very short, but strong impulse acting on the system. Such localised and impulsive sources are plentiful in the solar physics, occurring over a very large spectrum of energies, e.g. Coronal Mass Ejections, flares of different energies, surges, and, in general, phenomena that are related to reconnections of oppositely oriented magnetic fields. As a result of such interaction, sudden energy releases (in form of e.g. shocks) take place. Such events can take place in any region of the solar atmosphere. Strictly speaking the delta-function (also known as the Dirac-delta function) is not a function in the normal sense as it is zero everywhere, except when $x = 0$, where the function is infinite. However, given its property, the delta-function can be a very useful function to evaluate integrals of the type shown by Eq. (4.81), as

$$\int_{-\infty}^{\infty} f(x)\delta(x-a)dx = f(a)$$

In reality, though, such very narrow drivers do not exist and this restriction will be relaxed later by considering a wider driver. The delta-function as a driver

has been used widely in solar physics application. For instance, Sutmann et al. (1998) investigated the initial value problem of the generation of slow sausage modes in gravitationally stratified plasmas and found that an initial delta-function pulse decays at a rate proportional to $t^{-3/2}$. In a similar fashion, Ballai et al. (2008) considered the generation of kink oscillations in coronal loops by the interaction of EIT global waves with individual coronal loops. In the first instance the EIT wave has been approximated by a delta-function pulse.

The delta-function perturbation gives a constant value in k -space, $v_{z0}(k) = \pi a l$. Straightforward calculations then result in

$$v_z(x, z, t) = \frac{a}{2}(\Gamma\theta t + |z|) \left[\frac{1}{(\Gamma\theta t + |z|)^2 + (C_k t - x)^2} + \frac{1}{(\Gamma\theta t + |z|)^2 + (C_k t + x)^2} \right]. \quad (4.82)$$

We can see that the above solution (Eq. 4.82) is a superposition of two signals, one propagating in the positive x -direction and the other in the negative x -direction with the phase speed C_k , while dispersing outwards in the z -direction, with phase-speed $\theta\Gamma$. As expected the result of a delta-function driver results in a signal that does not oscillate, however the impulsive driver generates a pulse that decays in intensity with time, due to energy leakage. The vertical velocity is symmetric either side of the interface. However the region in which this solution is physical (satisfying the condition in Eq. 4.60), has boundaries which propagate at speeds proportional to the Alfvén speed either side of the interface.

The solution also decays as $\mathcal{O}(t^{-1})$ as $t \rightarrow \infty$, as the energy “leaks” away and it is proportional to the angle θ . We should also note that, the solution to the initial value problem when written in terms of position, rather than wavenumber, decays as $|z| \rightarrow \infty$, unlike the oscillatory form, when given in terms of wavenumber.

4.6.2 Lorentz function driver

While a delta function may be a useful approximation of a large perturbation, centred at one position, there can never be a physical perturbation that is exactly a delta-function, since an infinite amplitude perturbation at a point, with infinitesimal width would be impossible. As a more physical initial condition, we now consider the Lorentz function, which has the form

$$v_{z0}(x) = \frac{al^2}{x^2 + l^2}, \quad (4.83)$$

where a once again is a constant velocity and l is a length describing the width of the initial perturbation. This profile has finite magnitude and non-zero width and, therefore, constitutes a much more realistic driver than the delta-function. In many applications it is much more convenient to use a Lorentz function driver than the standard Gaussian function as the Lorentz function

has a much simpler form (compared to the exponential form of the Gaussian function), and the two functions show a very close similarity.

The Fourier transform of the driver function is

$$v_{z0}(k) = \pi a l e^{-lk}. \quad (4.84)$$

Then it follows from Eq. (4.65) that

$$v_z(k, z, t) = \pi a l \cos(k C_k t) \exp[-k(|z| + l + \theta \Gamma t)]. \quad (4.85)$$

Again, after a straightforward calculation, we obtain

$$v_z(x, z, t) = \frac{al}{2} (\Gamma \theta t + |z| + l) \times \left[\frac{1}{(\Gamma \theta t + |z| + l)^2 + (C_k t - x)^2} + \frac{1}{(\Gamma \theta t + |z| + l)^2 + (C_k t + x)^2} \right]. \quad (4.86)$$

Similar to the case corresponding to the delta-function initial condition, this solution is also symmetric across the interface. The vertical velocity is shown in the region of the (x, z) -plane for which the above function is physical, for different times in Figure (4.4), for an inclination angle of 5° . The velocities are relatively low, since the initial amplitude was small, with $a = 1 \text{ kms}^{-1}$. The behaviour of v_z is quite similar to that given by Eq. (4.82) and it is a superposition of two perturbations propagating in the opposite directions with the phase speed C_k . The wave front decays with time as t^{-1} , confirming the attenuation of the waves, due to energy leakage. The amplitude also decays with the distance from the interface, as we would expect from a physical wave propagating away from an initial perturbation.

We also note that the expression given by Eq. (4.86) is almost equivalent to that given by Eq. (4.82), when $l = 0 \text{ km}$, apart from the factor of l . This property is in agreement with the fact that $l^2/(x^2 + l^2) \rightarrow \pi \delta(x)$ as $l \rightarrow 0$.

4.6.3 Sinusoidal Driver

We finally consider an initial condition, which is not centred with an intense amplitude at only one x -position and instead take a *sinusoidal* driver along the entire range of x , with $v_{z0}(x) = e^{i\kappa x}$, for some initial wavenumber, κ , which we assume is positive. This driver models a wave-like initial perturbation, which would be most applicable to modelling how an interface evolves after waves have developed (rather than an initial sinusoidal “kick” to the interface). This particular form of the driver gives an initial perturbation in terms of k of $v_{z0}(k) = 2\pi \delta(k - \kappa)$.

Using the method of finding components of velocity, shown before, we can find that

$$v_z(x, z, t) = 2e^{-\kappa(|z| + \theta \Gamma t)} \cos(\kappa C_k t) \cos(\kappa x). \quad (4.87)$$

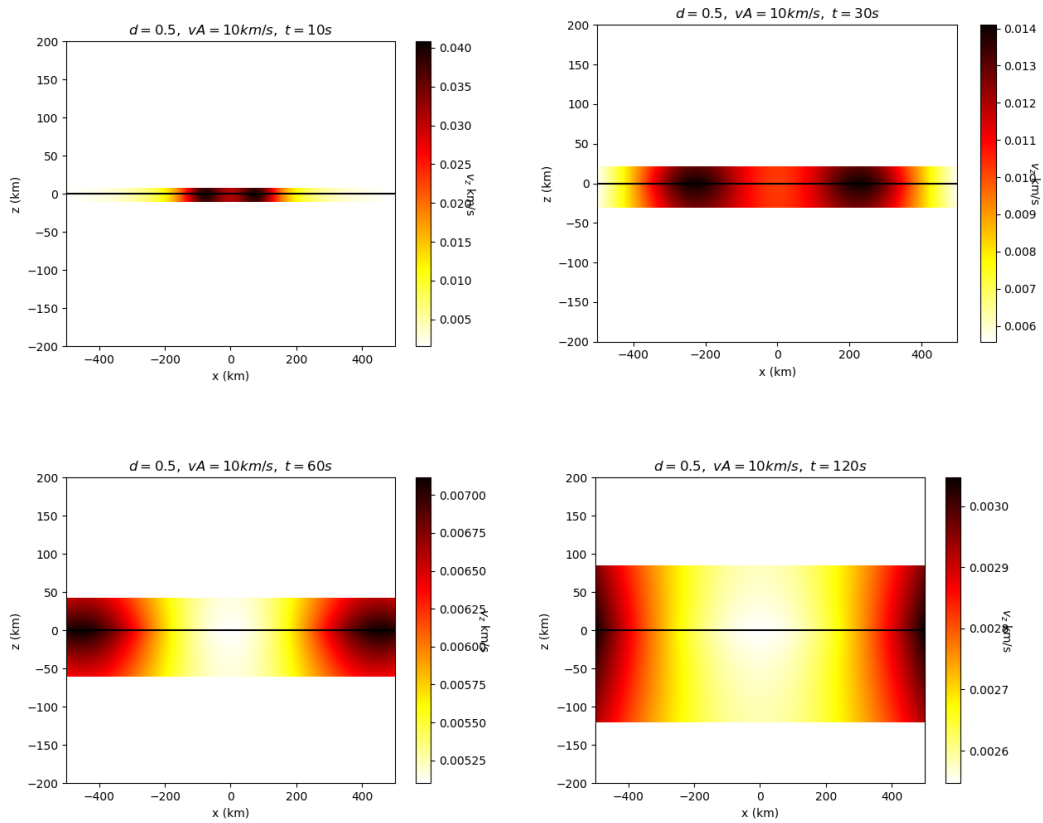


Figure 4.4: An intensity plot showing the vertical component of velocity in the (x, z) -plane over a minute, when subject to a Lorentzian driver, for $\theta = 5^\circ$, $d = 0.5$, $v_{A-} = 10 \text{ km s}^{-1}$, $a = 1$ and $l = 50 \text{ km}$. Solutions are only plotted in the region where $|z| < z_m(t)$.

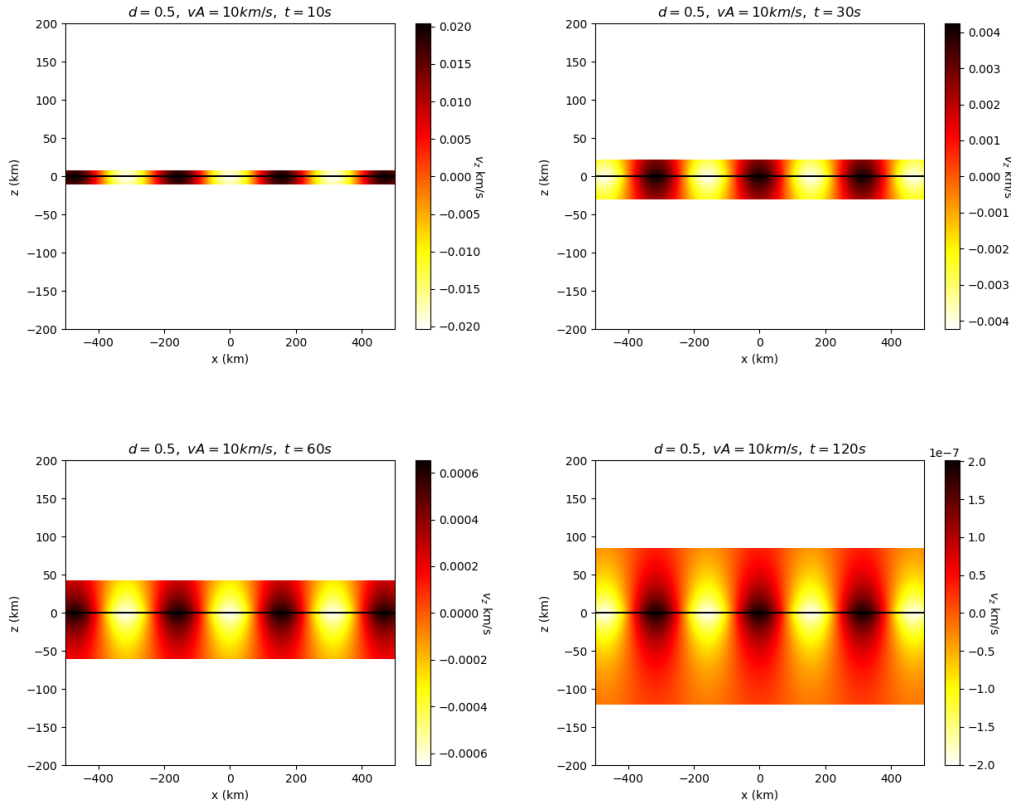


Figure 4.5: An intensity plot showing the vertical component of velocity in the (x, z) -plane over a minute, when subject to a sinusoidal initial driver, for $\theta = 5^\circ$, $d = 0.5$, $v_{A-} = 10 \text{ km s}^{-1}$, $a = 1$ and $l = 50 \text{ km}$. Solutions are only plotted in the region where $|z| < z_m(t)$.

We note that in this case the wave propagating along the interface decays in time as e^{-t} , confirming the leaky nature of the waves, while also decaying exponentially as $|z| \rightarrow \infty$. However, since the initial driver is not centred on one value, the solution does not ripple out along the x -axis in the same way as the solution for delta function or Lorentzian initial conditions.

The time for the amplitude of these MHD waves to decay to $1/e$ of the initial value, the attenuation time is independent of the initial kick and is simply given by $1/(\Gamma\theta\kappa)$. Hence, as $\theta \rightarrow 0$, the attenuation time tends towards infinity, which gives us an intuitive understanding as to why MHD waves along a tangential discontinuity do not display attenuation, while waves along a contact discontinuity do. By replacing k by κ , we obtain the formula for attenuation time given by Eq. (4.71) and so for $\kappa = 10^{-5} \text{ m}^{-1}$, we achieve the attenuation times given by Table (4.1).

Finally, we point out that in order to derive Eqs. (4.82), (4.86) and (4.87) we used Eq. (4.65), which is only valid when the conditions given by Eq. (4.60) are satisfied. Taking into account that Eq. (4.65) is derived for $\theta \ll 1$, we conclude that Eqs. (4.82) and (4.86) are only valid when the following conditions are

satisfied:

$$t \geq \frac{z_m}{\theta} \max \left(\frac{1}{v_{A-}}, \frac{1}{v_{A+}} \right), \quad -t\theta v_{A-} \leq z \leq t\theta v_{A+}. \quad (4.88)$$

We recall that z_m is determined by the condition that $v_{z0}(z) = 0$ for $|z| \geq z_m$, while there is such $z \in (-z_m, z_m)$ that $v_{z0}(z) \neq 0$.

4.7 Conclusions

This chapter confirmed many of the results of the previous chapter, including the leaky nature of waves, causing attenuation, while further providing an explicit description of the wave dynamics in terms of time and positions, for possible initial conditions.

While the previous chapter used an eigenmode analysis to study waves at a contact discontinuity, this chapter explored the same configuration as an initial value problem, for the incompressible case. Since compressibility was neglected, magnetic tension was the only restoring force, so only one mode was present, reducing the complexity of the problem as compared with the compressible case, allowing time-dependent analytical solutions to be found. The solution was obtained using a Laplace transform and the initial perturbations were assumed to be localised to the interface. These Laplace-transformed solutions were then inverted using a contour integration to achieve solutions for perturbations in terms of wavenumber and time. Solutions are only determined in the interval $-tv_{A-} < z < tv_{A+}$, proportional to the time it takes perturbations to propagate away from the interface.

We, once again, showed that leaky modes were present when the equilibrium magnetic field was inclined. The amplitudes of these modes exponentially decay with time and exponentially increase with the distance from the contact discontinuity, showing that the contact discontinuity supports qualitatively different modes than the tangential discontinuity. Moreover, as with the time-independent case, the amplitude of the modes were oscillatory in z and the wavelength of these amplitude oscillations is proportional to the inclination angle, so becomes highly spatially oscillatory for small inclination of the magnetic field. As previously, this suggested that there is no smooth transition to the tangential case, however, by introducing an average with respect to z over an interval of length $2\sqrt{\theta}/k$, we showed that the averaged quantities tend to the tangential solutions as $\theta \rightarrow 0$.

By performing inverse Fourier transforms, we found solutions in terms of position, rather than wavenumber, for some possible initial perturbations. This provides some examples of how leaky modes at surface discontinuities may appear in physical observations of the solar atmosphere. Two of the examples of initial conditions used were a Lorentz function and a delta function, which have a large initial amplitude centred at one position. The delta-function pulse has been used previously to model both kink and sausage waves in coronal structures, started by an impulsive event (see Sutmann et al. 1998, Ballai et al. 2008) The solutions with delta-function and Lorentz-function initial drivers

could also model waves along the transition region, excited by the buffeting from spicules, below, such as in the model of transition region quakes, described by Scullion et al. (2011). The third initial condition example was sinusoidal, providing a possible model for contact discontinuities, in many solar structures, when incident with an MHD waves, such as those produced throughout the solar atmosphere after large-scale CMEs and related events. However, the sinusoidal initial perturbation may be more relevant as a model of how an interface evolves after waves have developed. All of these solutions, for all three initial conditions, clearly show wave attenuation over time; as there are no outside energy sources or sinks and there are no other methods of energy dissipation are present, this must clearly be due to energy leaking outwards. Using typical solar atmospheric values we found that the attenuation of waves due to wave leakage is very effective. The region in which these solutions are physical propagates outwards over time, as do the velocity perturbations, which demonstrate the energy flow away from the interface, while, for a given time, the amplitude exponentially decays away from the interface.

CHAPTER 5

An Introduction to Instabilities

The hydrodynamic Rayleigh-Taylor instability (RTI), first explored by Rayleigh (1900) and later by Taylor (1950), for the incompressible case in the context of fluid dynamics, concerns the instability of an interface, separating two fluids with different properties, where a dense fluid is supported above a lighter fluid, in the presence of a vertical gravitational force. The Magnetic Rayleigh-Taylor (MRT) instability was studied for the case of a horizontal magnetic field by (e.g. Kruskal and Schwarzschild 1954, Parker 1966). The magnetic field in this case was found to provide a stabilising effect to perturbations propagating in the direction of the magnetic field, by supplying magnetic tension, which counteracts buoyancy. The magnetic field also introduces a preferential direction, as perturbations perpendicular to the magnetic field are not supported by magnetic tension and so are analogous to the hydrodynamic case. The particular effect of inclination on wave propagation, with respect to magnetic field direction, was most notably investigated by Chandrasekhar (1961).

Over the years, many advances have been made in the theory of MRT instabilities that helped to understand its complex properties. Among other effects, compressibility has been widely investigated (Vandervoort 1961, Shivamoggi 1982, Bernstein and Book 1983, Ribeyre et al. 2004) and is in general found to stabilise against MRT instability. Recently developments have been made to analyse the effect of sheared magnetic fields (Ruderman et al. 2014, Ruderman 2017). The growth time of unstable modes was found to be dependent on the shear angle and, by using the growth rate of instabilities, the shear angle of observed prominences was determined, using an estimation of the Alfvén speed and lifetimes of the prominence threads. Partial ionisation has also been introduced into the models describing the generation of MRT instability in the lower part of the atmosphere (Díaz et al. 2014, Ruderman, Ballai, Khomenko and Collados 2018), and the results show that, in partially ionised plasmas, the interface becomes unstable for all wavelengths, provided the plasma is partially ionised on both sides of the interface.

Interest in MRT instabilities has grown recently, due to their many applications in an astrophysical context. For example, the filamentary structure of the Crab Nebula, could well be due to Rayleigh-Taylor instability, as was corroborated by comparisons made by Hester et al. (1996) between the observed structuring and MRT instability simulations, made by Jun and Norman (1995). Other examples of where MRT instabilities may develop are in supernovae (Jun

et al. 1996, Chevalier 1982), accretion discs (Wang and Nepveu 1983, Kulkarni and Romanova 2008), buoyant magnetic bubbles in galaxies (Robinson et al. 2004, Jones and De Young 2005) and relativistic jets (Matsumoto and Masada, 2013).

Of particular note to the present thesis, there are many examples where MRT may be at work in the solar atmosphere. Isobe suggested (Isobe et al. 2005, Isobe et al. 2006) that the “fingers” that develop in MRT instabilities are responsible for the filamentary structure in emerging flux regions. Most notably, solar prominences are likely to become Rayleigh-Taylor unstable, since they are composed of cool, dense plasma, suspended above much lighter plasma. Filamentary threads of prominences were modelled analytically by Terradas et al. (2012), who found that the MRT instability caused filaments in quiescent prominences to have very short lifetimes, but that in active regions, the magnetic tension may be sufficient to stabilise these prominences. MRT instabilities in observed prominences have been investigated by Ryutova et al. (2010) to explain plumes and even to determine the magnetic field strength from the wavelength and growth rate of instabilities. This was expanded upon by (Innes et al., 2012), who used the critical wavelength to estimate the Alfvén speed, and (Carlyle et al., 2014), who used a most unstable mode analysis to find the magnetic field strength, in fragmenting eruptions of filaments. For a more comprehensive review, see Hillier (2018).

5.1 Gravitational Instabilities

When a sharp interface separates a dense fluid, above, from a less dense fluid, below, the Rayleigh-Taylor instability may occur. When a magnetic field is present in a plasma, with a horizontal component, the magnetic tension helps to support the plasma against gravity. However, over a threshold density ratio (for a given wavenumber), or under a threshold wavenumber (for a given density ratio), the system is still prone to instabilities: a magnetic variation on the Rayleigh-Taylor instability. This is sometimes referred to as either the Parker instability, if the wave-vector, \mathbf{k} is parallel to the magnetic field (see Parker 1966), or the Kruskal-Schwarzschild instability, if \mathbf{k} is perpendicular to the magnetic field, as well as gravity (see Kruskal and Schwarzschild 1954).

Although we intend to study the possibility of magnetic Rayleigh-Taylor instability generation at a contact discontinuity (later in Chapter 6), it is important to understand the manifestations of other instabilities in order to separate any effects of these from our results and to focus solely on RTI. For instance, the collapse seen in the Jeans’ instability may appear similar to the downward “fingers” of the RTI, also, the continuing motion of perturbations in convective instabilities may seem like plasma motions either side of the RTI, depending on the direction of perturbations, since the onset of instabilities may all appear similar.

In order to understand the way this important instability appears and what the effects of different physical parameters are in its development, we are going to briefly review the family of gravity-induced instabilities. In a plasma where

gravitational effects may not be ignored, there are three predominant kinds of instabilities that may arise: Rayleigh-Taylor, Convective and Gravitational instabilities.

Gravitational instabilities occur where a plasma collapses under its own weight. The simplest case is that of a homogeneous plasma, known as the Jeans instability, which occurs primarily in interstellar gas clouds (Jeans, 1902). However, since this is due to the height dependence of gravity and it is customary to only consider self-gravity when discussing Jeans instability, it will not be considered further in the present work.

5.1.1 Convective instabilities

The second form of instability that may be present are convective instabilities. These occur in plasmas where the stratification is insufficient to stabilise the buoyancy force. In a homogeneous plasma this has the effect that, if a plasma element is displaced upwards, it will continue to rise, with the rest of that column of plasma, uninhibited. This sort of instability is thought to operate in the solar convective zone, helping the hot plasma at the base of the region to rise against gravity and form the granular pattern on the solar surface.

A vertically stratified, non-magnetic, fluid is convectively stable if the Brunt-Väisälä frequency, N satisfies the condition $N^2 > 0$, where

$$N^2 = -g \left(\frac{1}{\rho} \frac{\partial \rho_0}{\partial z} + \frac{g}{c_s^2} \right),$$

where gravitational stratification is taken to occur in the z -direction. In a magnetized plasma, this frequency is modified by the magnetic field. In the case of a horizontal magnetic field, this frequency was determined previously by Chen and Lykoudis (1972) and for the more general case of an inclined magnetic field in a spherical coordinate system, the value of N was found by Ershkovich and Israelevich (2000). The derivation given by the latter is repeated here, for a Cartesian geometry, where linearisation has not been applied.

The Lorentz force acting upon a plasma element is given by

$$\mathbf{F}_L = (\nabla \times \mathbf{B}) \times \mathbf{B} / \mu_0 = -\frac{1}{2\mu_0} \nabla B^2 + \frac{1}{\mu_0} (\mathbf{B} \cdot \nabla) \frac{\mathbf{B}}{B},$$

where \mathbf{B} is the total magnetic field. If there is primarily inhomogeneity in the z -direction only (e.g. due to gravitational stratification), the equilibrium field would depend mostly on z , therefore $(\mathbf{B} \cdot \nabla) \mathbf{B} \approx B_z \partial B / \partial z$, where B_z is the component of magnetic field in the z -direction. This approximation will be used to find an expression for the magnetic Brunt-Väisälä frequency, under the assumption that inhomogeneity perpendicular to gravity is negligible.

The momentum equation for a plasma in hydrostatic equilibrium is

$$-\nabla p + \mathbf{F}_L + \rho \mathbf{g} = 0.$$

By using the expression for the Lorentz force given above, we are able to find that the z-component of the momentum balance gives,

$$\frac{dp}{dz} = -\frac{1}{\mu_0}B\frac{dB}{dz} + \frac{1}{\mu_0}\frac{B_z^2}{B}\frac{dB}{dz} - \rho g = -v_{A_h}^2\frac{\rho}{B}\frac{dB}{dz} - \rho g, \quad (5.1)$$

where $v_{A_h}^2 = (B^2 - B_z^2)/\mu_0\rho$.

If we consider a plasma element, which is subject to a small vertical, translational perturbation, ξ from the equilibrium, in the z direction, the change in pressure within the plasma element is given by

$$\delta p_{in} = c_s^2\delta\rho_{in} = -v_{A_h}^2\frac{\rho}{B}\frac{dB}{dz}\xi - \rho g\xi,$$

where δp_{in} and $\delta\rho_{in}$ are the changes in pressure and density, respectively within the plasma element and c_s is the sound speed. Due to the frozen-in nature of the magnetic field, \mathbf{B}/ρ is conserved, hence

$$c_s^2\delta\rho_{in} = -v_{A_h}^2\delta\rho_{in} - \rho g\xi.$$

Therefore, the change in density inside the plasma element is

$$\delta\rho_{in} = -\frac{\rho g\xi}{c_s^2 + v_{A_h}^2}.$$

On the other hand, the change in density outside of the perturbed element is simply

$$\delta\rho_{out} = \frac{d\rho}{dz}\xi.$$

Using Archimedes' law, which states that the buoyancy force for a fluid element is given by $g(\delta\rho_{out} - \delta\rho_{in})$, the motion of the displaced plasma element is described by

$$\rho\frac{d^2\xi}{dt^2} + g\left(\frac{\partial\rho_0}{\partial z} + \frac{g\rho}{c_s^2 + v_{A_h}^2}\right)\xi = 0.$$

This equation describes oscillations of the fluid element, with a frequency given by the magnetically modified Brunt-Väisälä frequency,

$$N_B^2 = -g\left(\frac{1}{\rho}\frac{\partial\rho_0}{\partial z} + \frac{g}{c_s^2 + v_{A_h}^2}\right). \quad (5.2)$$

For the inclined field case, considered in this thesis, the equilibrium magnetic field is given by $\mathbf{B}_0 = B_0(\cos\theta, 0, \sin\theta)$. Hence, the magnetic Brunt-Väisälä is given by,

$$N_B^2 = -g\left(\frac{1}{\rho}\frac{\partial\rho_0}{\partial z} + \frac{g}{c_s^2 + v_A^2\cos^2\theta}\right). \quad (5.3)$$

The criterion for convective stability is simply that N_B^2 , given in Eq. (5.3), is positive. This may equivalently be written,

$$-\frac{d\rho_0}{dz} > \frac{\rho_0^2 g}{\gamma p_0 + B_t^2}, \quad (5.4)$$

where B_t is the tangential component of the magnetic field, i.e. $B_t^2 = B_x^2 + B_y^2$. The Brunt-Väisälä frequency for the magnetic case is higher than the corresponding value for the fluid case, which means that the magnetic field stabilises the system against convective instability. If we assume that on the local scale, stratification is negligible, i.e. $\frac{d\rho_0}{dz} \rightarrow 0$, the above criterion is not satisfied, so for a homogeneous plasma there must be convective instability. The maximum growth rates, given by the imaginary part of the frequency, are found in Newcomb (1960) to be

$$\max(\Im(\omega)) = \left\{ \frac{g}{\rho} \left(\frac{\rho^2 g}{\gamma p + B_t^2} + \frac{d\rho}{dz} \right) \right\}^{1/2} \quad \text{if} \quad -\frac{d\rho}{dz} < \frac{\rho^2 g \gamma p}{(\gamma p + B_t^2)^2}, \quad (5.5)$$

$$\max(\Im(\omega)) = \left\{ \frac{\rho g}{B_t^2} \left[1 - \left(\frac{-\gamma p}{\rho^2 g} \frac{d\rho}{dz} \right)^{1/2} \right]^2 \right\}^{1/2} \quad \text{if} \quad \frac{\rho^2 g \gamma p}{(\gamma p + B_t^2)^2} < -\frac{d\rho}{dz} < \frac{\rho^2 g}{\gamma p}. \quad (5.6)$$

Thus, for the homogeneous case,

$$\max(\omega_I^2) = \frac{\rho g^2}{\gamma p + B_t^2}.$$

Hence, we have two necessary conditions to test whether a given instability is convective. Firstly, if Eq. (5.4) is not satisfied, then there is instability. Secondly, the growth rate of the instability must not exceed the values given by Eqs. (5.5) and (5.6). If either one of these conditions are not satisfied, the instability cannot be generated due to convection.

5.2 Hydrodynamic Rayleigh-Taylor Instabilities

Now let us consider the Rayleigh-Taylor instability in detail. The most straightforward case of the Rayleigh-Taylor instability is that of the purely hydrodynamic case, where two homogeneous incompressible fluids are separated by a sharp horizontal interface. We take gravity to act in the negative z -direction, i.e. $\mathbf{g} = -g\hat{\mathbf{z}}$, and the interface to be situated at $z = 0$.

In the absence of a magnetic field, linear fluid dynamics are described by the two equations

$$\frac{\partial \rho}{\partial t} + \mathbf{v} \cdot \nabla \rho_0 = 0, \quad (5.7)$$

$$\rho_0 \frac{\partial \mathbf{v}}{\partial t} = -\nabla p - \rho g \hat{\mathbf{z}}, \quad (5.8)$$

that should be considered together with the incompressibility condition,

$$\nabla \cdot \mathbf{v} = 0. \quad (5.9)$$

Perturbations are assumed to be wavelike in the (x, y) -plane, so are of the form $f = \hat{f} \exp[i(k_x x + k_y y - \omega t)]$, where, as usual, \hat{f} is the amplitude of an

arbitrary perturbation, that can depend on z and the background density is dependent only on height, $\rho_0 = \rho_0(z)$. Hence, the governing equations are written in terms of components as,

$$-i\omega\hat{\rho} + \hat{v}_z \frac{\partial \rho_0}{\partial z} = 0 \quad (5.10)$$

$$i\omega\rho_0\hat{v}_x = ik_x\hat{p}, \quad (5.11)$$

$$i\omega\rho_0\hat{v}_y = ik_y\hat{p}, \quad (5.12)$$

$$i\omega\rho_0\hat{v}_z = \frac{\partial \hat{p}}{\partial z} + \hat{\rho}g. \quad (5.13)$$

Applying the same ansatz to the incompressibility condition results in

$$i(k_x\hat{v}_x + k_y\hat{v}_y) + \frac{\partial \hat{v}_z}{\partial z} = 0. \quad (5.14)$$

We multiply Eq.(5.11) by ik_x and Eq.(5.12) by ik_y , sum the two and use Eq.(5.14), to obtain,

$$i\omega\rho_0 \frac{\partial \hat{v}_z}{\partial z} = k^2\hat{p}, \quad (5.15)$$

where $k^2 = k_x^2 + k_y^2$. Substituting expressions for $\hat{\rho}$ and \hat{p} given by Eqs. (5.10) and (5.15) into the z -component of the momentum equation, Eq. (5.13), the *governing equation* is found to be

$$\frac{\partial}{\partial z} \left(\rho_0 \frac{\partial \hat{v}_z}{\partial z} \right) - k^2 \rho_0 \hat{v}_z = \frac{gk^2}{\omega^2} \hat{v}_z \frac{\partial \rho_0}{\partial z}. \quad (5.16)$$

The *gravitational scale-height* of the medium, H , gives a measure of how quickly the pressure and density change with height. In an isothermal atmosphere, $H = c_s^2/g$ and the height-dependence of density is given as

$$\rho_0(z) = \rho_0(z=0) \exp\left(\frac{-z}{H}\right). \quad (5.17)$$

If the vertical length scales of perturbations in the system are small compared to the scale-height, the fluid may be considered *locally homogeneous* and so the density (and pressure) may be considered as constants on the small scale. This allows us to take $\rho'_0 \rightarrow 0$, so Eq. (5.16) reduces to

$$\frac{\partial^2 \hat{v}_z}{\partial z^2} - k^2 \hat{v}_z = 0,$$

which has solutions $\hat{v}_z \sim e^{\pm kz}$. Further, requiring that solutions are evanescent far away from the interface, we obtain

$$\hat{v}_z = \begin{cases} A_- e^{kz}, & z < 0, \\ A_+ e^{-kz}, & z > 0, \end{cases} \quad (5.18)$$

where the amplitudes A_- and A_+ will be determined by imposing the necessary boundary conditions at the interface.

The requirement that the component of velocity perpendicular to the interface is continuous across the interface, gives that $A_- = A_+$. Further, integrating Eq. (5.16) with respect to z across the boundary, the second jump condition is found to be

$$\left[\left[\rho_0 \frac{\partial \hat{v}_z}{\partial z} \right] \right] = \frac{gk^2}{\omega^2} \hat{v}_z \llbracket \rho_0 \rrbracket. \quad (5.19)$$

This is equivalent to the condition for continuity of pressure across the interface, given in Section (2.3). Very often, in hydrodynamics these jump conditions (or boundary conditions) are called the kinematic and dynamic boundary conditions. Using the solutions found above (Eq. 5.18), the frequency of the waves is given by

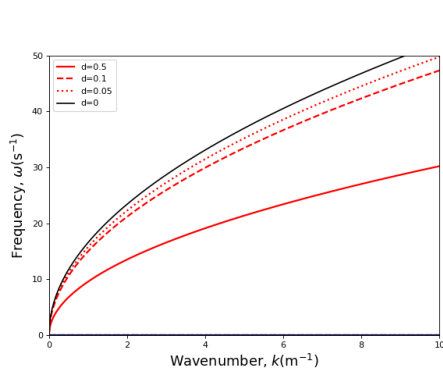
$$\omega = \pm \sqrt{-gk \frac{\rho_+ - \rho_-}{\rho_+ + \rho_-}}. \quad (5.20)$$

This expression becomes imaginary if $\rho_+ > \rho_-$. Thus, rather unsurprisingly, the system is unstable if the upper fluid is denser. The growth-rate is higher, the greater the difference between the two densities, though this is reduced as the total of the two densities increases. This is seen more clearly if we introduce the density ratio, $d = \rho_-/\rho_+$, so that the frequency is given by

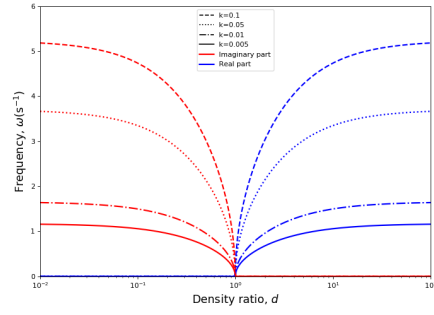
$$\omega = \pm \sqrt{-gk \frac{1-d}{d+1}}. \quad (5.21)$$

There is a limiting value as $d \rightarrow 0$, since the instability rate cannot be higher than that due to pure gravitational acceleration of a fluid parcel. It may also be seen, from the above expression for ω , that the system is more unstable to short wavelength perturbations. These two results are illustrated in the plots shown in Figure (5.1).

It is clear that the growth rate of the instability increases with the wavenumber, for any density ratio, and all rates are smaller than the limiting value we obtain for $d \rightarrow 0$. In the right-hand side panel we plot the variation of the frequency for a large spectrum of density ratio, and for several values of the wavenumber, k . The RT instability occurs when $d < 1$ (the left-hand side branch or curves, shown in red), while the right-hand side branch (curves shown in blue) correspond to propagating surface gravity waves, that propagate with no amplification due to gravity .



(a) Imaginary part of the frequency of hydrodynamic Rayleigh-Taylor instability as a function of wavenumber, for varying density ratio. The limit of $d \rightarrow 0$ is shown in black.



(b) Frequency of hydrodynamic Rayleigh-Taylor instability as a function of density ratio, for several wavenumber values. The propagating modes, corresponding to $d > 1$ are purely real and are plotted in blue. The RT unstable modes are purely imaginary and are shown in red.

Figure 5.1: Solutions for the hydrodynamic RTI and propagating modes, in terms of wavenumber and density ratio.

5.3 Stability of a Plasma Supported by a Horizontal Magnetic field

Since the present thesis deals with solar plasmas, where magnetic fields play a crucial role, we will expand this introductory section to review some characteristics of the RTI in the presence of magnetic fields, and here we will discuss the properties of this instability when the ambient magnetic field is horizontal and vertical, i.e. parallel and perpendicular to the density interface. The case of RTI in the presence of a horizontal magnetic field was first investigated by Kruskal and Schwarzschild (1954). The following derivation is based on that presented in Chandrasekhar (1961).

The background magnetic field is set to be horizontal and parallel to the interface, i.e. $\mathbf{B}_0 = B_0 \hat{\mathbf{x}}$, and the gravity is taken to be in the negative z -direction, i.e. $\mathbf{g} = -g \hat{\mathbf{z}}$ (see Fig.5.2). The linearised, incompressible, ideal MHD equations for this situation (once again taking perturbations to be of the form $f = \hat{f} \exp[i(k_x x + k_y y - \omega t)]$) are,

$$-i\omega \hat{p} + \hat{v}_z \frac{\partial \rho_0}{\partial z} = 0, \quad (5.10)$$

$$-i\omega \rho_0 \hat{v}_x = -ik_x \hat{p}, \quad (5.11)$$

$$-i\omega \rho_0 \hat{v}_y + \frac{B_0}{\mu} [ik_y \hat{b}_x - ik_x \hat{b}_y] = -ik_y \hat{p}, \quad (5.22)$$

$$-i\omega \rho_0 \hat{v}_z = -\frac{\partial \hat{p}}{\partial z} - \frac{B_0}{\mu} \left[\frac{\partial \hat{b}_x}{\partial z} - ik_x \hat{b}_z \right] - \hat{\rho} g \hat{\mathbf{z}}, \quad (5.23)$$

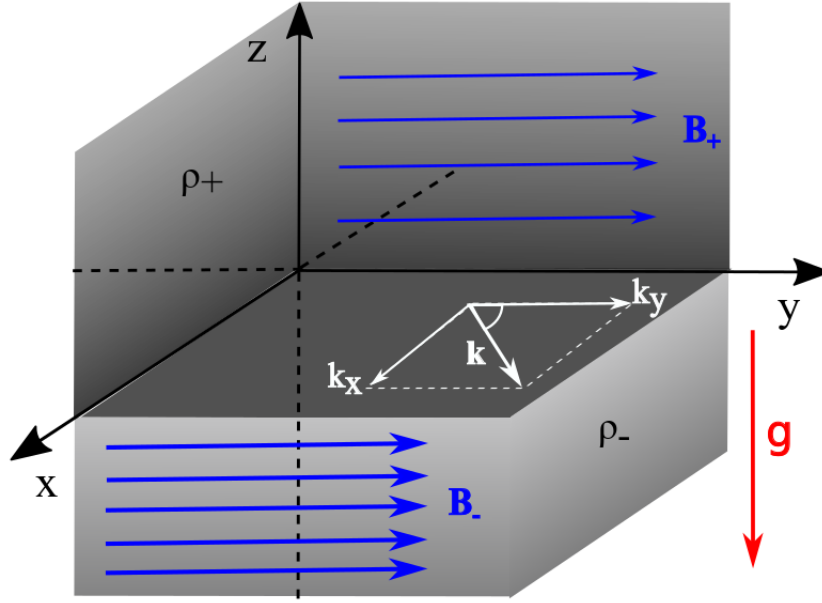


Figure 5.2: A sketch of the equilibrium configuration for the case of a horizontal magnetic field. The equilibrium state consists of a surface separating two regions, each with different density. The magnetic field is horizontal and uniform in each region. The configuration is invariant in the x - and y -directions and perturbations are in the direction of the wavevector \mathbf{k} in the (x, y) -plane.

$$-i\omega\hat{\mathbf{b}} = ik_x B_0 \hat{\mathbf{v}}, \quad (5.24)$$

$$ik_x \hat{v}_x + ik_y \hat{v}_y + \frac{\partial \hat{v}_z}{\partial z} = ik_x \hat{b}_x + ik_y \hat{b}_y + \frac{\partial \hat{b}_z}{\partial z} = 0. \quad (5.25)$$

By using the condition of incompressibility, as well as the solenoidal constraint (given by Eq.5.25), we may write the y -components of the velocity and magnetic field perturbation in terms of the x and z -components as,

$$\hat{v}_y = \frac{i}{k_y} \left(ik_x \hat{v}_x + \frac{\partial \hat{v}_z}{\partial z} \right), \quad \hat{b}_y = \frac{i}{k_y} \left(ik_x \hat{b}_x + \frac{\partial \hat{b}_z}{\partial z} \right), \quad (5.26)$$

and so the y -component of the momentum equation, Eq. (5.22) becomes

$$\frac{\omega}{k_y} \rho_0 \left(ik_x \hat{v}_x + \frac{\partial \hat{v}_z}{\partial z} \right) + \frac{B_0}{\mu} \left[ik_y \hat{b}_x + \frac{k_x}{k_y} \left(ik_x \hat{v}_x + \frac{\partial \hat{v}_z}{\partial z} \right) \right] = -ik_y \hat{p}. \quad (5.27)$$

Using equations (5.10), (5.11) and (5.22), we can find the expressions for $\hat{\rho}$, \hat{p} and $\hat{\mathbf{b}}$, in terms of $\hat{\mathbf{v}}$ and, therefore, the y and z -components of the momentum equation are found to be,

$$-i \frac{k^2}{k_x} \left[k_x^2 \frac{B_0^2}{\mu} - \rho_0 \omega^2 \right] \hat{v}_x = \left[k_x^2 \frac{B_0^2}{\mu} - \rho_0 \omega^2 \right] \frac{\partial \hat{v}_z}{\partial z}, \quad (5.28)$$

$$\left[i\omega^2 \rho_0 - ik_x^2 \frac{B_0^2}{\mu} + ig \frac{\partial \rho_0}{\partial z} \right] \hat{v}_z = \frac{\omega^2}{k_x} \frac{\partial}{\partial z} (\rho_0 \hat{v}_x) - \frac{B_0^2 k_x}{\mu} \frac{\partial \hat{v}_x}{\partial z}. \quad (5.29)$$

Equation (5.28) simplifies to give that

$$\hat{v}_x = i \frac{k_x}{k^2} \frac{\partial \hat{v}_z}{\partial z},$$

so we may formulate Eq.(5.29) in terms of v_z alone as the *governing equation*,

$$\frac{\partial}{\partial z} \left[\rho_0 \frac{\partial \hat{v}_z}{\partial z} \right] - \frac{k_x^2 B_0^2}{\mu \omega^2} \left[\frac{\partial^2}{\partial z^2} - k^2 \right] \hat{v}_z - k^2 \rho_0 \hat{v}_z = \frac{gk^2}{\omega^2} \hat{v}_z \frac{d\rho_0}{dz}. \quad (5.30)$$

After comparing this governing equation with Eq. (1.17), it is clear that the second term in the above equation is the addition due to the presence of the magnetic field.

We now consider the situation when a horizontal interface separates two plasmas, which may each be taken to be *locally homogeneous*. The densities either side of the interface are thus given by ρ_- in the lower region and ρ_+ in the upper region and are taken to be constants, close to the interface (locally homogeneous). In the two plasma regions, Eq. (5.30) becomes,

$$(\omega^2 - k_x^2 v_A^2) \left[\frac{\partial^2 \hat{v}_z}{\partial z^2} - k^2 \hat{v}_z \right] = 0, \quad (5.31)$$

which, similar to the hydrodynamic case, has evanescent solutions in the form $v_z = A_{\pm} e^{\pm kz}$, where, again, the two coefficients, A_{\pm} will be determined once boundary conditions at the interface are applied and the \pm subscript denotes values below ($z < 0$) and above ($z > 0$) the interface. Using the continuity of v_z across the interface, $A_+ = A_- = A$ and so the surface wave solutions are

$$\hat{v}_z = A \begin{cases} e^{kz}, & z < 0, \\ e^{-kz}, & z > 0. \end{cases} \quad (5.32)$$

Integrating Eq. 5.30 across the boundary we arrive at

$$\left[\rho_0 \frac{\partial \hat{v}_z}{\partial z} \right] - \frac{k_x^2 B_0^2}{\mu \omega^2} \left[\frac{\partial \hat{v}_z}{\partial z} \right] = \frac{gk^2}{\omega} \hat{v}_z(z=0) \llbracket \rho_0 \rrbracket. \quad (5.33)$$

This equation is identical to the condition we would obtain by imposing the continuity of pressure in the presence of gravity (see Section (2.3)). Substituting in the solutions (5.32) and rearranging, we find,

$$\omega^2 = \frac{gk(\rho_- - \rho_+)}{\rho_- + \rho_+} + \frac{2k_x^2 B_0^2}{\mu(\rho_- + \rho_+)}. \quad (5.34)$$

Once again, using the density ratio, $d = \rho_-/\rho_+$, and also using the Alfvén speed, $v_{A-} = \sqrt{B_0^2/\mu\rho_-}$, this stability criterion may be written as,

$$\omega^2 = -\frac{gk(1-d)}{d+1} + \frac{2dk_x^2 v_{A-}^2}{d+1}. \quad (5.35)$$

Since the second term of the above relation is strictly positive, we see that the magnetic field has a stabilising effect, with a higher magnetic field strength

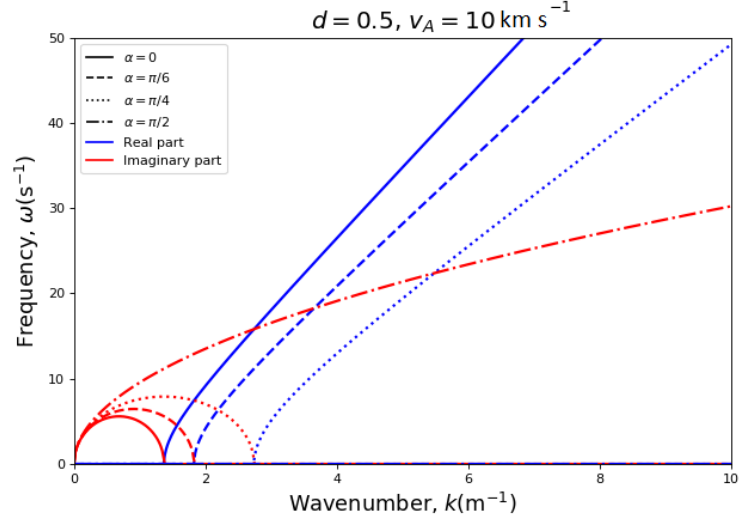


Figure 5.3: Frequency of waves in the presence of a horizontal magnetic field, in terms of wavenumber. The real part of solutions is shown in blue and the imaginary part in red, while solutions for different propagation directions are shown with different line-styles.

reducing the growth rate, if it is unstable. This result is easy to understand, as the horizontal magnetic field is (through the magnetic tension) opposing perturbations in the vertical direction, in a similar manner to surface tension in a hydro-dynamic case.

For perturbations in the x -direction, (i.e. $k_y = 0$, $k = k_x$), the magnetic field also reduces the range of k values for which instability exists. It must now be in the range

$$0 < k < \frac{g(1-d)}{2dv_{A-}^2},$$

if the system is to remain unstable. For any given value of k , there is a much stricter condition on the densities for instability to take place than for the hydrodynamic case, i.e,

$$\rho_+ > \rho_- + \frac{2k^2v_A^2}{gk}.$$

However, when $k_x = 0$, so $k = k_y$, the stability criterion is identical to the hydrodynamic case. Thus, we see that the direction of the perturbations also has an effect on the stability. In order to make this clearer, we introduce α , to indicate the angle between the wave vector \mathbf{k} and the x -axis, so that $k_x = k \cos \alpha$ and $k_y = k \sin \alpha$. The numerical analysis of the above stability criterion is shown in Fig. (5.3). It is clear that there is always a critical wavenumber, k_c , below which waves are RT unstable. For $k > k_c$, waves are propagating. For the y -propagating case, we see that $k_c = 0$, like the hydrodynamic case. Similar to the hydrodynamic case, here we introduced α as the angle between the ambient magnetic field and the direction of propagation.

5.4 Stability of Plasma Permeated by a Vertical Magnetic Field

While the previous section has given us an understanding of the effect of a magnetic field on Rayleigh-Taylor instabilities at a tangential discontinuity, this thesis is concerned with contact discontinuities. We therefore need to consider the case of a magnetic field with a component intersecting the interface. We begin with the simplest magnetic field configuration for a contact discontinuity, i.e. the case where the magnetic field is purely perpendicular to the interface and parallel to gravity. Hence, using the same gravitational field configuration as before, $\mathbf{g} = -g\hat{\mathbf{z}}$, and the background magnetic field is now taken to be $\mathbf{B}_0 = B_0\hat{\mathbf{z}}$. Once again, this instability is considered at an interface between two homogeneous plasmas, with the denser plasma supported above the sparser plasma ($\rho_- < \rho_+$). This problem has been considered initially by Chandrasekhar (1961) (among others), and key points of the derivation are repeated here for completeness.

When written in terms of Fourier expanded components, the linearised, incompressible, ideal MHD equations for this case, in the incompressible limit in the presence of a vertical magnetic field, are

$$-i\omega\hat{\rho} + \hat{v}_z\rho'_0 = 0 \quad (5.10)$$

$$-i\omega\rho_0\hat{v}_x = -ik_x\hat{p} + \frac{B_0}{\mu} \left(\frac{\partial\hat{b}_x}{\partial z} - ik_x\hat{b}_z \right), \quad (5.36)$$

$$-i\omega\rho_0\hat{v}_y = -ik_y\hat{p} + \frac{B_0}{\mu} \left(\frac{\partial\hat{b}_y}{\partial z} - ik_y\hat{b}_z \right), \quad (5.37)$$

$$-i\omega\rho_0\hat{v}_z = -\frac{\partial\hat{p}}{\partial z} - \hat{\rho}g, \quad (5.38)$$

$$-i\omega\hat{\mathbf{b}} = B_0\frac{\partial\hat{\mathbf{v}}}{\partial z}, \quad (5.39)$$

where $\rho'_0 = \partial\rho_0/\partial z$. The above system of equation has to be supplemented by the incompressibility condition, $\nabla \cdot \mathbf{v} = 0$ and the solenoidal constraint, $\nabla \cdot \mathbf{b} = 0$.

For a locally homogeneous plasma, the above equations may be combined, using a similar method as for the horizontal magnetic field, into the *governing equation*,

$$\left(\frac{\partial^2}{\partial z^2} - k^2 \right) \left(v_A^2 \frac{\partial^2}{\partial z^2} + \omega^2 \right) (\hat{v}_z) = 0. \quad (5.40)$$

The solutions of the above governing equation are of the form $\hat{v}_z \sim e^{\Gamma z}$, where

$$\Gamma = \pm k, \pm \frac{i\omega}{v_A}.$$

We require once again that solutions decay away from the interface. *Instability* rather than attenuation of perturbations is being investigated, so it is assumed that $\Im(\omega) \geq 0$ and so evanescent solutions are given by

$$\hat{v}_z = \begin{cases} A_- e^{kz} + B_- e^{\frac{-i\omega}{v_{A-}}z} & z < 0, \\ A_+ e^{-kz} + B_+ e^{\frac{i\omega}{v_{A+}}z} & z > 0, \end{cases} \quad (5.41)$$

where, again, the \pm subscript refers to solutions above and below the interface and $v_{A\pm}$ denote the Alfvén speeds in the two regions.

This is a contact discontinuity, with gravity taken into account, so the appropriate continuity conditions across the interface are (see the derivation in Section (2.3))

$$\llbracket \hat{v}_z \rrbracket = 0, \quad \llbracket \hat{v}_{\parallel} \rrbracket = 0, \quad \llbracket \hat{b}_z \rrbracket = 0, \quad \llbracket \hat{b}_{\parallel} \rrbracket = 0, \quad \llbracket \left[\frac{\partial \hat{p}}{\partial z} - g\rho_0 \hat{v}_z \right] \rrbracket = 0,$$

where $v_{\parallel} = \sqrt{v_x^2 + v_y^2}$. Using the MHD equations, (5.10), (5.36) - (5.39), these jump conditions can be given in terms of \hat{v}_z as,

$$\begin{aligned} \llbracket \hat{v}_z \rrbracket = 0, \quad \llbracket \left[\frac{\partial \hat{v}_z}{\partial z} \right] \rrbracket = 0, \quad \llbracket \left[\frac{\partial^2 \hat{v}_z}{\partial z^2} \right] \rrbracket = 0, \\ \llbracket \left[g\rho_0 \hat{v}_z - \frac{1}{k^2} \left[\frac{B_0^2}{\mu} \left(\frac{\partial^2}{\partial z^2} - k^2 \right) + \omega^2 \rho_0 \right] \frac{\partial \hat{v}_z}{\partial z} \right] \rrbracket = 0 \end{aligned}$$

Using the solutions, shown by Eq. (5.41) the continuity conditions may be combined into a matrix equation, to give

$$MA = \begin{bmatrix} 1 & 1 & -1 & -1 \\ k & -\frac{i\omega}{v_{A-}} & k & -\frac{i\omega}{v_{A+}} \\ k^2 & -\frac{\omega^2}{v_{A-}^2} & -k^2 & \frac{\omega^2}{v_{A+}^2} \\ \rho_- \left(g - \frac{\omega^2}{k} \right) & \rho_- (g - i\omega v_{A-}) & -\rho_+ \left(g + \frac{\omega^2}{k} \right) & -\rho_- (g + i\omega v_{A+}) \end{bmatrix} \begin{bmatrix} A_- \\ B_- \\ A_+ \\ B_+ \end{bmatrix} = 0. \quad (5.42)$$

Non-trivial solutions of the above system of equations are given by $\det(M) = 0$. This equation may be written explicitly as the *dispersion relation*,

$$(\omega - ikv_{A-}) (\omega - ikd^{1/2}v_{A-}) q = 0 \quad (5.43)$$

where,

$$q = (1+d)\omega^3 + 2ikv_{A-}(d^{1/2}+1)\omega^2 + k[2kv_{A-}^2 + g(d-1)]\omega - 2igk^2v_{A-}(d^{1/2}-1), \quad (5.44)$$

and the density ratio is defined as $d = \rho_-/\rho_+$. As noted by Chandrasekhar (1961), the roots given by $\omega = ikv_{A-}$ and $\omega = ikd^{1/2}v_{A-}$ lead to trivial solutions for velocity. Removing these factors, the remaining cubic polynomial has three solutions, but only one solution has non-negative imaginary part, which

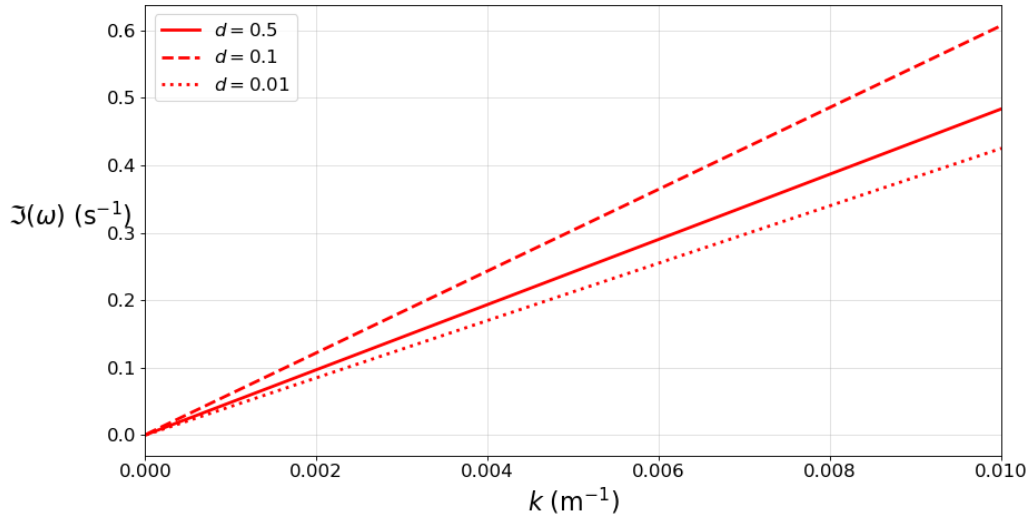


Figure 5.4: Imaginary part of the frequency against wavenumber for the case of vertical magnetic field, i.e. normal to the density interface.

was a necessary condition in the current calculation. This solution is unstable for all values of wavenumber, when the upper plasma is denser, i.e. $d < 1$. In fact, when $d < 1$, this solution has no real part, so is a pure instability, rather than an unstable propagating wave.

Solutions of the only physical root of the equation $q = 0$, for various density ratios, are plotted against wavenumber in Figure (5.4). We can see that the instability rate increases with wavenumber and also increases as d decreases. Unlike the tangential case however, the system is unstable for all wavenumbers, provided $d < 1$. The propagation direction has no effect, since the system is rotationally symmetric with respect to the z -axis.

As $k \rightarrow \infty$ the frequency tends to a fixed value, $\omega \rightarrow (1 - d^{1/2})/\sqrt{1 + d}$, unlike the hydrodynamic case, where ω increases indefinitely with k .

CHAPTER 6

Magnetic Rayleigh-Taylor Instability at a Contact Discontinuity

Despite the horizontal and vertical magnetic field configurations of the MRT instability having been extensively studied by previous authors, little work has been done to investigate the effect of magnetic field inclination on stability of density interfaces. The present chapter is dedicated to the analysis of this case, relevant to several solar applications. For example, arcade-type prominences, with typical “dipped” magnetic field structure, which intersects the denser upper plasma are excellent cases where the stability of contact discontinuities become pertinent, (see Figure 1.4). We will determine the governing equations of wave propagation and analytically calculate the growth rate of instability in terms of equilibrium parameters, for the case of a contact discontinuity, of an incompressible plasma.

Although this is inherently a 3D problem, we will begin with the simpler cases, looking at the problem in two dimensions: considering the problem in the plane of the field inclination (the (x, z) -plane) and perpendicular to this (the (y, z) -plane), separately. These preliminary studies will show clearly some of the important factors at work, that may be obscured in the more complicated three-dimensional case. It will also be useful as a comparison tool, to the fully 3-dimensional case, in order to check it is physically correct.

6.1 x -propagating waves

Initially, we will consider the 2-dimensional case in the (x, z) -plane. Like the equilibrium in Chapter 3, an interface located at $z = 0$, separates the space into two plasma regions of different densities, as

$$\rho_0(z) = \begin{cases} \rho_-, & z < 0, \\ \rho_+, & z > 0. \end{cases} \quad (6.1)$$

This chapter is based on the following submitted journal article:

- Vickers, E., Ballai, I., Erdélyi, R. (2019); Magnetic Rayleigh-Taylor Instability at Contact Discontinuity, *Astron. Astrophys.*, submitted

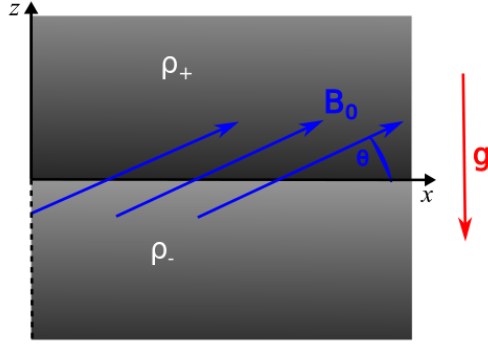


Figure 6.1: 2D sketch of the equilibrium configuration for the case of waves propagating in the x -direction. The equilibrium state consists of a surface separating two regions, each with different density. The magnetic field is uniform throughout both regions and is inclined within the (x, z) -plane at an angle, θ , with respect to the x -direction. The configuration is invariant in the x -direction.

A homogeneous equilibrium magnetic field is, once again, present across the entire space, with field lines inclined at an angle, θ to the interface, with $\mathbf{B}_0 = B_0(\cos \theta, 0, \sin \theta)$. In this situation, gravity also acts in the negative z -direction as $\mathbf{g} = g\hat{\mathbf{z}}$. The schematic representation of the equilibrium configuration is shown in Fig (6.1). As we are currently treating the problem only in 2-dimensions, we take $k_y = 0$ and only consider x and z perturbations, setting $b_y = v_y = 0$. The MHD equations for this case, when supplemented with the incompressibility condition, $\nabla \cdot \mathbf{v} = 0$, are given by

$$\frac{\partial \rho}{\partial t} + \rho'_0 v_z = 0, \quad (5.10)$$

$$\rho_0 \frac{\partial v_x}{\partial t} = -\frac{\partial p}{\partial x} + \frac{1}{\mu} B_0 \sin \theta \left(\frac{\partial b_x}{\partial z} - \frac{\partial b_z}{\partial x} \right), \quad (3.2)$$

$$\rho_0 \frac{\partial v_z}{\partial t} = -\frac{\partial p}{\partial z} + \frac{1}{\mu} B_0 \cos \theta \left(\frac{\partial b_z}{\partial x} - \frac{\partial b_x}{\partial z} \right) - \rho g, \quad (6.2)$$

$$\frac{\partial b_x}{\partial x} + \frac{\partial b_z}{\partial z} = 0, \quad (3.5)$$

$$\frac{\partial b_x}{\partial t} = B_0 \left(\sin \theta \frac{\partial v_x}{\partial z} - \cos \theta \frac{\partial v_z}{\partial x} \right), \quad (3.6)$$

$$\frac{\partial b_z}{\partial t} = B_0 \left(\cos \theta \frac{\partial v_z}{\partial x} - \sin \theta \frac{\partial v_x}{\partial z} \right). \quad (3.7)$$

where $\rho'_0 = d\rho_0/dz$. Most of these equations are identical to the gravity free case considered in Chapter 3, however the continuity equation (5.10) is given in the hydrodynamic RTI case, taking incompressibility and stratification into account, and the z -component of the momentum equation (6.2) is supplemented by gravitational forces.

Once again, we are looking for waves propagating in the x -direction, meaning that all perturbations can be written as, $f = \hat{f} \exp[i(k_x x - \omega t)]$, and this

ansatz is applied here. The x -component of the momentum equation, Eq.(3.2) may be rearranged to give an expression for the perturbation to the pressure,

$$\hat{p} = \frac{\omega}{k_x} \rho_0 \hat{v}_x - \frac{i}{k_x} \frac{B_0}{\mu} \sin \theta \left(\frac{\partial \hat{b}_x}{\partial z} - ik_x \hat{b}_z \right). \quad (6.3)$$

From the mass conservation equation, Eq.(5.10), we can isolate the density perturbation, in terms of the transversal component of velocity, as

$$\hat{\rho} = -\frac{i}{\omega} \rho'_0 \hat{v}_z. \quad (6.4)$$

Next, using the incompressibility condition, $\nabla \cdot \mathbf{v} = 0$, and the solenoidal constraint, $\nabla \cdot \mathbf{b} = 0$, we are able to write the x -components of velocity and magnetic field perturbation in terms of the z -components. Finally, from the z component of the induction equation, Eq.(3.7), we obtain that,

$$\hat{b}_z = -\frac{B_0}{\omega} \left(k_x \cos \theta \hat{v}_z - i \sin \theta \frac{\partial \hat{v}_z}{\partial z} \right). \quad (6.5)$$

We combine all of these expressions for v_x , b_x , b_z , p and ρ , along with the vertical component of the momentum equation (6.2) to achieve the *governing equation*,

$$\begin{aligned} & \sin^2(\theta) \frac{B_0^2}{\mu} \frac{\partial^4 \hat{v}_z}{\partial z^4} + ik_x \frac{B_0^2}{\mu} \sin 2\theta \frac{\partial^3 \hat{v}_z}{\partial z^3} - k_x^2 \frac{B_0^2}{\mu} \frac{\partial^2 \hat{v}_z}{\partial z^2} - ik_x^3 \frac{B_0^2}{\mu} \sin 2\theta \frac{\partial \hat{v}_z}{\partial z} \\ & - k_x^2 \left[\omega^2 \rho_0 - k_x^2 \frac{B_0^2}{\mu} \cos^2 \theta \right] \hat{v}_z = k_x^2 g \frac{d\rho_0}{dz} \hat{v}_z - \omega^2 \frac{\partial}{\partial z} \left(\rho_0 \frac{\partial \hat{v}_z}{\partial z} \right). \end{aligned} \quad (6.6)$$

We will again assume local homogeneity, where the plasma densities either side of the interface, ρ_{\pm} , may be considered to be constants, provided that the length scale of the perturbations are much smaller than the gravitational scale-height. As we are concerned with the conditions required for Rayleigh-Taylor instabilities to occur, we will in particular consider the case where the upper plasma region is heavier, i.e. $\rho_+ > \rho_-$.

Either side of the interface, solutions to the governing equation are of the form $\hat{v}_z \sim e^{\Gamma z}$, with Γz a complex quantity, which describes how the wave amplitude changes away from the interface. After simple algebra, we can find the governing equation in the form

$$(\Gamma^2 - k_x^2)(v_A^2 \sin^2 \theta \Gamma^2 + 2ik_x v_A^2 \sin \theta \cos \theta \Gamma + \omega^2 - k_x^2 v_A^2 \cos^2 \theta) = 0, \quad (6.7)$$

which admits the straightforward solutions,

$$\Gamma = \pm k_x, m_{\pm}$$

where

$$m_{\pm} = \frac{i[\pm\omega - v_A k_x \cos \theta]}{v_A \sin \theta}. \quad (6.8)$$

These solutions represent the pure surface wave and fast-mode components of the perturbation, respectively.

Surface waves are expected to decay away from the interface, so we require that $\Re(\Gamma z) < 0$, such that $v_z \rightarrow 0$ as $z \rightarrow \pm\infty$.

As we are investigating a “top-heavy” equilibrium situation, we expect instabilities to occur and so we restrict our attention to the solutions that correspond to $\Im(\omega) > 0$. This means that for evanescent solutions we use $\Gamma = m_-$, in the lower plasma region, and $\Gamma = m_+$, in the upper region, with the suitable value of Alfvén speed for the region substituted in.

Hence, the surface wave solutions are given by

$$\hat{v}_z = \begin{cases} A_- e^{k_x z} + B_- e^{m_- z} & z < 0, \\ A_+ e^{-k_x z} + B_+ e^{m_+ z} & z > 0. \end{cases} \quad (6.9)$$

The constant coefficients, that appear as amplitudes in the above relations, can be found once the continuity conditions for variables are imposed at the boundary between the two media.

6.1.1 Continuity conditions

From Section (2.3), the continuity conditions across $z = 0$ are given to linear order by

$$[[v_z]] = 0, \quad [[v_x]] = 0, \quad [[b_x]] = 0, \quad [[b_z]] = 0, \quad \left[\left[\frac{\partial p}{\partial t} - g\rho_0 v_z \right] \right] = 0.$$

The above relations may be written in terms of \hat{v}_z alone, as,

$$\begin{aligned} [[\hat{v}_z]] &= 0, \quad \left[\left[\frac{\partial \hat{v}_z}{\partial z} \right] \right] = 0, \quad \left[\left[\frac{\partial^2 \hat{v}_z}{\partial z^2} \right] \right] = 0, \\ \sin^2 \theta \frac{B_0^2}{\mu} \left[\left[\frac{\partial^3 \hat{v}_z}{\partial z^3} \right] \right] + \omega^2 \left[\left[\rho_0 \frac{\partial \hat{v}_z}{\partial z} \right] \right] - k_x^2 g [[\rho_0 \hat{v}_z]] &= 0 \end{aligned} \quad (6.10)$$

Substituting the expressions for \hat{v}_z into the continuity conditions allows us to write the relations in linear form as

$$\begin{bmatrix} 1 & 1 & -1 & -1 \\ k_x & m_- & k_x & -m_+ \\ k_x^2 & m_-^2 & -k_x^2 & -m_+^2 \\ da_- & db_- & -a_+ & -b_+ \end{bmatrix} \begin{bmatrix} A_- \\ B_- \\ A_+ \\ B_+ \end{bmatrix} = M \begin{bmatrix} A_- \\ B_- \\ A_+ \\ B_+ \end{bmatrix} = 0, \quad (6.11)$$

where the quantities used in the expression of matrix L are defined as

$$\begin{aligned} a_- &= \sin^2 \theta k_x^3 v_{A-}^2 - gk_x^2 + k_x \omega^2, & b_- &= \sin^2 \theta m_-^3 v_{A-}^2 - gk_x^2 + m_- \omega^2, \\ a_+ &= -\sin^2 \theta k_x^3 d v_{A-}^2 - gk_x^2 - k_x \omega^2, & b_+ &= \sin^2 \theta m_+^3 d v_{A-}^2 - gk_x^2 + m_+ \omega^2, \end{aligned} \quad (6.12)$$

in terms of the *density ratio*, $d = \rho_-/\rho_+$. For non-trivial solutions, we require that the determinant of the matrix M vanishes, so we have the *dispersion relation*,

$$\det(M) = 0.$$

It is worth noting that m_-/k_x and m_+/k_x , when written in terms of the phase-speed, $c_{ph} = \omega/k_x$, are independent of k_x ,

$$\tilde{m}_- = \frac{m_-}{k_x} = \frac{-i[v_{A-} \cos \theta + c_{ph}]}{v_{A-} \sin \theta}, \quad \tilde{m}_+ = \frac{m_+}{k_x} = \frac{-i[\sqrt{d}v_{A-} \cos \theta - c_{ph}]}{\sqrt{d}v_{A-} \sin \theta}.$$

It is thus possible to re-write the continuity equations, and hence the dispersion relation, in a form, where k_x dependence is only introduced in the gravity terms of the fourth continuity condition. This is expected, since the only inherent length-scale in the system is the gravitational scale-height.

6.1.2 Solutions

The dispersion relation, may be expanded into a polynomial form,

$$(k_x + m_+)(k_x - m_-)Q(\omega) = 0, \quad (6.13)$$

where,

$$\begin{aligned} Q(\omega) = & (d^{1/2} + 1)(d + 1)\omega^3 + 2ik_x d^{1/2} v_{A-} \sin \theta (d^{1/2} + 1)^2 \omega^2 \\ & - (d^{1/2} + 1) [2dv_{A-}^2 k_x^2 + gk_x(d - 1)] \omega - 2ik_x^2 d^{1/2} v_{A-} \sin \theta g(d - 1). \end{aligned} \quad (6.14)$$

The dispersion relation, Eq. (6.13) has five solutions, two of which are the explicit solutions to $k_x - m_- = 0$ and $k_x + m_+ = 0$, i.e.

$$\omega_1 = -k_x v_{A-} \cos \theta + ik_x v_{A-} \sin \theta, \quad \omega_2 = k_x \sqrt{d} v_{A-} \cos \theta + ik_x \sqrt{d} v_{A-} \sin \theta. \quad (6.15)$$

These solutions are linear in k_x and v_{A-} and ω_2 is proportional to \sqrt{d} . However these solutions would lead to the result that the velocity perturbation is given simply by $v_z = A_{\mp} e^{\pm k_x z}$, and the jump conditions would give that $A_- = A_+ = 0$. These trivial solutions are thus neglected in the following analysis.

The three solutions to the cubic polynomial, Q , may be found using the cubic formula, however, due to the complexity of these solutions, they will not be written explicitly. Only one of these three solutions has positive imaginary part and, thus, corresponds to an instability, evanescent from the interface. This solution is shown in figures (6.2) and (6.3) and is the only physical solution, so is the only solution considered subsequently.

In Figure (6.2), the evanescent solution that satisfies the equation, $Q = 0$ is shown in terms of the wavenumber, k_x , along with solutions corresponding to the tangential case, for the same plasma parameters (shown here in green), for comparison. For the sake of completeness we also plot the real part of the solution corresponding to the contact discontinuity (blue lines), but these values are zero. For low wavenumber, the solution for the inclined case is nearly identical to the tangential case, though for higher wavenumber the solutions show a very different behaviour. The tangential solution has a cut-off value k_c (given in the previous Chapter), for the wavenumber, above which solutions

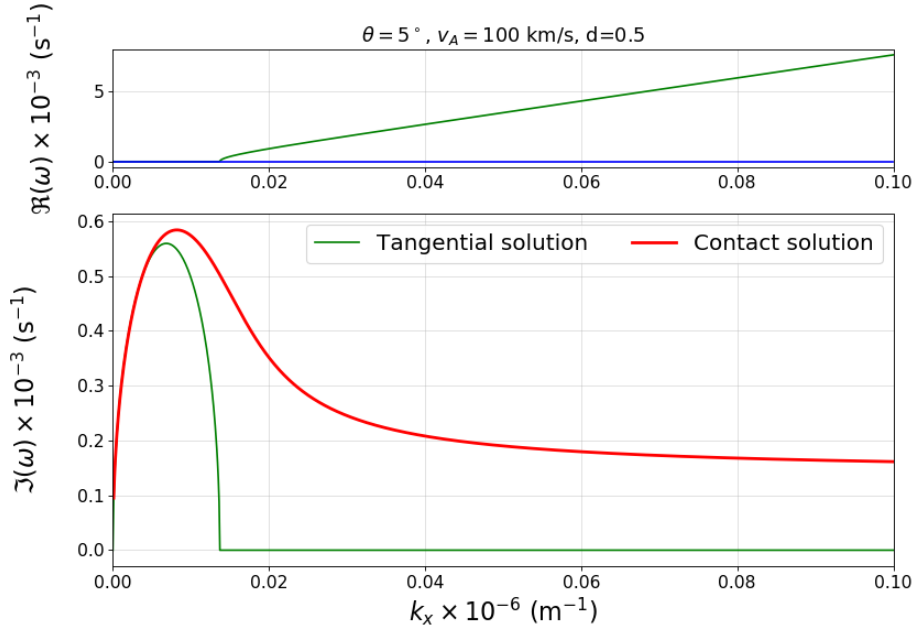


Figure 6.2: Solutions for longitudinally propagating waves, where $d = 0.5$, $v_A = 100 \text{ km s}^{-1}$, $\theta = 5^\circ$. Imaginary part of frequency is plotted in red in lower panel, whereas the real part is shown in blue in the upper panel. The solution to the tangential case is shown in green

are purely propagating and below which solutions are pure instabilities. The solution corresponding to an inclined magnetic field (contact discontinuity) has no such cut-off value: solutions are pure instabilities for all values of k_x , for any inclination angle. Hence, the inclination of the field qualitatively changes the nature of solutions, no longer permitting the presence of propagating waves.

In Figure (6.3) we plot the imaginary part of the physical solution to $Q = 0$, for varying inclination angle, θ , and it shows unstable behaviour for every value of θ . The growth rate increases as the field tends towards vertical, since there is a smaller component of magnetic tension opposing gravity.

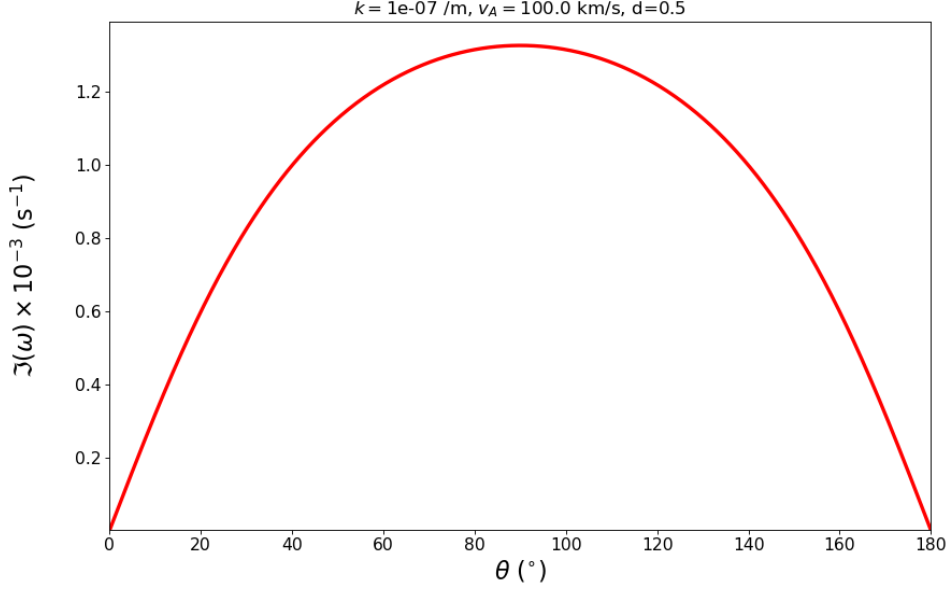


Figure 6.3: Imaginary part of the solution for x -propagating waves, where $d = 0.5$, $v_A = 100 \text{ km s}^{-1}$, $k_x = 0.0025$.

6.2 y -propagating waves

Let us now consider the other extreme, where waves are propagating in the transverse direction (y -direction), therefore $k_x = 0$ and perturbations in velocity and magnetic field have no x -component, i.e. $v_x = b_x = 0$. The MHD equations for this case are now given by

$$\frac{\partial \rho}{\partial t} + \rho'_0 v_z = 0, \quad (5.10)$$

$$\rho_0 \frac{\partial v_y}{\partial t} = -\frac{\partial p}{\partial y} + \frac{1}{\mu} B_0 \sin \theta \left(\frac{\partial b_y}{\partial z} - \frac{\partial b_z}{\partial y} \right), \quad (6.16)$$

$$\rho_0 \frac{\partial v_z}{\partial t} = -\frac{\partial p}{\partial z} - \rho g, \quad (6.17)$$

$$\frac{\partial b_x}{\partial y} + \frac{\partial b_z}{\partial z} = 0, \quad (6.18)$$

$$\frac{\partial \mathbf{b}}{\partial t} = B_0 \sin \theta \frac{\partial \mathbf{v}}{\partial z}. \quad (6.19)$$

It is expected that this is equivalent to the case with a vertical magnetic field, with field strength equal to the vertical component for this case, i.e. $B_z = B_0 \sin \theta$. In other words, inclination of the magnetic field should not affect the stability condition, compared to the case of a vertical field, when only considering waves propagating perpendicular to the plane of inclination, although, it is expected to modify the growth rate.

Using similar techniques to the x -propagating case and using the ansatz

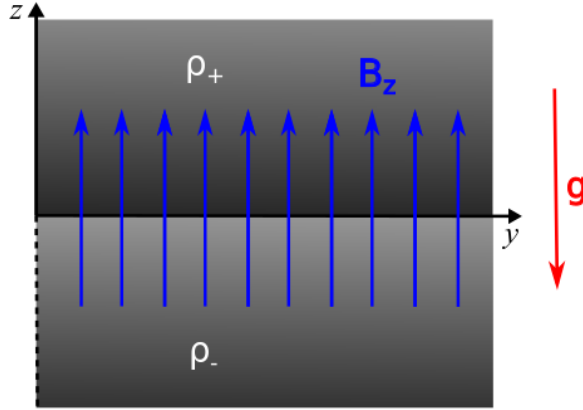


Figure 6.4: 2D sketch of the equilibrium configuration for the case of waves propagating in the y -direction. The equilibrium state consists of a surface separating two regions, each with different density. The magnetic field is uniform throughout both regions and is inclined within the (x, z) -plane at an angle, θ , with respect to the x -direction, so has a component $B_z = B_0 \sin \theta$ within the (y, z) -plane. The configuration is invariant in the y -direction.

for y -propagating wave perturbations, $f \sim \exp[i(k_y y - \omega t)]$, the governing equation is found to be,

$$\frac{\partial}{\partial z} \left(\rho_0 \frac{\partial \hat{v}_z}{\partial z} \right) + \frac{B_z^2}{\mu \omega^2} \left(\frac{\partial^2}{\partial z^2} - k_y^2 \right) \frac{\partial^2 \hat{v}_z}{\partial z^2} = k_y^2 \rho_0 \hat{v}_z + \frac{g k_y^2}{\omega^2} \rho_0' \hat{v}_z. \quad (6.20)$$

When the plasma is locally homogeneous either side of the interface, the plasma density is constant, hence, either side of the interface, the vertical component of velocity has the form $\hat{v}_z \sim e^{\Gamma z}$, where the effective wavenumbers, Γ are the solutions to the bi-quadratic equation,

$$\frac{B_z^2}{\mu} \Gamma^4 + \left[\rho_0 \omega^2 - \frac{B_z^2}{\mu} k_y^2 \right] \Gamma^2 - \omega^2 k_y^2 \rho_0 = 0. \quad (6.21)$$

Solutions are simply given by $\Gamma = \pm k_y$, n_{\pm} , where

$$n_- = \frac{i\omega}{v_{A-} \sin \theta}, \quad n_+ = \frac{i\omega}{v_{A+} \sin \theta}.$$

The surface wave solutions, evanescent away from the interface, for unstable solutions with $\Im(\omega) \geq 0$, are

$$\hat{v}_z = \begin{cases} A_- e^{k_y z} + B_- e^{-n_- z} & z < 0, \\ A_+ e^{-k_y z} + B_+ e^{n_+ z} & z > 0, \end{cases} \quad (6.22)$$

where the four coefficients that appear in these expressions will be determined using the jump conditions imposed at the interface.

Solutions obtained for both regions must be matched at the interface using the continuity conditions for a contact discontinuity (see Section 2.3), i.e.

$$[[v_z]] = 0, \quad [[v_y]] = 0, \quad [[b_y]] = 0, \quad [[b_z]] = 0,$$

$$\left[\left[\frac{\partial p}{\partial t} - g\rho_0 v_z \right] \right] = \left[i\omega p + g\rho_0 v_z \right] = 0.$$

In terms of the transversal component of velocity, \hat{v}_z , these jump conditions become,

$$\begin{aligned} \left[\hat{v}_z \right] &= 0, & \left[\left[\frac{\partial \hat{v}_z}{\partial z} \right] \right] &= 0, & \left[\left[\frac{\partial^2 \hat{v}_z}{\partial z^2} \right] \right] &= 0, \\ gk_y^2 \left[\rho_0 \hat{v}_z \right] - \omega^2 \left[\left[\rho_0 \frac{\partial \hat{v}_z}{\partial z} \right] \right] - \frac{B_z^2}{\mu} \left[\left[\frac{\partial^3 \hat{v}_z}{\partial z^3} \right] \right] &= 0. \end{aligned} \quad (6.23)$$

With the help of Eq. (6.22), we can cast the equations that arise, after applying the four jump conditions, into a matrix equation of the form $N\mathbf{A} = 0$, given by

$$N = \begin{bmatrix} 1 & 1 & -1 & -1 \\ k_y & -n_- & k_y & -n_+ \\ k_y^2 & n_-^2 & -k_y^2 & -n_+^2 \\ a_- & b_- & -a_+ & -b_+ \end{bmatrix}, \quad \mathbf{A} = \begin{bmatrix} A_- \\ B_- \\ A_+ \\ B_+ \end{bmatrix} \quad (6.24)$$

In the expression of N we introduce the notations,

$$a_- = d(gk_y^2 - k_y\omega^2 - k_y^3 v_{A-}^2 \sin^2 \theta), \quad b_- = d(gk_y^2 + n_- \omega^2 + n_-^3 v_{A-}^2 \sin^2 \theta), \quad (6.25)$$

$$a_+ = gk_y^2 + k_y\omega^2 + k_y^3 dv_{A-}^2 \sin^2 \theta, \quad b_+ = gk_y^2 - n_+ \omega^2 - n_+^3 dv_{A-}^2 \sin^2 \theta. \quad (6.26)$$

Non-trivial solutions to the matrix equation above are given by $\det(N) = 0$, and this leads to the *dispersion relation* of waves propagating along the interface in the y direction. The dispersion relation can be written in expanded form as

$$k(k + n_-)(k + n_+)R = 0,$$

where the polynomial, R is given by

$$\begin{aligned} R(\omega) &= (d^{1/2} + 1)(d - 1)\omega^3 - 2ik_y d^{1/2} v_{A-} \sin \theta (d^{1/2} + 1)^2 \omega^2 \\ &\quad + (d^{1/2} + 1)[2dv_{A-}^2 k_y^2 \sin^2 \theta + gk_y(d - 1)]\omega + 2ik_y^2 d^{1/2} v_{A-} g \sin \theta (d - 1). \end{aligned} \quad (6.27)$$

As expected, by setting $\theta = \pi/2$, we obtain the expression Q , given in Eq. (6.14), from the dispersion relation for a vertical magnetic field configuration.

By substituting the expressions for n_{\pm} , the first two terms of the dispersion relation give purely imaginary solutions in frequency, with

$$\omega_1 = id^{1/2} k_y v_{A-} \sin \theta, \quad \omega_2 = ik_y v_{A-} \sin \theta.$$

These roots describe purely unstable, non-propagating solutions, with linear dependence on both wavenumber and Alfvén speed. The solutions ω_1 and ω_2 correspond to the solutions for the vertical magnetic field case which lead to trivial solutions, as noted by Chandrasekhar (1961).

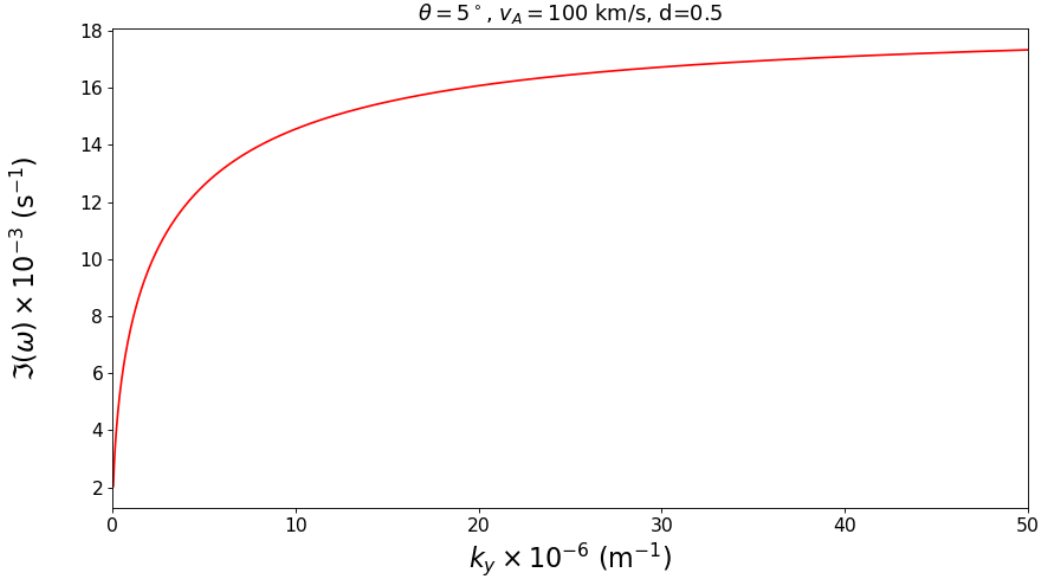


Figure 6.5: A solution for transversally propagating waves in terms the wavenumber, k_y , which $d = 0.5$, $v_A = 100 \text{ km s}^{-1}$, $\theta = 22.5^\circ$.

The remaining three solutions are given by $R = 0$. As R is a cubic polynomial, the roots of $R = 0$ may be found explicitly, however, it may be shown that only one solution has positive imaginary part. This unstable solution is shown in Fig. (6.5), for values of the variables appropriate to the chromosphere: $g = 274 \text{ m s}^{-2}$, $\theta = \pi/8$, $d = 0.5$, $v_{A-} = 100 \text{ km s}^{-1}$. Figure (6.5) shows that the growth rate increases with k_y and $\Im(\omega)$ is positive for all values of k_y . Hence, as with a vertical field, there is no critical wavenumber and instabilities are present for every k_y value. Unlike the longitudinally propagating case, the instability rate increases monotonically with the wavenumber, since there is no horizontal component of the magnetic field directed within the (y, z) -plane, to act against gravity.

It is interesting to note that the growth rate is bounded. For $k_y \rightarrow \infty$, we may perform an asymptotic expansion of the dispersion relation, which, to highest order, gives us a linear equation in ω , of the form

$$\Im(\omega) \rightarrow \frac{g}{\sin \theta v_{A+}} \frac{1-d}{\sqrt{d+1}}.$$

This implies that the growth rate tends towards a constant value for high wavenumber.

On the other extreme, we can expand the function $R(\omega, k_y)$, into series solutions for $k_y \rightarrow 0$. Keeping only linear terms in k_y , we obtain a quadratic equation in ω

$$\omega^2 \approx -\frac{1-d}{d+1} k_y g, \quad (6.28)$$

which is the same stability condition as for the hydrodynamic case, for waves propagating in the y -direction. It also constitutes the dispersion relation of

internal gravity modes, known from hydrodynamics, for the case of a denser lower plasmas, i.e. $d > 1$. Therefore for large wavelengths, the magnetic field has insignificant effect on waves propagating in the y -direction.

6.3 Three-Dimensional Analysis

While the previous 2D analyses have given us useful information about how the waves may propagate and the instability thresholds, to understand the stability of this system fully, it is necessary to investigate the problem in all three dimensions, where waves propagate in the (x, y) -plane. That is why we consider the case where the interface is in the (x, y) -plane, situated at $z = 0$, with density changing sharply at this interface, according to Eq. (6.1). Once again, we consider a homogeneous equilibrium magnetic field intersecting the interface at an angle θ , meaning that the equilibrium magnetic field is given by $\mathbf{B}_0 = B_0(\cos \theta, 0, \sin \theta)$. Thus, a contact discontinuity is achieved. Due to the constraint of continuity of magnetic field strength across the interface, the background magnetic field has the same value in both plasma regions and B_0 is constant. The equilibrium configuration is shown in Fig. (6.6).

6.3.1 Dispersion relation of waves propagating along the interface

Similar to the cases discussed previously, we are going to consider that all perturbations are proportional to the exponential ansatz introduced in Section 2, i.e. $f \sim \hat{f} \exp[i(k_x x + k_y y - \omega t)]$. In this case, the dynamics of waves are described with the help of the ideal, incompressible MHD equations,

$$-i\omega \hat{\rho} + \hat{v}_z \rho'_0 = 0 \quad (6.29)$$

$$-i\omega \rho_0 \hat{v}_x = -ik_x \hat{p} + \frac{B_0}{\mu} \sin \theta \left(\frac{\partial \hat{b}_x}{\partial z} - ik_x \hat{b}_z \right), \quad (6.30)$$

$$-i\omega \rho_0 \hat{v}_y = -ik_y \hat{p} + \frac{B_0}{\mu} \sin \theta \left(\frac{\partial \hat{b}_y}{\partial z} - ik_y \hat{b}_z \right) + \frac{B_0}{\mu} \cos \theta \left(ik_x \hat{b}_y - ik_y \hat{b}_x \right), \quad (6.31)$$

$$-i\omega \rho_0 \hat{v}_z = -\frac{\partial \hat{p}}{\partial z} + \frac{B_0}{\mu} \cos \theta \left(ik_x \hat{b}_z - \frac{\partial \hat{b}_x}{\partial z} \right) - \hat{\rho} g, \quad (6.32)$$

$$-i\omega \hat{\mathbf{b}} = B_0 \left(ik_x \cos \theta \hat{\mathbf{v}} + \sin \theta \frac{\partial \hat{\mathbf{v}}}{\partial z} \right). \quad (6.33)$$

We may substitute the induction equation, (6.33), into the x -component of the momentum equation, Eq. (6.30), to obtain an expression for \hat{p} in terms of

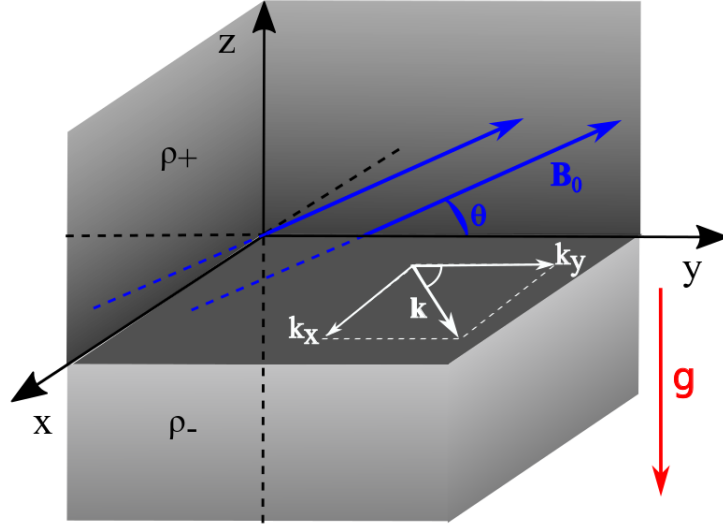


Figure 6.6: Schematic representation of the equilibrium configuration used in the present section. The equilibrium state consists of a surface separating two regions, each with different density. The magnetic field is uniform throughout both regions and is inclined within the (x, z) -plane at an angle, θ , with respect to the x -direction. The configuration is invariant in the x - and y -directions. Perturbations are described by the wavevector, \mathbf{k} , in the (x, y) -plane.

the components of velocity,

$$\begin{aligned}
\hat{p} &= \frac{\omega}{k_x} \rho_0 \hat{v}_x - \frac{i}{k_x} \frac{B_0^2}{\mu\omega} \sin \theta \left(i \sin \theta \frac{\partial^2 \hat{v}_x}{\partial z^2} - k_x \cos \theta \frac{\partial \hat{v}_x}{\partial z} + k_x \frac{\partial \hat{v}_z}{\partial z} + i k_x^2 \cos \theta \hat{v}_z \right) \\
&= \left[\frac{1}{k_x} \frac{B_0^2}{\mu\omega} \sin^2 \theta \frac{\partial^2}{\partial z^2} + i \frac{B_0^2}{\mu\omega} \cos \theta \sin \theta \frac{\partial}{\partial z} + \frac{\omega}{k_x} \rho_0 \right] (\hat{v}_x) \\
&\quad + \left[-i \frac{B_0^2}{\mu\omega} \sin^2 \theta \frac{\partial}{\partial z} + k_x \frac{B_0^2}{\mu\omega} \cos \theta \sin \theta \right] (\hat{v}_z). \tag{6.34}
\end{aligned}$$

The incompressibility condition, $\nabla \cdot \mathbf{v} = 0$, can be used to obtain a relationship between \hat{v}_y and the other two components of velocity, as

$$\hat{v}_y = \frac{1}{k_y} \left(i \frac{\partial \hat{v}_z}{\partial z} - k_x \hat{v}_x \right). \tag{6.35}$$

Finally, Eq. (6.29) allows us to express the density perturbation as

$$\hat{\rho} = -\frac{i}{\omega} \rho_0' \hat{v}_z. \tag{6.36}$$

The above expressions for density, pressure and the y -component of velocity can be inserted into the y and z -components of the momentum equation (6.31) and (6.32), to obtain two relations that connect \hat{v}_x and \hat{v}_z :

$$i \frac{k^2}{k_x} f(\hat{v}_x) = -f \left(\frac{\partial \hat{v}_z}{\partial z} \right), \quad \frac{1}{k_x} \left[f \left(\frac{\partial \hat{v}_x}{\partial z} \right) + \omega^2 \frac{\rho_0'}{\rho_0} \hat{v}_x \right] = i \left[f(\hat{v}_z) + g \frac{\rho_0'}{\rho_0} \hat{v}_z \right], \tag{6.37}$$

where $k^2 = k_x^2 + k_y^2$ and the operator function, f , is defined as

$$f = v_A^2 \sin^2 \theta \frac{\partial^2}{\partial z^2} + 2ik_x v_A^2 \cos \theta \sin \theta \frac{\partial}{\partial z} + (\omega^2 - k_x^2 v_A^2 \cos^2 \theta). \quad (6.38)$$

When the vertical length scales of the perturbations are much smaller than the gravitational scale-height, such as at the onset of instability in the problem currently being explored, we can take the long scale-height limit and so treat the plasma either side of the interface as uniform. Given this approximation of *local homogeneity*, we will simplify our treatment by taking $\rho'_0 \rightarrow 0$. We are, therefore, able to combine the equations given by (6.37), into the *governing equation* for wave propagation in the incompressible plasma,

$$\left(k^2 - \frac{\partial^2}{\partial z^2}\right) f(\hat{v}_z) = 0. \quad (6.39)$$

We assume that the above equation has solutions of the form $\hat{v}_z \sim e^{\Gamma z}$, where the quantity Γ is complex. The governing equation for this case (6.39) thus simplifies to

$$(\Gamma^2 - k^2)(v_A^2 \sin^2 \theta \Gamma^2 + 2ik_x v_A^2 \sin \theta \cos \theta \Gamma + \omega^2 - k_x^2 v_A^2 \cos^2 \theta) = 0, \quad (6.40)$$

which gives the roots $\Gamma = \pm k, m_{\pm}$, where the expression for m_{\pm} is given by Eq. (6.8).

The form of the governing equation, Eq. (6.39) implies that the frequency of waves will be complex, with the imaginary part of ω describing the temporal evolution of perturbations' amplitude. According to the temporal variation of perturbations assumed earlier, it is clear that a positive imaginary part of ω will describe unstable amplification of the amplitude. Since we are interested in waves localised at the surface, we assume that far away from the interface waves will be evanescent, therefore, the z -component of the velocity will be of the form,

$$\hat{v}_z = \begin{cases} A_- e^{kz} + B_- e^{m_- z}, & z < 0, \\ A_+ e^{-kz} + B_+ e^{m_+ z}, & z > 0, \end{cases} \quad (6.41)$$

where the amplitudes, A_{\pm} and B_{\pm} are arbitrary constants. We are only interested in unstable perturbations, hence we assume that $\Im(\omega) > 0$. This ensures that waves will be evanescent (via the roots m_{\pm}). The first terms (A) in Eq. (6.41) represent an exponential decay with z , while the second terms (B) describe an oscillatory decay. It is clear that when $\theta = 0$, in Eq. 6.40, the second terms of (6.41) vanish and we recover the result of a tangential discontinuity.

The present assumption of local homogeneity is valid when $1/|\Re(\Gamma)|$ is much less than the gravitational scale-height, H , i.e.

$$H \gg \max\left(\frac{1}{k}, \frac{v_{A-} \sin \theta}{\Im(\omega)}, \frac{v_{A+} \sin \theta}{\Im(\omega)}\right). \quad (6.42)$$

In other words, stratification effects due to gravity may be ignored, so long as the wavelength of perturbations is sufficiently small, as well as the product of the growth time, $\Im(\omega)^{-1}$, with the Alfvén speeds.

6.3.1.1 Boundary Conditions

The solutions obtained for the two plasma regions, given by Eq. (6.41), will now be connected at the interface, using the boundary conditions for a contact discontinuity in the presence of gravity. The jump conditions across the interface are given in Chapter 2 by Eq. (2.61) and the condition for pressure continuity across $z = 0$ is more explicitly given by Eq. (2.64). These equations state that we require continuity of all components of velocity and magnetic field perturbations, as well as continuity across the unperturbed interface of $i\omega p + g\rho_0 v_z$. Using the surface wave solutions (6.41), we may now express these jump conditions in terms of \hat{v}_x and \hat{v}_z , using the same methods as previously. These are found to be

$$\llbracket \hat{v}_z \rrbracket = 0, \quad \llbracket \frac{\partial \hat{v}_z}{\partial z} \rrbracket = 0, \quad \llbracket \frac{\partial^2 \hat{v}_z}{\partial z^2} \rrbracket = 0 \quad (6.43)$$

along with the dynamic boundary condition,

$$\llbracket i\rho_0 \left(v_A^2 \sin^2 \theta \frac{\partial^2 \hat{v}_x}{\partial z^2} + \omega^2 \hat{v}_x \right) + k_x g \rho_0 \hat{v}_z \rrbracket = 0. \quad (6.44)$$

These boundary conditions will be used to connect the solutions from both sides of the interface, in order to derive the dispersion relation of waves.

6.3.1.2 Derivation of Dispersion Relation

In order to use the boundary conditions specified above, we must first find the expression for \hat{v}_x using the expression of \hat{v}_z given by Eq. (6.41). In the local homogeneity limit we may combine Eqs. (6.37) into a governing equation for \hat{v}_x of the same form as the governing equation for \hat{v}_z , though with different constants. Therefore, we write \hat{v}_x as

$$\hat{v}_x = \begin{cases} a_- A_- e^{kz} + b_- B_- e^{m-z} & z < 0, \\ a_+ A_+ e^{-kz} + b_+ B_+ e^{m+z} & z > 0, \end{cases} \quad (6.45)$$

where a_{\pm} , b_{\pm} are to be found using the boundary conditions. Using the explicit expressions for \hat{v}_x and \hat{v}_z , Eq.(6.37a) transforms into

$$i \frac{k^2}{k_x} f(a_{\pm} A_i e^{\mp kz}) = -\frac{\partial}{\partial z} f(A_{\pm} e^{\mp kz}), \quad (6.46)$$

since $f(e^{n \pm z}) = 0$. As a result, the coefficients a_{\pm} are

$$a_- = i \frac{k_x}{k}, \quad a_+ = -i \frac{k_x}{k}.$$

However, these expressions give no information about the coefficients b_i . By combining the coefficients b_{\pm} and B_{\pm} into a new unknown quantity, C_{\pm} , \hat{v}_x may be written as,

$$\hat{v}_x = \begin{cases} i \frac{k_x}{k} A_- e^{kz} + C_- e^{m-z} & z < 0, \\ -i \frac{k_x}{k} A_+ e^{-kz} + C_+ e^{m+z} & z > 0. \end{cases} \quad (6.47)$$

Using the exponential forms of \hat{v}_x and \hat{v}_z given by Eqs 6.41 and 6.45, we can now apply the boundary conditions, Eqs. (??) - (6.44). After long but straightforward calculations, we obtain a system of linear equations for the unknown six constants, that in matrix form, can be given as,

$$\begin{bmatrix} 1 & 1 & 0 & -1 & -1 & 0 \\ i\frac{k_x}{k} & 0 & 1 & i\frac{k_x}{k} & 0 & -1 \\ k & m_- & 0 & k & -m_+ & 0 \\ k^2 & m_-^2 & 0 & -k^2 & -m_+^2 & 0 \\ ik_x & 0 & m_- & -ik_x & 0 & -m_+ \\ \alpha_- & \beta_- & \gamma_- & -\alpha_+ & -\beta_+ & -\gamma_+ \end{bmatrix} \begin{bmatrix} A_- \\ B_- \\ C_- \\ A_+ \\ B_+ \\ C_+ \end{bmatrix} = M \begin{bmatrix} A_- \\ B_- \\ C_- \\ A_+ \\ B_+ \\ C_+ \end{bmatrix} = 0, \quad (6.48)$$

where the various expressions in the newly defined matrix M are,

$$\begin{aligned} \alpha_- &= dk_x g - \frac{k_x}{k} (dv_{A-}^2 k^2 \sin^2 \theta + d\omega^2), \\ \alpha_+ &= k_x g + \frac{k_x}{k} (dv_{A-}^2 k^2 \sin^2 \theta + \omega^2), \\ \beta_- &= dk_x g, \\ \beta_+ &= k_x g, \\ \gamma_- &= i (dv_{A-}^2 m_-^2 \sin^2 \theta + d\omega^2), \\ \gamma_+ &= i (dv_{A-}^2 m_+^2 \sin^2 \theta + d\omega^2). \end{aligned} \quad (6.49)$$

The non-trivial solution to the homogeneous system of equations (6.48) only exists when $\det(M) = 0$, which will give us the dispersion relation of waves propagating along the interface, in the presence of gravity and inclined magnetic field. This dispersion relation is explicitly given to be

$$(m_+ - m_-)(k - m_-)(k + m_+)S(\omega) = 0, \quad (6.50)$$

where

$$\begin{aligned} S(\omega) &= (d^{1/2} + 1)(d - 1)\omega^3 - 2ikd^{1/2}v_{A-} \sin \theta (d^{1/2} + 1)^2 \omega^2 \\ &+ (d^{1/2} + 1)[2dv_{A-}^2(k^2 - k_y^2 \cos^2 \theta) + gk(d - 1)]\omega \\ &+ 2ik^2 d^{1/2} v_{A-} g \sin \theta (d - 1), \end{aligned} \quad (6.51)$$

and $d = \rho_-/\rho_+ < 1$ is the density ratio. The dispersion relation, Eq. (6.50) has six roots in terms of ω . The first multiplier in the dispersion relation clearly corresponds to a trivial solution. The second and third brackets admit the two roots,

$$\begin{aligned} \omega_1 &= k_x v_{A-} \cos \theta - ik v_{A-} \sin \theta \\ \omega_2 &= k_x \sqrt{d} v_{A-} \cos \theta - ik \sqrt{d} v_{A-} \sin \theta. \end{aligned} \quad (6.52)$$

The solutions ω_1 and ω_2 lead to trivial solutions for velocity perturbations, but even so they both have negative imaginary parts and these solutions are necessarily disregarded, because we only consider that physical solutions correspond to $\Im(\omega) > 0$. Hence, we consider the three solutions to $S = 0$.

In order to simplify discussion, we use one single Alfvén speed (v_{A-}), and write the Alfvén speed in the upper plasma region as, $v_{A+} = \sqrt{d}v_{A-}$. To gain more information about the unstable solutions, the dispersion relation may be reformatted in terms of $\Omega = -i\omega$, such that $\Re(\Omega) = \Im(\omega)$ and the unstable solutions are given by solutions where the real part of Ω is positive. With the help of this re-scaling we obtain that $S = -i\sigma$, where the function σ is given by

$$\begin{aligned} \sigma = & (d^{1/2} + 1)(1 - d)\Omega^3 + 2kd^{1/2}v_{A-} \sin \theta (d^{1/2} + 1)^2 \Omega^2 \\ & + (d^{1/2} + 1)[2dv_{A-}^2(k^2 - k_y^2 \cos^2 \theta) - gk(1 - d)]\Omega \\ & - 2k^2d^{1/2}v_{A-}g \sin \theta (1 - d). \end{aligned} \quad (6.53)$$

Given that the coefficients of Ω^3 and Ω^2 are both positive (when $d < 1$), the sum of the roots must be negative and since the coefficient of Ω^0 is negative, the product of the roots must be positive. Assuming that at least one solution is unstable, i.e. positive Ω , these two conditions lead to the fact that the other two roots for Ω must have negative real parts and so are non-physical, amplifying modes. This leaves one physical solution, that we display graphically, to explore the effects of varying wavenumber, k , inclination angle, θ , density ratio, d , and propagation direction, α , shown in Figures (6.7 - 6.10).

6.3.2 Solutions and results

In order to simplify the discussion, let us introduce the propagation angle of the perturbations within the (x, y) -plane, α , such that

$$k_x = k \cos \alpha, \quad k_y = k \sin \alpha.$$

We note that, even before plotting solutions, we see that taking the limit $\alpha \rightarrow 0$, i.e. considering waves only propagating in the x -direction, the polynomial, $S(\omega)$ simplifies to the polynomial, $Q(\omega)$ for the 2D case in the (x, z) -plane, given by Eq. (6.14) and so, too, does the solution tend to the solutions for the 2D case in the (x, z) -plane. As $\alpha \rightarrow \pi/2$ we consider waves propagating in the y -direction, and the polynomial $S(\omega)$ tends towards the polynomial $R(\omega)$ derived for the 2D case in the (y, z) -plane. As the propagation direction changes smoothly from x -aligned to y -aligned, there is a smooth change in the solution. This may initially seem like a trivial comment, but in the 2-dimensional cases considered in Sections (6.1 and 6.2), it was assumed that there were no perturbations to velocity or magnetic field perpendicular to the direction of propagation. Thus, for the 3D case, simply changing the direction of propagation of the wave reduces the problem, by removing perpendicular components of perturbations. This also confirms that the results and conclusions discussed in the previous sections are relevant to the fully 3D problem.

The variation of the only physically acceptable root of $S(\omega) = 0$, with various physical parameters, is investigated numerically. First, in Fig. (6.7) we plot the variation of the real and imaginary part of the frequency with respect to the wavenumber, k , for a small field inclination angle. In order

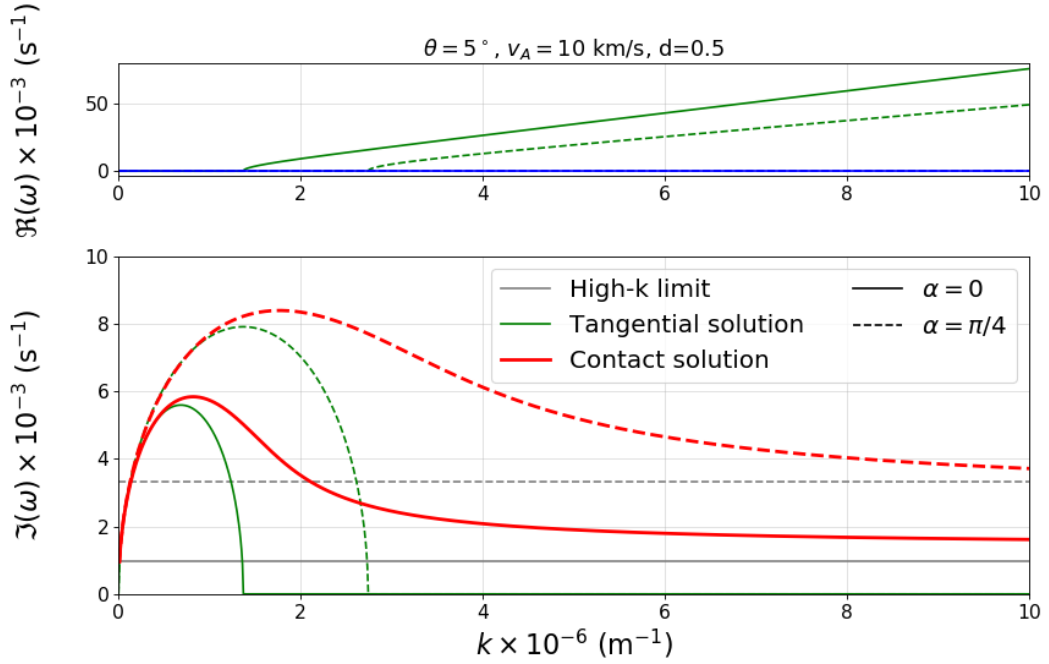


Figure 6.7: Solutions for the dispersion relation for waves propagating in the (x, y) -plane, for two propagation directions ($\alpha = 0$ solid line, and $\alpha = \pi/4$ dashed line), with respect to wavenumber, k . The density ratio is $d = 0.5$, the Alfvén speed of the lower plasma is $v_A = 10 \text{ km s}^{-1}$, and the magnetic field inclination angle $\theta = 5^\circ$. The upper panel shows the real part of the frequency, while the imaginary part is plotted in the lower panel. The limiting value of $\Im(\omega)$ when $k \rightarrow \infty$ is shown by the grey horizontal lines, in the lower panel. For illustration we also show the real and imaginary part of the frequency in the case of a tangential discontinuity ($\theta = 0$), plotted here in green.

to compare our results with the well-known results obtained in the case of a tangential discontinuity, we also plot the results we obtain for $\theta = 0$ (green lines). We choose to plot solutions for two values of the propagation direction: $\alpha = 0$ (propagation along the x -axis, solid line) and $\alpha = \pi/4$ (dashed line). The smallest instability increment (longest amplification time) is obtained for propagation parallel to the x -axis, while increasing the direction of propagation away from $\alpha = 0$ we see an increase in the instability rate. The maximum of the instability rate is obtained at a smaller wavelength than in the case of a tangential discontinuity, and, in general, the maximum of the rate is higher than the one obtained for tangential discontinuity. This result is easy to interpret, as at contact discontinuity only the horizontal (x -directed) component of the equilibrium magnetic field is able to stabilise the plasma.

In the case of a tangential discontinuity, there is always a critical wavenumber, below which the solution is purely imaginary and hence gives rise to instability. However, above this critical value, the solution is real and the wave is propagating. In contrast, for the contact discontinuity, this is no longer the case; solutions are unstable for all values of wavenumber, k . Moreover, for

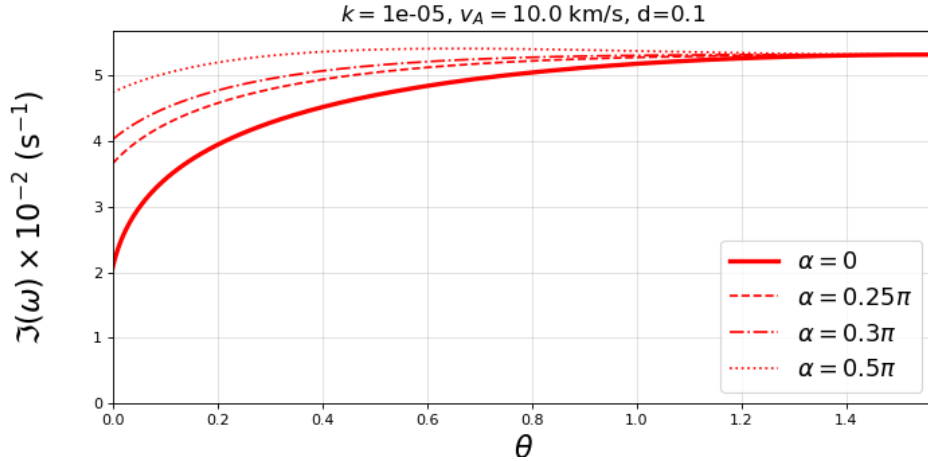


Figure 6.8: Imaginary part of the frequency for waves propagating in the (x, y) -plane, for several propagation directions, with respect to the magnetic field inclination, θ . The density ratio is assumed to be $d = 0.5$, the reference Alfvén speed is $v_{A-} = 10 \text{ km s}^{-1}$, and the value of the wavenumber fixed at $k = 10^{-5} \text{ m}^{-1}$.

very large wavenumbers, the imaginary part of the frequency tends towards a fixed value, given by

$$\Im(\omega) \rightarrow \frac{g \sin \theta (1 - d)}{v_{A-} d^{1/2} (1 - \sin^2 \alpha \cos^2 \theta) (d^{1/2} + 1)}. \quad (6.54)$$

These values are shown in grey in Fig. (6.7). It may also be seen that the instability rate decreases for higher wavenumber.

Interestingly, the behaviour of the imaginary part of the frequency (and the disappearance of the critical wavenumber) is similar to the results obtained by Díaz et al. (2014), where these authors studied the effect of partial ionization on MRT instability in a single-fluid approximation. In their study, the change in the imaginary part of the frequency was attributed to the ambipolar diffusion in the induction equation, i.e. the modification was due to the presence of neutrals, that can diffuse in the perpendicular direction to the ambient magnetic field. This suggests that changes occurring in the transversal direction (relative to the interface) will notably modify the behaviour of the instability increment. One important difference is that, for the partially ionised case considered by Díaz et al. (2014), the instability rate tends to zero for high wavenumbers, however, in our case this quantity never reaches the zero value.

In the other limit, when the propagation direction is along the y -axis ($\alpha = \pi/2$), solutions are identical to the 2D y -propagating case in Section (6.2) and the only wave that can propagate is the gravity surface wave. The magnetic field begins to have an effect on the propagation characteristics of waves, as the propagation direction inclines towards the x -axis.

Let us investigate how the inclination angle of the magnetic field, θ , affects the stability of incompressible waves propagating along the interface. Now, the value of the wavenumber is fixed at $k = 10^{-5} \text{ m}^{-1}$ (a typical value for

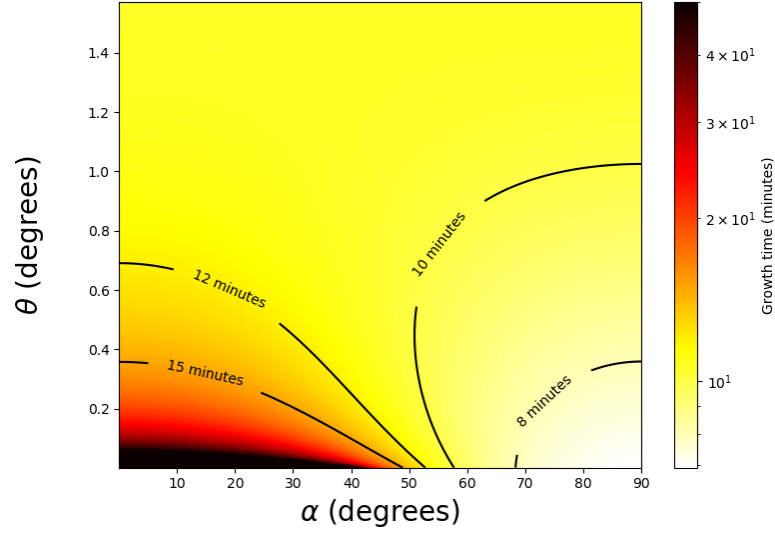


Figure 6.9: Growth time for $k = 2.5 \times 10^{-3} \text{ m}^{-1}$, $d = 0.5$ $v_A = 10 \text{ kms}^{-1}$, in terms of propagation angle, α and field inclination θ .

oscillations in prominences) and we choose a number of characteristic values for the propagation angle, α . The numerical result of our analysis is shown in Fig. (6.8). Again, the mode that has the smallest instability rate is the one that propagates strictly along the x -axis and this rate shows a pronounced increase for smaller values of θ , after which this rates saturates and becomes independent of the inclination angle of the magnetic field. With increasing propagation angle, the instability rate increases, meaning that the amplification time reduces. This result is something that can be understood if we keep in mind that, with increasing the propagation angle, the magnetic tension has less effect on the stabilisation of the interface. It is clear that, regardless of the propagation angle of waves, the instability increments tend to a steady value of approximately $\Im(\omega) = 0.055 \text{ s}^{-1}$.

In Fig. (6.8), we see that regardless of the value of the propagation angle of the waves, for large inclination angle of the field, all modes will tend towards the same instability rate. In order to translate our results into observable quantities, we show the contour plots of the inverse of the instability rate (the growth time, in minutes) for a particular wavenumber, density ratio, d and Alfvén speed in terms of the inclination angle, θ and propagation angle, α (see Fig. 6.9), i.e. we plot the pair of the angles that satisfy the given growth time. In this plot, we see two distinct behaviours. While on the left-hand side of the plot we see that for shorter growth time we require higher inclination angle, the mode that appears on the right-hand side shows a different behaviour for very large values of inclination angle. However, this mode is not an Alfvén mode; instead it is the surface gravity mode that appears for a nearly perpendicular propagation. Similarly to the findings shown in Fig.(6.8), for large inclination angle of the magnetic field, the growth time of instability becomes independent of α .

It is well known that magnetic field can stabilise the unstable interface,

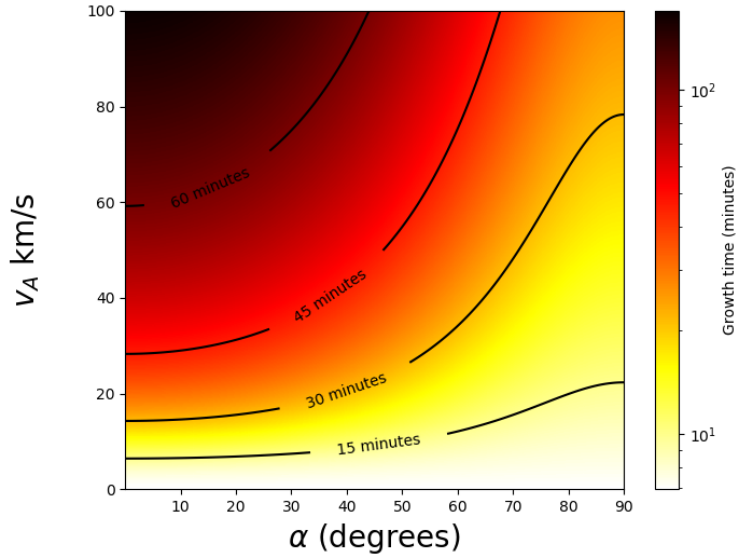


Figure 6.10: Growth time for $k = 2.5 \times 10^{-3} \text{ m}^{-1}$, $d = 0.5$ $\theta = \pi/8$, in terms of propagation angle, α and Alfvén speed of the lower plasma, v_A .

which is why we investigate the variation of the growth time with respect to the propagation angle of waves and Alfvén speed, keeping the wavenumber, density ratio and magnetic field inclination constant (see Fig.(6.10)). Since the density ratio is constant, changing Alfvén speed means a change in the intensity of the magnetic field. An increase in the magnetic field intensity means that the growth time increases, i.e. the magnetic field has a stabilising effect, for any propagation direction, as expected. In addition, the value of the propagation angle becomes more important for stronger magnetic fields.

Finally, we investigate the effect of changing density ratio on the growth rate of unstable modes and we obtain that the growth rate decreases monotonically towards zero as the density ratio is increased, towards $d = 1$. In the case of the tangential MRT instability (but also true for the hydrodynamic case), as the density of the upper plasma increases in comparison to the density of the lower plasma (d decreasing), the system becomes less stable. Taking the limit of $d \rightarrow 0$, the instability rate tends towards a fixed value. By taking the solution of $S(\omega) = 0$, when $d \rightarrow 0$, the limiting value of the growth rate is found to be $\Im(\omega) \rightarrow \sqrt{gk}$. This is clearly independent of both inclination angle and magnetic field strength and gives the dynamics of a plasma element falling freely under gravity.

6.3.3 Symmetry

We will once again consider how viewing this system from a different orientation may affect the mathematical results. This analysis is slightly less essential than for the gravity-free case, since the direction of gravity will introduce a preferential direction into the system. Nevertheless, for completeness, we include a discussion of the symmetry problem in what follows.

We assume that in the original orientation the variables are given by $\mathbf{k} = (K_x, K_y, 0)$, $d = D$, $\theta = \Theta$ and the gravity pointing downwards to be $g = G$. If we once again rotate the system by 180° , the variables in the standard viewpoint are given by $\mathbf{k} = (-K_x, K_y, 0)$, $d = D$, $\theta = \Theta$ and $g = -G$. The magnitude of the wavevector, k is unchanged. In this orientation the Alfvén speeds also have exchanged subscripts.

Considering the expression for m_\pm is given by Eq. (6.8), along with the condition for evanescence, we see that

$$m_\pm \left(d = \frac{1}{D}, \mathbf{k} = (-K_x, K_y, 0) \right) = -m_\mp (d = D, \mathbf{k} = (K_x, K_y, 0)).$$

The condition that $k_x = -K_x$ also gives us that, $a_- \longleftrightarrow a_+$. These two conditions, along with our altered variables, in turn, give that $\alpha_- \longleftrightarrow -\alpha_+$, $\beta_- \longleftrightarrow -\beta_+$, and $\gamma_- \longleftrightarrow -\gamma_+$. Thus, the matrix which leads us to the dispersion relation becomes

$$M = \begin{bmatrix} 1 & 1 & 0 & -1 & -1 & 0 \\ i\frac{K_x}{k} & 0 & 1 & i\frac{K_x}{k} & 0 & -1 \\ k & -m_+ & 0 & k & m_- & 0 \\ k^2 & m_+^2 & 0 & -k^2 & -m_-^2 & 0 \\ -iK_x & 0 & -m_+ & iK_x & 0 & m_- \\ -\alpha_+ & -\beta_+ & -\gamma_+ & \alpha_- & \beta_- & \gamma_- \end{bmatrix}, \quad (6.55)$$

which, through simple matrix manipulation, may be rewritten as the matrix for the original orientation. Thus, we have once again confirmed that viewing the system for a different orientation will not change the mathematical results.

6.3.4 Applications to Solar Prominences

Solar prominences are magnetic features suspended in the solar corona that are made from dense, cold plasma surrounded by tenuous and hot coronal plasma. High-resolution observations show that prominences present threads along which plasma can flow and waves propagate (see Sections 1.1.3 and 1.1.5 for more detail on prominences). Such an observation was carried out, using Hinode/SOT instrument by Okamoto et al. (2007), who observed an active region prominence (NOAA AR 10921) in a 0.3 nm broadband region centred at 396.8 nm. They found that a multi-thread prominence was suspended above the main sunspot. Their analysis showed in-phase, oscillatory motions with periods 130-250 s. These authors concluded that the observed waves are propagating or standing Alfvén waves.

Terradas et al. (2008) used these oscillations to carry out a seismological study and determined Alfvén speeds in both the prominence and corona in terms of the density ratio. The threads were considered to be thin flux tubes (observations showed that they have a small radius), in the presence of a flow that slightly influenced the period of waves. Using a few simplifications (e.g. straight flux tubes, homogeneous plasma, longitudinal magnetic field, non-stratified plasma, threads have equal length, linear approximation) these

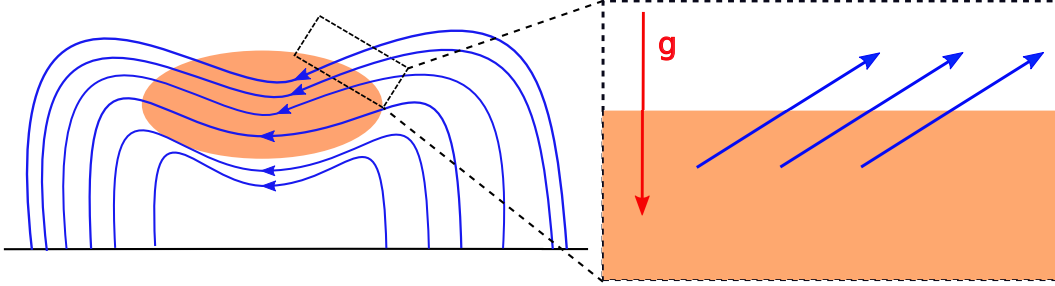


Figure 6.11: A diagram showing the dense prominence plasma (orange) supported by magnetic field lines (blue) and how this relates to the contact discontinuity at an interface investigated in the present work.

authors obtained that the minimum Alfvén speed varies between 120 and 350 km s^{-1} . Although not analysed in the above studies, Ruderman et al. (2014), found that the typical lifetimes of threads under investigation is 10 minutes. If the MRT is responsible for these short lifetimes, then we may suppose that the instability time is approximately equal to the thread lifetime. This gives us the necessary information to find the magnetic field inclination, θ , in terms of the propagation direction α , for a given density ratio, using our model. Figure (6.11) shows how our investigation of a contact discontinuity at an interface, relates to prominences and gives some justification for this technique.

Using the observations by Okamoto et al. (2007), we can use the analysis presented by Terradas et al. (2008) (their Eq. 3) to determine the wavenumbers and Alfvén speeds for three possible density ratios ($d = 0.1, 0.2, 0.5$). With these values, we solve numerically Eq.(6.51) and this determines the pair of values for magnetic field inclination and propagation direction satisfying the observed variables. We note that not all observable data sets have solutions for any α and θ values; these are shown by dashes in the table of results. This suggests that only certain density ratios may be possible in those circumstances, thus giving even more information about hard-to-observe variables. The solutions, in terms of magnetic field inclination and propagation direction, are displayed for all six observed threads in Figure (6.12) and the relevant data, including the maximum possible inclination angle (when the wave is directed in the same plane as the magnetic field i.e x -propagating), are shown in Table ??.

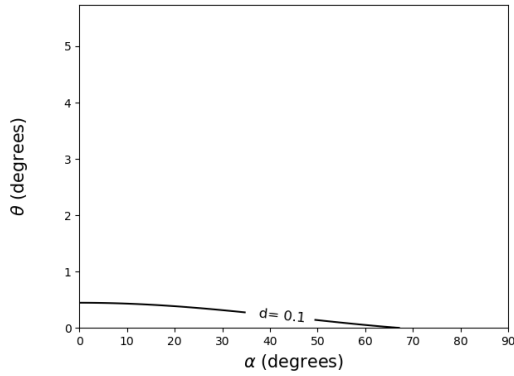
It is clear that for all threads the 10 min growth time can be satisfied only for particular values of density ratio and a particular combination of field inclination angle and propagation angle. Thread 1 shows only solutions for a density ratio of $d = 0.1$, with the maximum field inclination only about half a degree that is attained when the wave propagates along the x -axis. Threads 4, 5 and 6 all have solutions for $d = 0.2$ with maximum inclination of approximately 1° . In addition thread 4 has a solution for $d = 0.5$ with a noticeably higher maximum inclination of 4° . Thread 2 shows a higher maximum θ for the $d = 0.2$ solution than the other three, of 3° , and a lower maximum θ for the $d = 0.5$ solution than thread 4 of approximately 1° . Finally, thread 3 has a solution only for $d = 0.5$, but with much higher maximum

#	Wavenumber (10^{-7} m^{-1})	d=0.1		d=0.2		d=0.5	
		v_A (km s^{-1})	max θ ($^\circ$)	v_A (km s^{-1})	max θ ($^\circ$)	v_A (km s^{-1})	max θ ($^\circ$)
1	34.9	1331	0.5	1237	-	1172	-
2	7.85	1336	-	1015	2.9	897	1.1
3	18.8	1116	-	983	-	899	25.8
4	57.1	1220	-	1164	1.4	1126	4.0
5	35.9	1710	-	1583	1.1	1511	-
6	7.39	861	-	827	1.1	806	-

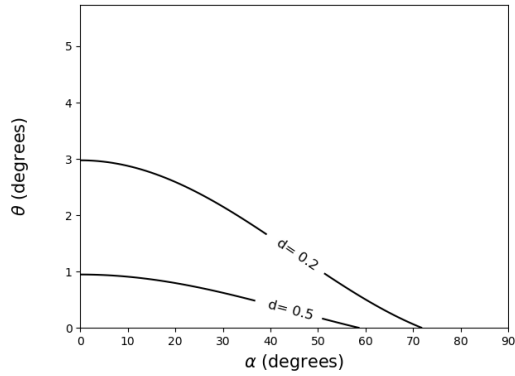
Table 6.1: The wavenumber and coronal Alfvén speeds derived for the six prominence threads. The maximum value of the inclination angle of the field is shown for the three values of the density ratio, d .

inclination than any of the other threads, with $\theta = 25^\circ$. Although all of the magnetic field inclinations found are relatively low (except thread 3), the inclination is only zero if the propagation direction is almost perpendicular to the magnetic field, which would be very unlikely for MHD waves in the solar atmosphere. This also gives a justification for the study explored in Chapters 3 and 4, where small magnetic field inclinations were considered for MHD waves at a contact discontinuity.

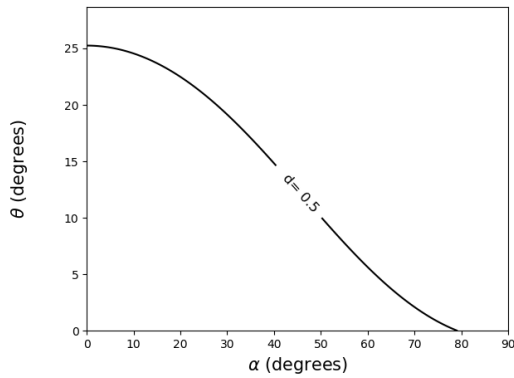
We should note that, in the context of solar prominences, compressibility would have a pronounced effect in stabilising the interface, therefore, a model including compressibility would need to be developed to give more pertinent results. The density ratios present in prominences also, in general, give lower d values than those considered here, destabilising the system further. We can thus suppose that solutions would be of a similar order of magnitude to those considered here.



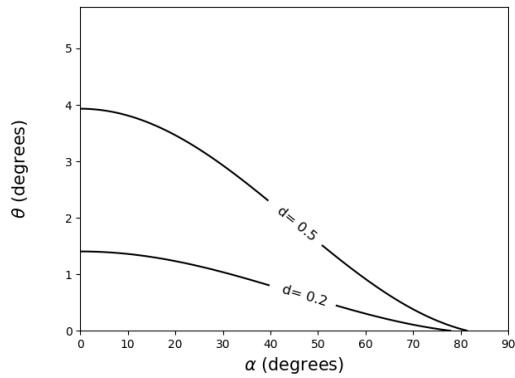
(a) Thread 1



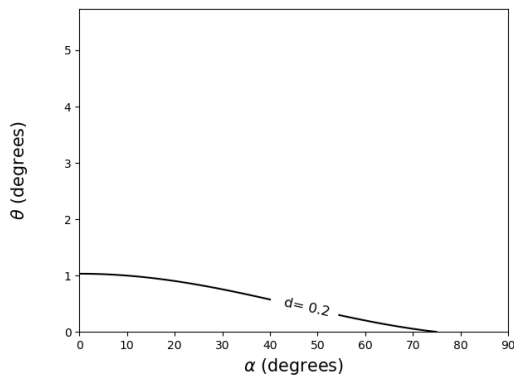
(b) Thread 2



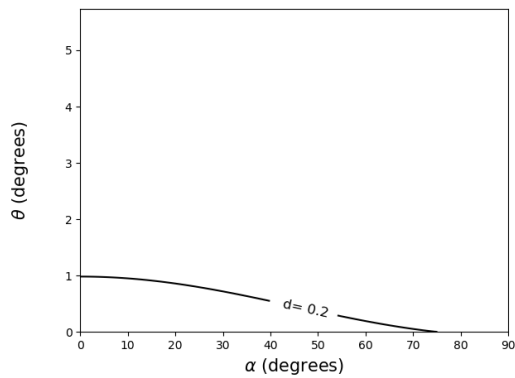
(c) Thread 3



(d) Thread 4



(e) Thread 5



(f) Thread 6

Figure 6.12: Solutions of the dispersion relation for a given growth time in terms of magnetic field inclination (θ) and propagation direction (α), for six observed prominence threads, for three possible density ratios. Observational data has been adapted from Okamoto et al. (2007).

6.4 Conclusions

This chapter has presented the results of the study on the generation of Rayleigh-Taylor instability of waves propagating along a density interface in the presence of an oblique magnetic field that crosses an interface. For simplicity the plasma was considered to be incompressible. The component of the magnetic field across the interface, makes the interface a contact discontinuity.

We have shown that, for even a small inclination of the magnetic field, the system is unstable for any wavenumber. This results is in contrast to the findings obtained in the case of a tangential discontinuity, where there is always a “critical wavenumber”, above which the system is stable. The instability rate we obtained is also higher than the rate we would obtain for the tangential case, however the magnetic tension stabilises against gravity, so the instability rate is lower than for the purely hydrodynamic case and is reduced with increasing Alfvén speed. The instability rate was found to be considerably higher for perturbations perpendicular to the plane in which the magnetic field is inclined, than for perturbations in the direction of the field and there is a smooth change between these two extremes, as the magnetic tension has a less pronounced effect as a restoring force.

The geometry investigated provides a good model for the edges of prominences, where the high density gradients, between the low density coronal plasma and the higher density plasma of the prominence itself, are readily modelled by a sharp interface. The edges of these prominences are often intersected by inclined magnetic fields, making this investigation relevant to Rayleigh-Taylor instabilities. The results of this study thus suggest that, even with a high magnetic field strength, instabilities are able to develop for perturbations of any wavelength, where the field intersects the prominence edge. This gives us information about where in the prominences plumes are most likely to develop.

Using the dispersion relation derived in the current study, an inversion technique has been performed on observations of oscillating prominences, which can give us information on the angle of inclination of the magnetic field and direction of the wave propagation. A simple analysis of six prominence threads observed by Hinode/SOT was performed, which found that the typical maximum inclination angles of the magnetic field was $1 - 4^\circ$. The inversion technique applied in this Chapter also provided information about the possible density ratios, for each prominence thread considered.

CHAPTER 7

Conclusions

7.1 Overview of Thesis

The present thesis is concerned with the properties of waves propagating along a density interface, when the interface is permeated by a homogeneous magnetic field. Such configuration defines a contact discontinuity.

Chapter 2 introduces important background information required for the body of this thesis, including an introduction to linear MHD wave theory, as well as revising MHD waves propagating in a homogeneous medium. In this chapter we present a rigorous derivation of jump conditions at an interface. These jump conditions are effective as when matching solutions at the interface and, in this sense, act as boundary conditions at the interface. This chapter also summarises a previous work, exploring MHD waves at a tangential discontinuity (Roberts, 1981*a*).

Chapter 3 was based on the published study, Vickers et al. (2018), and introduces the concept of wave propagation in the presence of magnetic field inclination across the interface, for the first time. Following the method used by Roberts (1981*a*), which was summarised in Chapter 2, a governing equation is found, which describes the transverse velocity component, either side of the interface. In order to solve the governing equation analytically and hence find the dispersion relation, it was necessary to consider an approximation of small inclination angle. Solutions to the dispersion relation were found numerically.

In Chapter 4, based upon work by Ruderman, Vickers et al. (2018), we analysed the initial value problem for incompressible waves propagating along contact discontinuities. Time-dependent solutions, in terms of wavenumber, are found in terms of initial drivers for v_z , which is assumed to be localised at the interface. There, x -dependent solutions are found analytically for small field inclination for several different initial conditions.

Background information on gravitational instabilities is given in Chapter 5 and, in particular, magnetic Rayleigh-Taylor instabilities, which are considered at a tangential discontinuity, as well as at a contact discontinuity with vertical magnetic field.

In Chapter 6, we take into account the effect of gravity and explore the effect of magnetic field inclination on the magnetic Rayleigh-Taylor instability, for the case where the upper plasma is denser. Unlike the studies covered in

the previous chapters, a two-dimensional analysis is not sufficient to investigate whether a given state is stable, so a three-dimensional analysis is employed to analyse the incompressible problem. A dispersion relation is found and solved analytically, to give the instability rate in terms of two angles (as well as the ratio of the densities, the wavenumber, and one of the Alfvén speeds): the direction of propagation of the initial perturbation, and the inclination of the field with respect to the interface. This expression was then used to find the range of possible angles for both propagation direction and field inclination for observed magnetic Rayleigh-Taylor instabilities on prominence filaments.

7.2 Summary of Results

7.2.1 Chapter 3

The first two chapters of the present thesis are devoted to the introduction of the mathematical and physical framework of the thesis, including the jump conditions that will be used throughout our calculation.

Chapter 3 used an eigenmode technique to find the phase-speed of waves propagating along a contact discontinuity. A governing equation for the transverse component of velocity was found either side of the interface, in the presence of an inclined magnetic field. Solutions to this equation showed that the variation of wave amplitude with height had an oscillatory component, due to the complex effective wavenumber. Using a small angle approximation for the magnetic field inclination, the dispersion relation was found analytically, from these solutions. Phase-speed solutions to the dispersion relation were calculated numerically and were found to be complex, which implied complex values for frequency. Complex values for frequency correspond to amplification (if $\Im(\omega) > 0$) or attenuation (if $\Im(\omega) < 0$). Since there is no outside energy source, the only physical solutions must be the attenuated modes, where the attenuation is due to energy leaking away from the interface. This result corresponds to the amplitude of the waves decreasing over time, but increasing away from the interface. Thus, even a small inclination of the magnetic field qualitatively changes the modes that may exist, from stable surface modes at the tangential discontinuity to attenuating leaky modes at the contact discontinuity. While this distinct change exists for velocity solutions, by averaging over a small boundary layer, values are found to change continuously to the tangential solutions, as the direction of the magnetic field tends towards horizontal.

7.2.2 Chapter 4

Chapter 4 expanded upon the previous chapter by introducing time-dependence, i.e. an analysis of time evolution of MHD waves at a contact discontinuity. In this chapter, we solved an initial value problem for incompressible waves propagating along the density interface. This method required performing a

Laplace transform of the perturbed quantities. However, in order to make analytical progress, only the incompressible case was considered. Through use of the continuity equations for a contact discontinuity, solutions for the Laplace transform of velocity are found. Complex analysis techniques are used to find the velocities in terms of wavenumber and the initial velocity perturbation. The initial velocity perturbation was assumed to be purely vertical and localised at the interface. These solutions for perturbations are valid within a certain distance of the interface, given in terms of the time and the speed at which the waves propagate outwards. In order to draw parallels to the previous chapter, as well as to aid in following calculations, the small angle approximation was once again considered. We have shown that, in the limit of the inclination angle tending toward zero (approaching a tangential discontinuity), the velocity did not change continuously to the value corresponding to the tangential discontinuity. However, when the solutions corresponding to the contact discontinuity were averaged over a small boundary layer, these averaged values tended towards the tangential solution.

The x -dependent solutions were found by performing an inverse Fourier transform for three different initial drivers: a delta function, a Lorentz function and a sinusoidal driver. The delta function and Lorentz function give a good approximation of the case when the interface is hit in one location. An example of this particular driver in the solar atmosphere may be the case of spicules hitting the transition region, which on a large scale may be viewed as an interface. The sinusoidal driver represents a wave perturbing the interface. In agreement with the previous chapter, it was shown that the amplitude of the wave decays for large time, regardless of the type of initial conditions. For the first two forms of the solution, we see that the solutions take the form of two pulses propagating forwards and backwards at the same speed along the interface, whilst spreading outwards in the vertical direction.

7.2.3 Chapter 6

While the previous chapters were concerned with how field inclination affected wave propagation, this chapter explored the effect of field inclination on the onset of magnetic Rayleigh-Taylor instability in an incompressible plasma. Initially, the problem is explored in two dimensions, firstly, in the plane in which the field is inclined, and then in the plane perpendicular to the magnetic field lines. Finally, the three-dimensional problem is explored. All three cases follow similar methods to find the time independent solutions. Unstable solutions are sought, which are evanescent far from the interface, when the upper plasma is denser than the lower plasma. The dispersion relation is found and solved analytically for a general inclination angle. The two 2D cases are found to be identical to the 3D case, when the propagation direction of perturbations is respectively parallel to and perpendicular to the plane in which the magnetic field is inclined. The general solution admits five solutions, but only one of them is found to be physical. This solution is unstable for every value of wavenumber and the instability rate tends towards a non-zero value for high

wavenumber. This result is unlike MRT instability at the tangential discontinuity, where solutions are only unstable for wavenumbers below some critical value and solutions are stable and propagating above this critical value. However, the closer to parallel the magnetic field is, the more stable the system is, as a greater component of the magnetic tension is directed vertically, stabilising against gravity. The magnetic field has a greater stabilising effect for perturbations directed parallel to the field in which the magnetic field is inclined varying smoothly with propagation direction. When the propagation direction is perpendicular to the magnetic field, solutions are identical to the case of a perpendicular magnetic field of field strength equal to strength of the vertical component of the inclined field.

These results were used to find pairs of angles of propagation direction and field inclination for observed unstable prominence threads. Six threads were observed, using Hinode, by Okamoto et al. (2007), on which Terradas et al. (2008) performed a seismological study to determine the Alfvén speeds. It was assumed that the instability time was roughly equal to the thread lifetime, which had previously been observed to be approximately 10 minutes. Using these quantities, the expression for the instability rate, derived earlier, was used to calculate the angles of propagation direction and field inclination, for three possible density ratios. The given instability time was found to be possible for a density ratio of $d = 0.2$ in four of the threads, for $d = 0.5$ in three of the threads and for $d = 0.1$ in only one thread. The maximum field inclinations were given when the propagation was directed parallel to the plane of magnetic field inclination and was found to be generally low (approximately one degree) except in one case, where the inclination was approximately twenty five degrees. The inclination of the field was only found to be zero for a propagation direction almost perpendicular to the magnetic field, an unlikely scenario, which confirms the presence of magnetic field inclination in prominence threads. While this was a first, simplified study, it lay the groundwork for more detailed future studies and showed validity for further research into contact discontinuities in the solar atmosphere.

7.3 Future Work

While this thesis presents some initial studies into the effect of magnetic field inclination upon waves and instabilities at an interface, there are many ways in which this work could be expanded, to be more applicable to structures in the solar atmosphere.

A fairly obvious extension to the work presented here would be to consider the models explored in the first two studies in all three dimensions. The compressible leaky modes explored in Chapter 3 could be explored for magnetic fields close to vertical, or solutions for a more general inclination could be found numerically. A time dependent analysis of the MRT instability (investigated in Chapter 6) would be interesting, however non-linear effects may need to be considered once the Rayleigh-Taylor “fingers” begin to develop. These extensions would help us to refine and expand upon the inversion introduced in

section 6.3.4 and help to determine field configurations in all three dimensions.

Although the first study (covered in Chapter 3) looked at the case of compressible plasma, incompressibility was assumed for the next two chapters. It would be expected that including compressibility to the initial value study of leaky waves (Chapter 4), would make it possible for two more modes to propagate simultaneously; representing the fast and slow magnetoacoustic modes, rather than the purely magnetic mode featured here. It is also known that compressibility stabilises plasma dynamics, so there may be qualitative differences to the stability of the MRT problem, discussed in Chapter 6.

The entirety of this thesis has assumed the plasma is fully ionised and has, thus, been concerned with a single-fluid approach. However, much of the solar atmosphere (photosphere and much of the chromosphere) is not fully ionised, so a two-fluid investigation may be more appropriate to modelling some regions of the solar atmosphere. A study of magnetic Rayleigh-Taylor instability at a tangential discontinuity has already been performed for a partially ionised plasma by Díaz et al. (2014), who found similar results to the solutions shown in Chapter 6 for the inclined field. This suggests that by including partial ionisation as well as field inclination may increase the instability rate for high wavenumber even further.

In all of our studies, we have considered a sharp interface between plasmas of two different densities, which clearly does not always describe reality. A more realistic (though still idealised) configuration would be to replace the sharp interface with a thin boundary layer, i.e. we can study the effects of field inclination in the presence of dispersion, another effect that affects the phase-speed of waves. This will have particular pertinence to modelling the transition region and the field lines intersecting it. If we are able to model this effectively, for the time-dependent case, we could use this to represent the effect of spicules on the transition region, in terms of waves that may propagate as well as energy leakage. It's also conceivable that this energy leakage could contribute to heating of the lower corona.

Our study was predominantly theoretical and numerical investigations have been used whenever the equations to be solved became too complicated to be solved analytically. Another possible path in which the research presented here could be continued is to connect our results to observations, i.e. to explore the diagnostic capabilities of the theoretical results presented here.

With all of these refinements, our model will be much more applicable to the solar environment and give us greater understanding of wave propagation, as well as energy leakage and instabilities in prominences, the transition region and other features with waves propagating obliquely to magnetic fields. This will help us to understand energy flow and its effects on wave observations in the solar atmosphere in ever greater detail.

APPENDIX A

Calculation of residues and time-dependent velocities

We aim to calculate explicitly the time dependent form of v_z , given by

$$v_z(t) = -2\pi i [\text{res}_{\omega_-} (\hat{v}_z e^{-i\omega t}) + \text{res}_{\omega_+} (\hat{v}_z e^{-i\omega t})].$$

In order to calculate the residues, required to find the time-dependent solutions for velocity, we introduce the expressions for B_+ and C_- , given by Eqs. (4.41) and (4.42), into the expressions for \hat{v}_z , given by Eqs. (4.29) and (4.31). As a result, we write

$$\hat{v}_{z\pm}(\omega) = X_{\pm}(\omega)A(\omega) + \frac{Y_{\pm}(\omega)}{\sin \theta},$$

where

$$X_- = \frac{k}{\rho_-(\omega^2 - k^2 v_{A-}^2 e^{-2i\theta})} \left[\frac{v_{A-} v_{A+}}{v_{A-} + V_{A+}} \sin \theta e^{i\lambda_{1-} z} (i\lambda_{2+} - k) + i\omega e^{kz} \right] \\ + \frac{k}{\rho_+(\omega^2 - k^2 v_{A+}^2 e^{2i\theta})} \left[\frac{v_{A-} v_{A+}}{v_{A-} + V_{A+}} \sin \theta e^{i\lambda_{1-} z} (i\lambda_{2+} + k) \right],$$

$$X_+ = \frac{k}{\rho_-(\omega^2 - k^2 v_{A-}^2 e^{-2i\theta})} \left[\frac{v_{A-} v_{A+}}{v_{A-} + V_{A+}} \sin \theta e^{i\lambda_{2+} z} (i\lambda_{1-} - k) \right] \\ + \frac{k}{\rho_+(\omega^2 - k^2 v_{A+}^2 e^{2i\theta})} \left[\frac{v_{A-} v_{A+}}{v_{A-} + V_{A+}} \sin \theta e^{i\lambda_{2+} z} (i\lambda_{1-} + k) + i\omega e^{-kz} \right],$$

$$Y_- = \frac{e^{i\lambda_{1+} z}}{2v_{A-}} \int_{-\infty}^z v_{z0} e^{-i\lambda_{1+} z'} dz' - \frac{e^{i\lambda_{1-} z}}{2v_{A-}} \int_0^z v_{z0} e^{-i\lambda_{1-} z'} dz' \\ + \frac{v_{A-} e^{i\lambda_{1-} z}}{v_{A+}(v_{A-} + v_{A+})} \int_0^{\infty} v_{z0} e^{-i\lambda_{2-} z} dz + \frac{(v_{A+} - v_{A-}) e^{i\lambda_{1-} z}}{2v_{A-}(v_{A-} + v_{A+})} \int_{-\infty}^0 v_{z0} e^{-i\lambda_{1+} z} dz,$$

$$Y_+ = \frac{e^{i\lambda_{2-} z}}{2v_{A+}} \int_z^{\infty} v_{z0} e^{-i\lambda_{2-} z'} dz' - \frac{e^{i\lambda_{2+} z}}{2v_{A+}} \int_0^z v_{z0} e^{-i\lambda_{2+} z'} dz' \\ + \frac{v_{A+} e^{i\lambda_{2+} z}}{v_{A-}(v_{A-} + v_{A+})} \int_{-\infty}^0 v_{z0} e^{-i\lambda_{1+} z} dz + \frac{(v_{A-} - v_{A+}) e^{i\lambda_{2+} z}}{2v_{A+}(v_{A-} + v_{A+})} \int_0^{\infty} v_{z0} e^{-i\lambda_{2-} z} dz.$$

Since $Y_{\pm}/\sin\theta$ has no poles in ω , the residues must be given simply by the residues of $X_{\pm}A$. We may write the expression, $D(\omega)$, in the definition for $A(\omega)$ as,

$$D(\omega) = (\rho_- + \rho_+)(\omega - \omega_-)(\omega - \omega_+).$$

This means that, when calculating the residue, we may use the result,

$$\lim_{\omega \rightarrow \omega_{\pm}} [(\omega - \omega_{\pm})A(\omega)] = \frac{H(\omega_{\pm})G(\omega_{\pm})}{\pm 2\omega_r(\rho_- + \rho_+)},$$

where G and H are defined in Eqs. (?? and 4.46). Thus, the time dependent form of the velocity, either side of the interface, is found to be

$$v_z(z, t) = -i\pi \left[\frac{X(\omega_+)H(\omega_+)G(\omega_+)}{\omega_+} e^{-i\omega_+t} - \frac{X(\omega_-)H(\omega_-)G(\omega_-)}{\omega_-} e^{-i\omega_-t} \right],$$

which, when written explicitly, is

$$v_z(t, z) = e^{\omega_i t} \left\{ e^{-i\omega_r t} \left[U_{1+} e^{kz} + W_{1+} \exp \left(\frac{[\omega_i - i(kv_{A-} \cos \theta + \omega_r)]z}{v_{A-} \sin \theta} \right) \right] - e^{i\omega_r t} \left[U_{1-} e^{kz} + W_{1-} \exp \left(\frac{[\omega_i - i(kv_{A-} \cos \theta - \omega_r)]z}{v_{A-} \sin \theta} \right) \right] \right\} \quad (\text{A.1})$$

for $z < 0$, and

$$v_z(t, z) = e^{\omega_i t} \left\{ e^{-i\omega_r t} \left[U_{2+} e^{-kz} - W_{2+} \exp \left(-\frac{[\omega_i + i(kv_{A+} \cos \theta - \omega_r)]z}{v_{A+} \sin \theta} \right) \right] - e^{i\omega_r t} \left[U_{2-} e^{-kz} - W_{2-} \exp \left(-\frac{[\omega_i + i(kv_{A+} \cos \theta + \omega_r)]z}{v_{A+} \sin \theta} \right) \right] \right\}, \quad (\text{A.2})$$

for $z > 0$, where $U_{1,2\pm}$ and $W_{1,2\pm}$ are given by the expressions,

$$U_{1\pm} = \frac{\rho_+ \omega_{\pm} G(\omega_{\pm})(v_{A-} - v_{A+})(\omega_{\pm} + kv_{A+} e^{i\theta})}{2\omega_r(\rho_- + \rho_+)(\omega_{\pm} + kv_{A-} e^{-i\theta})}, \quad (\text{A.3})$$

$$U_{2\pm} = \frac{\rho_- \omega_{\pm} G(\omega_{\pm})(v_{A+} - v_{A-})(\omega_{\pm} - kv_{A-} e^{-i\theta})}{2\omega_r(\rho_- + \rho_+)(\omega_{\pm} - kv_{A+} e^{i\theta})}, \quad (\text{A.4})$$

$$W_{1\pm} = \frac{G(\omega_{\pm})v_{A-}(v_{A+} - v_{A-})}{2\omega_r(\rho_- + \rho_+)(v_{A-} + v_{A+})(\omega_{\pm} + kv_{A-} e^{-i\theta})} \times [(\rho_- + \rho_+)\omega_{\pm}^2 + 2ik\omega_{\pm}\rho_+v_{A+} \sin \theta - 2k^2\rho v_A^2 e^{-i\theta} \cos \theta], \quad (\text{A.5})$$

$$W_{2\pm} = \frac{G(\omega_{\pm})v_{A+}(v_{A+} - v_{A-})}{2\omega_r(\rho_- + \rho_+)(v_{A-} + v_{A+})(\omega_{\pm} - kv_{A+} e^{i\theta})} \times [(\rho_- + \rho_+)\omega_{\pm}^2 + 2ik\omega_{\pm}\rho_-v_{A-} \sin \theta - 2k^2\rho v_A^2 e^{i\theta} \cos \theta]. \quad (\text{A.6})$$

APPENDIX B

Expressions for time-dependent averages

The expressions in Eq. (4.79) are given to be,

$$\begin{aligned}
\Upsilon_1 = & \exp[-kz(\Gamma/v_{A-} + i/\theta)] \left\{ \frac{\exp[-ikC_k(t + z/\theta v_{A-})]}{(C_k + v_{A-})(C_k + v_{A+})} \right. \\
& \times \left[\exp\left(\frac{\sqrt{\theta}\Gamma}{v_{A-}} + \frac{i}{\sqrt{\theta}}(1 + C_k/v_{A-})\right) - \exp\left(\frac{-\sqrt{\theta}\Gamma}{v_{A-}} - \frac{i}{\sqrt{\theta}}(1 + C_k/v_{A-})\right) \right] \\
& - \frac{\exp[ikC_k(t + z/\theta v_{A-})]}{(C_k - v_{A-})(C_k - v_{A+})} \\
& \left. \times \left[\exp\left(\frac{\sqrt{\theta}\Gamma}{v_{A-}} + \frac{i}{\sqrt{\theta}}(1 - C_k/v_{A-})\right) - \exp\left(\frac{-\sqrt{\theta}\Gamma}{v_{A-}} - \frac{i}{\sqrt{\theta}}(1 - C_k/v_{A-})\right) \right] \right\}, \tag{B.1}
\end{aligned}$$

$$\begin{aligned}
\Upsilon_2 = & \exp[kz(\Gamma/v_{A+} - i/\theta)] \left\{ \frac{\exp[-ikC_k(t - z/\theta v_{A+})]}{(C_k - v_{A-})(C_k - v_{A+})} \right. \\
& \times \left[\exp\left(\frac{\sqrt{\theta}\Gamma}{v_{A+}} - \frac{i}{\sqrt{\theta}}(1 - C_k/v_{A+})\right) - \exp\left(\frac{-\sqrt{\theta}\Gamma}{v_{A+}} + \frac{i}{\sqrt{\theta}}(1 - C_k/v_{A+})\right) \right] \\
& - \frac{\exp[ikC_k(t - z/\theta v_{A+})]}{(C_k + v_{A-})(C_k + v_{A+})} \\
& \times \left[\exp\left(\frac{\sqrt{\theta}\Gamma}{v_{A+}} - \frac{i}{\sqrt{\theta}}(1 + C_k/v_{A+})\right) \right. \\
& \left. - \exp\left(\frac{-\sqrt{\theta}\Gamma}{v_{A+}} + \frac{i}{\sqrt{\theta}}(1 + C_k/v_{A+})\right) \right] \left. \right\}, \tag{B.2}
\end{aligned}$$

and

$$\begin{aligned}
\Upsilon_t = & \frac{4i(C_k^2 + v_{A-}v_{A+}) \sin(kC_k t)}{(C_k^2 - v^2)(C_k^2 - v_{A+}^2)} \\
& + e^{-ikz/\theta} \left(\frac{\exp[\sigma_{1+} - ikC_k t] - \exp[\sigma_{2-} + ikC_k t]}{(C_k + v_{A-})(C_k + v_{A+})} \right. \\
& \left. - \frac{\exp[\sigma_{1-} + ikC_k t] - \exp[\sigma_{2+} - ikC_k t]}{(C_k - v_{A-})(C_k - v_{A+})} \right), \tag{B.3}
\end{aligned}$$

where

$$\begin{aligned}\sigma_{1\pm} &= \frac{\sqrt{\theta} - kz}{v_{A-}} \left(\Gamma \pm \frac{iC_k}{\theta} \right) + \frac{i}{\sqrt{\theta}}, \\ \sigma_{2\pm} &= \frac{\sqrt{\theta} + kz}{v_{A+}} \left(\Gamma \mp \frac{iC_k}{\theta} \right) - \frac{i}{\sqrt{\theta}}.\end{aligned}\tag{B.4}$$

Bibliography

- Andries, J., Arregui, I. and Goossens, M. (2005), ‘Determination of the Coronal Density Stratification from the Observation of Harmonic Coronal Loop Oscillations’, *Astrophys. J. Lett.* **624**(1), L57–L60.
- Anfinogentov, S., Nisticò, G. and Nakariakov, V. M. (2013), ‘Decay-less kink oscillations in coronal loops’, *A&A* **560**, A107.
URL: <https://doi.org/10.1051/0004-6361/201322094>
- Arregui, I. (2015), ‘Wave heating of the solar atmosphere’, *Philosophical Transactions of the Royal Society of London Series A* **373**(2042), 20140261–20140261.
- Arregui, I., Oliver, R. and Ballester, J. L. (2018), ‘Prominence oscillations’, *Living Reviews in Solar Physics* **15**(1), 3.
- Arregui, I., Terradas, J., Oliver, R. and Ballester, J. L. (2010), ‘The Sun and the Solar System’, *Astrophysics and Space Science Proceedings* **14**, 446.
- Aschwanden, M. J. (2003), ‘Review of Coronal Oscillations - An Observer’s View’, *arXiv e-prints* pp. astro-ph/0309505.
- Aschwanden, M. J., Fletcher, L., Schrijver, C. J. and Alexander, D. (1999), ‘Coronal Loop Oscillations Observed with the Transition Region and Coronal Explorer’, *Astrophys. J.* **520**(2), 880–894.
- Avrett, E. H. and Loeser, R. (2008), ‘Models of the Solar Chromosphere and Transition Region from SUMER and HRTS Observations: Formation of the Extreme-Ultraviolet Spectrum of Hydrogen, Carbon, and Oxygen’, *Astrophys. J. Suppl.* **175**(1), 229–276.
- Ballai, I., Douglas, M. and Marcu, A. (2008), ‘Forced oscillations of coronal loops driven by EIT waves’, *Astron. Astrophys.* **488**(3), 1125–1132.
- Ballester, J. L. (2006), ‘Recent progress in prominence seismology’, *Philosophical Transactions of the Royal Society of London Series A* **364**(1839), 405–415.
- Bernstein, I. B. and Book, D. L. (1983), ‘Effect of compressibility on the Rayleigh-Taylor instability’, *Physics of Fluids* **26**(2), 453–458.

- Briskin, W. F. and Zirin, H. (1997), ‘New Data and Models of Running Penumbra Waves in Sunspots’, *Astrophys. J.* **478**(2), 814–816.
- Brynildsen, N., Brekke, P., Haugan, S. V. H., Kjeldseth-Moe, O., Maltby, P. and Wikstøl, Ø. (2000), ‘Structure and Dynamics in the Atmosphere Above Sunspot Regions’, *Advances in Space Research* **25**(9), 1743–1746.
- Cally, P. S. (1986), ‘Leaky and Non-Leaky Oscillations in Magnetic Flux Tubes’, *Solar Phys.* **103**(2), 277–298.
- Cally, P. S. (2003), ‘Coronal Leaky Tube Waves and Oscillations Observed with Trace’, *Solar Phys.* **217**(1), 95–108.
- Cally, P. S. and Schunker, H. (2006), Magnetic field inclination and atmospheric oscillations above solar active regions: theory, *in* ‘Proceedings of SOHO 18/GONG 2006/HELAS I, Beyond the spherical Sun’, Vol. 624 of *ESA Special Publication*, p. 64.
- Carlyle, J., Williams, D. R., van Driel-Gesztelyi, L., Innes, D., Hillier, A. and Matthews, S. (2014), ‘Investigating the Dynamics and Density Evolution of Returning Plasma Blobs from the 2011 June 7 Eruption’, *Astrophys. J.* **782**(2), 87.
- Chandrasekhar, S. (1961), *Hydrodynamic and hydromagnetic stability*.
- Chen, C.-J. and Lykoudis, P. S. (1972), ‘Velocity Oscillations in Solar Plage Regions’, *Solar Phys.* **25**(2), 380–401.
- Chevalier, R. A. (1982), ‘The radio and X-ray emission from type II supernovae.’, *Astrophys. J.* **259**, 302–310.
- De Moortel, I. and Nakariakov, V. M. (2012), ‘Magnetohydrodynamic waves and coronal seismology: an overview of recent results’, *Philosophical Transactions of the Royal Society of London Series A* **370**(1970), 3193–3216.
- DeForest, C. E. and Gurman, J. B. (1998), ‘Observation of Quasi-periodic Compressive Waves in Solar Polar Plumes’, *Astrophys. J. Lett.* **501**(2), L217–L220.
- Díaz, A. J., Khomenko, E. and Collados, M. (2014), ‘Rayleigh-Taylor instability in partially ionized compressible plasmas: One fluid approach’, *Astron. Astrophys.* **564**, A97.
- Dorotovič, I., Erdélyi, R., Freij, N., Karlovský, V. and Márquez, I. (2014), ‘Standing sausage waves in photospheric magnetic waveguides’, *Astron. Astrophys.* **563**, A12.
- Edwin, P. M. and Roberts, B. (1982), ‘Wave Propagation in a Magnetically Structured Atmosphere - Part Three - the Slab in a Magnetic Environment’, *Solar Phys.* **76**(2), 239–259.

- Einaudi, G., Chiuderi, C. and Califano, F. (1993), ‘Coronal heating and solar activity: The role of waves’, *Advances in Space Research* **13**(9), 85–94.
- Erdélyi, R. and Ballai, I. (2007), ‘Heating of the solar and stellar coronae: a review’, *Astronomische Nachrichten* **328**(8), 726–733.
- Erdélyi, R. and James, S. P. (2004), ‘Can ion-neutral damping help to form spicules?. II. Random driver’, *Astron. Astrophys.* **427**, 1055–1064.
- Erdélyi, R. and Taroyan, Y. (2008), ‘Hinode EUV spectroscopic observations of coronal oscillations’, *Astron. Astrophys.* **489**(3), L49–L52.
- Ershkovich, A. I. and Israelevich, P. L. (2000), ‘On the MHD analogue of the Brunt/Väisälä frequency in a magnetized plasma’, *Journal of Plasma Physics* **64**(2), 195–200.
- Giovanelli, R. G. (1972), ‘Oscillations and Waves in a Sunspot’, *Solar Phys.* **27**(1), 71–79.
- Goedbloed, J. P. H. and Poedts, S. (2004), *Principles of Magnetohydrodynamics*.
- Goossens, M., Andries, J., Soler, R., Van Doorselaere, T., Arregui, I. and Terradas, J. (2012), ‘Surface Alfvén Waves in Solar Flux Tubes’, *Astrophys. J.* **753**(2), 111.
- Hester, J. J., Stone, J. M., Scowen, P. A., Jun, B.-I., Gallagher, John S., I., Norman, M. L., Ballester, G. E., Burrows, C. J., Casertano, S., Clarke, J. T., Crisp, D., Griffiths, R. E., Hoessel, J. G., Holtzman, J. A., Krist, J., Mould, J. R., Sankrit, R., Stapelfeldt, K. R., Trauger, J. T., Watson, A. and Westphal, J. A. (1996), ‘WFPC2 Studies of the Crab Nebula. III. Magnetic Rayleigh-Taylor Instabilities and the Origin of the Filaments’, *Astrophys. J.* **456**, 225.
- Hillier, A. (2018), ‘The magnetic Rayleigh-Taylor instability in solar prominences’, *Reviews of Modern Plasma Physics* **2**(1), 1.
- Innes, D. E., Cameron, R. H., Fletcher, L., Inhester, B. and Solanki, S. K. (2012), ‘Break up of returning plasma after the 7 June 2011 filament eruption by Rayleigh-Taylor instabilities’, *Astron. Astrophys.* **540**, L10.
- Isobe, H., Miyagoshi, T., Shibata, K. and Yokoyama, T. (2005), ‘Filamentary structure on the Sun from the magnetic Rayleigh-Taylor instability’, *Nature* **434**(7032), 478–481.
- Isobe, H., Miyagoshi, T., Shibata, K. and Yokoyama, T. (2006), ‘Three-Dimensional Simulation of Solar Emerging Flux Using the Earth Simulator I. Magnetic Rayleigh-Taylor Instability at the Top of the Emerging Flux as the Origin of Filamentary Structure’, *Pub. Astron. Soc. Japan* **58**, 423–438.

- Jain, R. and Roberts, B. (1991), ‘Magnetoacoustic surface waves at a single interface’, *Solar Phys.* **133**(2), 263–280.
- Jeans, J. H. (1902), ‘The Stability of a Spherical Nebula’, *Philosophical Transactions of the Royal Society of London Series A* **199**, 1–53.
- Jess, D. B., Morton, R. J., Verth, G., Fedun, V., Grant, S. D. T. and Gigkiozis, I. (2015), ‘Multiwavelength Studies of MHD Waves in the Solar Chromosphere. An Overview of Recent Results’, *Space Sci. Rev.* **190**(1–4), 103–161.
- Jess, D. B., Reznikova, V. E., Van Doorselaere, T., Keys, P. H. and Mackay, D. H. (2013), ‘The Influence of the Magnetic Field on Running Penumbra Waves in the Solar Chromosphere’, *Astrophys. J.* **779**(2), 168.
- Joarder, P. S. and Nakariakov, V. M. (2006), ‘Hydromagnetic surface waves on a tangential discontinuity’, *Geophysical and Astrophysical Fluid Dynamics* **100**(1), 59–83.
- Jones, T. W. and De Young, D. S. (2005), ‘Magnetohydrodynamic Simulations of Relic Radio Bubbles in Clusters’, *Astrophys. J.* **624**(2), 586–605.
- Jun, B.-I., Jones, T. W. and Norman, M. L. (1996), ‘Interaction of Rayleigh-Taylor Fingers and Circumstellar Cloudlets in Young Supernova Remnants’, *Astrophys. J. Lett.* **468**, L59.
- Jun, B.-I. and Norman, M. L. (1995), ‘MHD Simulations of Rayleigh-Taylor Instability in Young Supernova Remnants’, *Astrophys. Space Sci.* **233**(1–2), 267–272.
- Kelvinsong (2012), ‘Sun poster’. Accessed: 23 September 2019.
- Khomenko, E. and Collados, M. (2015), ‘Oscillations and Waves in Sunspots’, *Living Reviews in Solar Physics* **12**(1), 6.
- Klimchuk, J. A. (2006), ‘On Solving the Coronal Heating Problem’, *Solar Phys.* **234**(1), 41–77.
- Kobanov, N. I. and Makarchik, D. V. (2004), ‘Propagating waves in the sunspot umbra chromosphere’, *Astron. Astrophys.* **424**, 671–675.
- Kruskal, M. and Schwarzschild, M. (1954), ‘Some Instabilities of a Completely Ionized Plasma’, *Proceedings of the Royal Society of London Series A* **223**(1154), 348–360.
- Kulkarni, A. K. and Romanova, M. M. (2008), Rayleigh-Taylor-Unstable Accretion and Variability of Magnetized Stars: Global Three-Dimensional Simulations, in R. Wijnands, D. Altamirano, P. Soleri, N. Degenaar, N. Rea, P. Casella, A. Patruno and M. Linares, eds, ‘American Institute of Physics Conference Series’, Vol. 1068 of *American Institute of Physics Conference Series*, pp. 99–102.

- Leighton, R. B. (1960), in R. N. Thomas, ed., ‘Aerodynamic Phenomena in Stellar Atmospheres’, Vol. 12 of *IAU Symposium*, pp. 321–325.
- Levy, R. H., Petschek, H. E. and Siscoe, G. L. (1964), ‘Aerodynamic aspects of the magnetospheric flow’, *AIAA Journal* **2**(12), 2065–2076.
- Lin, Y., Soler, R., Engvold, O., Ballester, J. L., Langanen, Ø., Oliver, R. and Rouppe van der Voort, L. H. M. (2009), ‘Swaying Threads of a Solar Filament’, *Astrophys. J.* **704**(1), 870–876.
- Lites, B. W., White, O. R. and Packman, D. (1982), ‘Photoelectric observations of propagating sunspot oscillations’, *Astrophys. J.* **253**, 386–392.
- Luna, M. and Karpen, J. (2012), ‘Large-amplitude Longitudinal Oscillations in a Solar Filament’, *Astrophys. J. Lett.* **750**(1), L1.
- Malherbe, J. M. and Priest, E. R. (1983), ‘Current sheet models for solar prominences. I Magnetohydrostatics of support and evolution through quasi-static models’, *Astron. Astrophys.* **123**(1), 80–88.
- Mather, J. F. and Erdélyi, R. (2016), ‘Magneto-Acoustic Waves in a Gravitationally Stratified Magnetized Plasma: Eigen-Solutions and their Applications to the Solar Atmosphere’, *Astrophys. J.* **822**(2), 116.
- Mathioudakis, M., Jess, D. B. and Erdélyi, R. (2013), ‘Alfvén Waves in the Solar Atmosphere. From Theory to Observations’, *Space Sci. Rev.* **175**(1–4), 1–27.
- Matsumoto, J. and Masada, Y. (2013), ‘Two-dimensional Numerical Study for Rayleigh-Taylor and Richtmyer-Meshkov Instabilities in Relativistic Jets’, *Astrophys. J. Lett.* **772**(1), L1.
- Moreton, G. E. and Ramsey, H. E. (1960), ‘Recent Observations of Dynamical Phenomena Associated with Solar Flares’, *Pub. Astron. Soc. Pac.* **72**(428), 357.
- Nakariakov, V. M. and Roberts, B. (1999), ‘Solitary autowaves in magnetic flux tubes’, *Physics Letters A* **254**(6), 314–318.
- Nakariakov, V. M., Roberts, B. and Murawski, K. (1999), MHD Waves in Open Magnetic Structures, in B. Schmieder, A. Hofmann and J. Staude, eds, ‘Third Advances in Solar Physics Euroconference: Magnetic Fields and Oscillations’, Vol. 184 of *Astronomical Society of the Pacific Conference Series*, pp. 243–247.
- Newcomb, W. A. (1960), ‘Hydromagnetic stability of a diffuse linear pinch’, *Annals of Physics* **10**(2), 232–267.
- Nye, A. H. and Thomas, J. H. (1974), ‘The Nature of Running Penumbra Waves’, *Solar Phys.* **38**(2), 399–413.

- Okamoto, T. J., Tsuneta, S., Berger, T. E., Ichimoto, K., Katsukawa, Y., Lites, B. W., Nagata, S., Shibata, K., Shimizu, T., Shine, R. A., Suematsu, Y., Tarbell, T. D. and Title, A. M. (2007), ‘Coronal Transverse Magnetohydrodynamic Waves in a Solar Prominence’, *Science* **318**(5856), 1577.
- Oliver, R. (2009), ‘Prominence Seismology Using Small Amplitude Oscillations’, *Space Sci. Rev.* **149**(1-4), 175–197.
- Parker, E. N. (1966), ‘The Dynamical State of the Interstellar Gas and Field’, *Astrophys. J.* **145**, 811.
- Parnell, C. E. and De Moortel, I. (2012), ‘A contemporary view of coronal heating’, *Philosophical Transactions of the Royal Society of London Series A* **370**(1970), 3217–3240.
- Paschmann, G., Sckopke, N., Bame, S. J., Asbridge, J. R., Gosling, J. T., Russell, C. T. and Greenstadt, E. W. (1979), ‘Association of low-frequency waves with suprathermal ions in the upstream solar wind’, *Geophys. Res. Lett.* **6**(3), 209–212.
- Priest, E. (2014), *Magnetohydrodynamics of the Sun*.
- Rayleigh, L. (1900), ‘On the Viscosity of Gases as Affected by Temperature’, *Proceedings of the Royal Society of London Series I* **67**, 137–139.
- Ribeyre, X., Tikhonchuk, V. T. and Bouquet, S. (2004), ‘Compressible Rayleigh-Taylor instabilities in supernova remnants’, *Physics of Fluids* **16**(12), 4661–4670.
- Roberts, B. (1981*a*), ‘Wave Propagation in a Magnetically Structured Atmosphere - Part One - Surface Waves at a Magnetic Interface’, *Solar Phys.* **69**(1), 27–38.
- Roberts, B. (1981*b*), ‘Wave Propagation in a Magnetically Structured Atmosphere - Part Two - Waves in a Magnetic Slab’, *Solar Phys.* **69**(1), 39–56.
- Robinson, K., Dursi, L. J., Ricker, P. M., Rosner, R., Calder, A. C., Zingale, M., Truran, J. W., Linde, T., Caceres, A., Fryxell, B., Olson, K., Riley, K., Siegel, A. and Vladimirova, N. (2004), ‘Morphology of Rising Hydrodynamic and Magnetohydrodynamic Bubbles from Numerical Simulations’, *Astrophys. J.* **601**(2), 621–643.
- Ruderman, M. S. (2017), ‘Compressibility Effect on the Rayleigh-Taylor Instability with Sheared Magnetic Fields’, *Solar Phys.* **292**(4), 47.
- Ruderman, M. S., Ballai, I., Khomenko, E. and Collados, M. (2018), ‘Rayleigh-Taylor instabilities with sheared magnetic fields in partially ionised plasmas’, *Astron. Astrophys.* **609**, A23.
- Ruderman, M. S. and Roberts, B. (2006), ‘Leaky and non-leaky kink oscillations of magnetic flux tubes’, *Journal of Plasma Physics* **72**(3), 285–308.

- Ruderman, M. S., Terradas, J. and Ballester, J. L. (2014), ‘Rayleigh-Taylor Instabilities with Sheared Magnetic Fields’, *Astrophys. J.* **785**(2), 110.
- Ruderman, M. S., Vickers, E., Ballai, I. and Erdélyi, R. (2018), ‘Propagation of leaky surface waves on contact magnetohydrodynamic discontinuities in incompressible plasmas’, *Physics of Plasmas* **25**(12), 122107.
- Ryutova, M., Berger, T., Frank, Z., Tarbell, T. and Title, A. (2010), ‘Observation of Plasma Instabilities in Quiescent Prominences’, *Solar Phys.* **267**(1), 75–94.
- Schunker, H. and Cally, P. S. (2006), ‘Magnetic field inclination and atmospheric oscillations above solar active regions’, *Mon. Not. Roy. Astron. Soc.* **372**(2), 551–564.
- Scullion, E., Erdélyi, R., Fedun, V. and Doyle, J. G. (2011), ‘The Response of A Three-dimensional Solar Atmosphere to Wave-driven Jets’, *Astrophys. J.* **743**(1), 14.
- Shivamoggi, B. K. (1982), ‘Rayleigh-Taylor instability of a compressible plasma in a horizontal magnetic field’, *Zeitschrift Angewandte Mathematik und Physik* **33**(5), 693–697.
- Solanki, S. K. (2003), ‘Sunspots: An overview’, *Astron. Astrophys. Rev.* **11**(2-3), 153–286.
- Spiegel, E. A. and Zahn, J. P. (1992), ‘The solar tachocline.’, *Astron. Astrophys.* **265**, 106–114.
- Sutmann, G., Musielak, Z. E. and Ulmschneider, P. (1998), ‘Acoustic wave propagation in the solar atmosphere. III. Analytic solutions for adiabatic wave excitations’, *Astron. Astrophys.* **340**, 556–568.
- Taylor, G. (1950), ‘The Instability of Liquid Surfaces when Accelerated in a Direction Perpendicular to their Planes. I’, *Proceedings of the Royal Society of London Series A* **201**(1065), 192–196.
- Terradas, J., Andries, J., Goossens, M., Arregui, I., Oliver, R. and Ballester, J. L. (2008), ‘Nonlinear Instability of Kink Oscillations due to Shear Motions’, *Astrophys. J. Lett.* **687**(2), L115.
- Terradas, J., Oliver, R. and Ballester, J. L. (2012), ‘The role of Rayleigh-Taylor instabilities in filament threads’, *Astron. Astrophys.* **541**, A102.
- Thomas, J. H. and Weiss, N. O. (2004), ‘Fine Structure in Sunspots’, *Ann. Rev. Astron. Astrophys.* **42**(1), 517–548.
- Thompson, B. J., Gurman, J. B., Neupert, W. M., Newmark, J. S., Delaboudinière, J. P., Cyr, O. C. S., Stezelberger, S., Dere, K. P., Howard, R. A. and Michels, D. J. (1999), ‘SOHO/EIT Observations of the 1997 April 7 Coronal Transient: Possible Evidence of Coronal Moreton Waves’, *Astrophys. J. Lett.* **517**(2), L151–L154.

- Vandervoort, P. O. (1961), ‘The Rayleigh-Taylor Instability in Compressible Fluids.’, *Astron. J.* **70**, 56.
- Vernazza, J. E., Avrett, E. H. and Loeser, R. (1981), ‘Structure of the solar chromosphere. III. Models of the EUV brightness components of the quiet sun.’, *Astrophys. J. Suppl.* **45**, 635–725.
- Verth, G., Erdélyi, R. and Jess, D. B. (2008), ‘Refined Magnetoseismological Technique for the Solar Corona’, *Astrophys. J. Lett.* **687**(1), L45.
- Verwichte, E., Nakariakov, V. M. and Cooper, F. C. (2005), ‘Transverse waves in a post-flare supra-arcade’, *Astron. Astrophys.* **430**, L65–L68.
- Vickers, E., Ballai, I. and Erdélyi, R. (2018), ‘Propagation of Leaky MHD Waves at Discontinuities with Tilted Magnetic Field’, *Solar Phys.* **293**(10), 139.
- Wang, Y. M. and Nepveu, M. (1983), ‘A numerical study of the nonlinear Rayleigh-Taylor instability, with application to accreting X-ray sources’, *Astron. Astrophys.* **118**(2), 267–274.
- Zirin, H. and Stein, A. (1972), ‘Observations of Running Penumbra Waves’, *Astrophys. J. Lett.* **178**, L85.
- Zsámberger, N. K., Allcock, M. and Erdélyi, R. (2018), ‘Magneto-acoustic Waves in a Magnetic Slab Embedded in an Asymmetric Magnetic Environment: The Effects of Asymmetry’, *Astrophys. J.* **853**(2), 136.